

Quantum Interference of Hydrodynamic Modes in a Dirty Marginal Fermi Liquid

Tsz Chun Wu,¹ Yunxiang Liao,^{2,3} and Matthew S. Foster^{1,4}

¹*Department of Physics and Astronomy, Rice University, Houston, Texas 77005, USA*

²*Joint Quantum Institute, University of Maryland, College Park, MD 20742, USA*

³*Condensed Matter Theory Center, Department of Physics,
University of Maryland, College Park, MD 20742, USA*

⁴*Rice Center for Quantum Materials, Rice University, Houston, Texas 77005, USA*

(Dated: June 7, 2022)

We study the electrical transport of a two-dimensional non-Fermi liquid with disorder, and we determine both the semiclassical dc conductivity and the first quantum correction. We consider a system with N flavors of fermions coupled to $SU(N)$ critical matrix bosons. Motivated by the SYK model, we employ the bilocal field formalism and derive a set of finite-temperature saddle-point equations governing the fermionic and bosonic self-energies in the large- N limit. Interestingly, disorder smearing induces marginal Fermi liquid (MFL) behavior. Consequently, the resistivity varies linearly with temperature on top of the Drude result. We also consider fluctuations around the saddle points and derive a MFL-Finkel'stein nonlinear sigma model. We find that the Altshuler-Aronov quantum conductance correction also gives linear- T resistivity, and in fact dominates at low temperatures. The strong temperature dependence of the quantum correction arises due to rapid relaxation of the mediating quantum-critical bosons. We verify that our calculations explicitly satisfy the Ward identity at the semiclassical and quantum levels. Our results establish that quantum interference persists in 2-particle hydrodynamic modes, even when quasiparticles are subject to strong (Planckian) dissipation.

CONTENTS

I. Introduction	2	2. Vertex correction $\delta\Gamma_{Vq}^{(i)}$	20
A. Summary of main results	2	B. Dynamical screening	20
B. A brief survey of strange-metal theory	4	C. Feynman diagrams for the interaction correction	21
C. Disordered, interacting Fermi liquids	5	1. Type-A diagrams	22
D. Technical approach of this work	5	2. Type-B diagrams	22
E. Outline	5	3. Total contribution	23
II. The model	6	D. Evaluation of the AA correction	24
III. Disorder averaging	8	1. Finite temperature, dc limit	24
IV. Bilocal field formulation	8	2. Zero temperature limit with finite external frequency	26
A. Saddle-point equations	9	VIII. Discussion and outlook	26
B. Marginal Fermi liquid dc resistivity at the saddle-point level	12	IX. Acknowledgment	27
V. Non-linear sigma model (“MFL-FNLsM”)	13	A. Evaluation of the thermal mass m_b^2	27
A. π - σ parametrization	14	B. Evaluation of $\mathcal{F}(t, x)$	28
1. Diffusion term	14	C. Derivation of the MFL-FNLsM	28
2. Interaction terms	15	1. Derivation for S_D , S_{qV} and S_V	29
3. Source field term	15	2. Derivation for $S_{\text{int I}}$ and $S_{\text{int II}}$	30
B. Feynman rules	16	D. Expressions for the type-B diagrams	32
1. Bare propagator	16	E. Numerical verification of the Ward identity	34
2. Interaction vertices	16	F. AA integral kernels	34
VI. Semiclassical result for the density response function	17	1. Intermediate temperature, ignoring dynamical screening	34
VII. Quantum interaction corrections to the density response function	19	2. Incorporating dynamical screening	34
A. Vertex corrections to the $q^{(2)}$ - V coupling	19	References	35
1. Vertex correction $\delta\Gamma_{Vq}^{(i)}$	19		

I. INTRODUCTION

There has been a recent surge of interest in non-Fermi liquids (NFLs), which cannot be described by the Landau quasiparticle paradigm. NFL properties are observed in a variety of correlated electron systems, including the cuprates [1, 2], iron-based superconductors [3, 4], ruthenates [5–8], twisted bilayer graphene [9, 10], and heavy fermion materials [11–13] tuned to quantum criticality. Some of these systems demonstrate a resistivity that increases linearly with temperature down to the low-temperature regime, in sharp contrast with ordinary metals in which the resistivity varies quadratically with temperature [14]. This “strange metal” phase has been ubiquitously observed in the normal state of high-temperature superconductors [1–4].

The anomalous properties observed in strange metals might indicate ultrafast “Planckian” dissipation, due to the extremely rapid collision dynamics between charge carriers [15, 16]. Arguably the most important question is why superconductivity, a macroscopic, coherent many-body quantum state, can paradoxically arise *at anomalously high temperatures* from a collision-dominated, seemingly incoherent strange metal. In this work, we address a precursor to this question: does some form of quantum coherence survive in a strange metal that simultaneously exhibits Planckian dissipation?

We consider the effects of both interactions and quenched disorder; the latter is certainly present in most quantum materials. Strange metals are typically quasi-two-dimensional, where quantum interference effects are strong and can induce Anderson localization for arbitrarily weak disorder [17, 18]. From a semiclassical (hydrodynamic or kinetic-theory) perspective, strong carrier-carrier collisions might be expected to wipe out interference effects like weak localization [19], particularly if the *electron transport dephasing time* τ_ϕ [20] due to inelastic carrier-carrier scattering becomes comparable to the elastic lifetime τ_{el} .

On the other hand, interactions can mediate other types of quantum interference: Altshuler-Aronov (AA) corrections to the conductivity [21, 22]. AA corrections can appear in the particle-hole channel, where a conservation law (the Ward identity) prevents the dephasing rate from directly modifying the hydrodynamic response function [23]. The coherent scattering of interacting electrons off the self-consistent potential due to impurity-induced Friedel oscillations results in AA corrections in Fermi liquids [22]. We show in this work that AA corrections can arise in a theory of a marginal Fermi liquid [1], and produce surprising effects. In our theory, interactions are mediated by quantum-critical bosons in the finite-temperature (quantum relaxational [24–26]) regime. As a result of the *rapid relaxation of the bosons*, the AA correction gives an additional source of linear-in-temperature dependence to the resistivity, which we show extends the marginal Fermi liquid phenomenology down to temperatures much smaller than the elastic scattering rate due

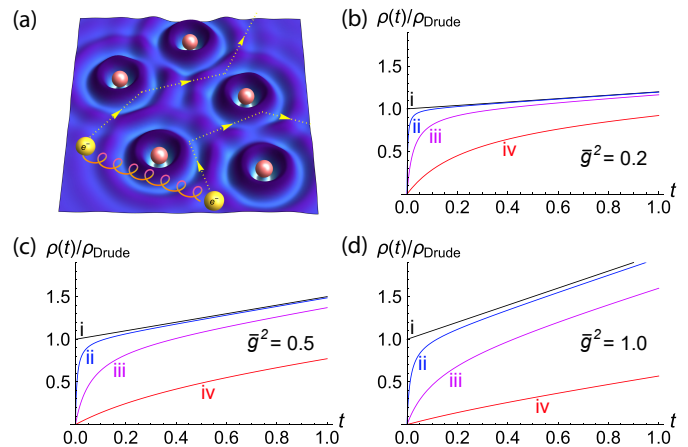


FIG. 1. (a) An impurity potential induces inhomogeneity in the single-particle wave functions, resulting in density Friedel oscillations. In a diffusive Fermi liquid, interacting electrons scatter coherently off of the Friedel oscillations, resulting in the Altshuler-Aronov (AA) quantum correction to conductance [21, 22]. (b)–(d) Plots of the dc resistivity $\rho(t)/\rho_{\text{Drude}}$ versus the temperature $t = T/\gamma_{\text{el}}$, from Eq. (1.4), incorporating the marginal Fermi liquid (MFL) saddle-point result and AA correction. We set the parameter $\mathcal{S} = 1$ in all plots. Panels (b), (c), and (d) depict results for three different values of the effective dimensionless squared-Yukawa coupling $\bar{g}^2 = \{0.2, 0.5, 1\}$, respectively. The black curve in each panel has $\bar{\rho}\mathcal{G}_{AA} = 0$, which neglects the AA correction. The other curves include the AA with $\bar{\rho}\mathcal{G}_{AA} \in \{0.001, 0.01, 0.1\}$ (blue to red, top to bottom). The antilocalizing AA correction drives $\rho(t)$ towards zero as $t \rightarrow 0$ and effectively shifts the resistivity downward, continuing the MFL phenomenology to very low temperatures.

to impurity scattering $1/\tau_{\text{el}}$, see Fig. 1.

Our most important takeaway is this: although individual quasiparticles rapidly decay in a strongly correlated marginal Fermi liquid, two-particle hydrodynamic modes can retain spatial quantum coherence, leading to virtual interference effects that modulate low-temperature transport. The key question for future work is to determine what implication this coherence may have for unconventional superconductivity [27–31].

A. Summary of main results

Much recent theoretical work incorporates multicomponent randomness (quenched “exchange” disorder) into the strange metal phase [16, 32–38]. These works draw upon or are inspired by progress in understanding of the Sachdev-Ye-Kitaev (SYK) model, as reviewed below in Sec. IB.

In this paper, we uncover an important role played by simple potential disorder in a model of a strange metal. We show that a two-dimensional (2D) system of fermions coupled to quantum-critical bosons, at finite temperature in the quantum relaxational regime of the latter

[24–26], exhibits a linear-in-temperature (linear- T) resistivity and a singular quantum interference correction that also gives linear- T resistivity at low temperature, where it dominates. The former (latter) arises from a marginal Fermi liquid self-energy (AA correction) that appears at the semiclassical/saddle-point (quantum one-loop) level, respectively. Specifically, we consider N flavors of fermions with finite density coupled to $N \times N$ matrix bosons representing magnetic collective fluctuations [39, 40]. The mass of the bosons is fine-tuned to zero at a zero-temperature quantum critical point (QCP), so that the interaction mediated by them becomes long-ranged in the temperature $T \rightarrow 0$ limit. In contrast to the SYK class of models [33–35, 37, 38, 41], the Yukawa coupling between the fermions and bosons here is uniform, not random. As a result, for every fixed realization of disorder, our system is manifestly $SU(N)$ invariant.

The starting point in this paper is the same large- N microscopic model considered in Ref. [40]. Different from that work, we construct a nonlinear sigma model based upon a distinct, finite-temperature saddle point. Our saddle point obtains from disorder-smearing of the clean NFL physics [39] and the generation of a thermal mass for the quantum relaxational bosons [26], leading to a fermion self-energy of exactly the marginal Fermi liquid type [1]. Our primary interest in strange-metal physics is as a platform for nucleating exotic correlated phases at finite temperature; we therefore do not consider the stability of our theory in the zero-temperature limit.

We derive a set of saddle point equations governing the self-energies in the large- N limit, treating non-perturbatively the effects of both disorder and interactions. We work in the Keldysh formalism at finite temperature [42–44]. Importantly, the singularity in the Landau-damped bosonic self-energy of the clean theory is smeared out due to disorder [34], leading to the effective retarded boson propagator

$$D_{\text{sp}}^R(\omega, \mathbf{k}) = -\frac{1}{2} [\mathbf{k}^2 + m_{\text{b}}^2 - i\alpha\omega]^{-1}. \quad (1.1)$$

Here

$$m_{\text{b}}^2 \simeq \alpha_m T \quad (1.2)$$

is the “thermal mass” [26, 45] of the critical matrix bosons in the quantum relaxational regime; such a mass generically arises due to interactions above a quantum critical point. In Eq. (1.2), T denotes the temperature, while α_m carries units of inverse diffusion constant and is independent of temperature in the leading approximation. We note that $SU(N)$ symmetry does *not* prevent the appearance of the thermal mass in the boson propagator; instead, the $SU(N)$ Ward identity constrains only correlation functions of the associated Noether currents (these are bosonic bilinears). The coefficient α in Eq. (1.1) carries units of inverse diffusion constant, and is independent of temperature. It takes a value $\alpha = 2\pi^2 \bar{g}^2 \nu_0 / N$. Here ν_0 is the bare density of states

per fermion species, and $\bar{g}^2 = g^2 / [(2\pi)^2 \gamma_{\text{el}}]$, with g the bare fermion-boson (Yukawa) coupling and γ_{el} the elastic impurity scattering rate.

At the same semiclassical saddle-point level, we obtain the retarded fermion self-energy

$$\Sigma_{\text{fermion}}^R(\omega, \mathbf{k}) = -i\gamma_{\text{el}} - \bar{g}^2 \left[\omega \ln \left(\frac{\omega_c}{x} \right) + i\frac{\pi}{2}x \right], \quad (1.3)$$

where $x = \max(|\omega|, JT)$ and ω_c is an ultraviolet cut-off. The second term in Eq. (1.3) takes exactly the form predicted 30 years ago in the phenomenological strange-metal theory of a “marginal Fermi liquid” (MFL) [1]. In Eq. (1.3), the constant $J = J(\alpha/\alpha_m)$ [Eq. (4.29)]. We note that $J \rightarrow 2 \ln(\alpha/\alpha_m)$ logarithmically diverges in the (artificial) limit of vanishing thermal mass, $\alpha_m \rightarrow 0$.

We also go beyond the saddle-point level, and derive a modified Finkel’stein nonlinear sigma model [44, 46–48] that governs quantum interference corrections on top of the MFL saddle-point. The sigma model incorporates the MFL self-energy [Eq. (1.3)] as well as an additional effective interaction channel [49, 50] that is induced relative to the Fermi-liquid case. We verify the consistency of our theory by explicitly confirming particle conservation (the Ward identity) for the density-density correlation function, at both the semiclassical and quantum levels at $T = 0$ through explicit calculations.

Our main physics result is the prediction of the temperature-dependent dc electrical resistivity, which takes the form

$$\frac{\rho(t)}{\rho_{\text{Drude}}} = \left[\frac{1}{1 + \mathcal{S} \bar{g}^2 t} + \bar{\rho} \mathcal{G}_{AA} \left(\frac{4\pi \bar{g}^2}{t} \right) \right]^{-1}, \quad (1.4)$$

where $t \equiv T/\gamma_{\text{el}}$ is the dimensionless temperature measured relative to the elastic scattering rate. The first term in the square brackets obtains from the Kubo formula, using the saddle-point MFL self-energy in Eq. (1.3). This term represents real inelastic emission and absorption of quantum relaxational bosons by the charge carriers. Vertex corrections can be neglected here since the bosons behave like damped simple harmonic oscillators (dissipative Einstein phonons) at finite temperature. In this paper, we do not consider the effects of strong fermion-boson drag, which can suppress the inelastic scattering contribution to the conductivity [38, 51].

The second term in the square brackets of Eq. (1.4) is the AA correction; here $\bar{\rho} = (Ne^2/h)\rho_{\text{Drude}}$ is the dimensionless Drude resistance per channel. Eq. (1.4) holds for $\bar{g}^2/N \lesssim t \lesssim 1$. The key observation is that the AA correction in Eq. (1.4) effectively continues the linear- T resistivity predicted by MFL phenomenology down to $t \ll 1$; without the AA correction, the saddle-point resistivity simply saturates to the Drude value $\rho(t \rightarrow 0) \sim \rho_{\text{Drude}}$. In Eq. (1.4), the parameters \mathcal{S} and \mathcal{G}_{AA} are dimensionless and order-one. The slope $\mathcal{S} \sim \pi J/2$ for $J \gtrsim 1$. The AA coefficient \mathcal{G}_{AA} becomes particularly simple in the limit of a static boson [$\alpha \rightarrow 0$ in Eq. (1.1)] and Fermi-liquid self-energy [$\bar{g}^2 = 0$ in Eq. (1.3)]. In that case,

\mathcal{G}_{AA} is a logarithmic function of $D\alpha_m$, independent of N and temperature. (This is the usual 2D AA logarithm [20, 21], automatically cut off here because we retain the irrelevant squared-momentum of the boson). In the general case of dynamical bosons and MFL fermions, \mathcal{G}_{AA} acquires weak temperature dependence, but remains order one for $D\alpha \gtrsim 1$ and $D\alpha_m \gtrsim 1$, see Sec. VIID and Figs. 15–17 for details.

The strong temperature dependence of the AA correction in Eq. (1.4) results directly from the thermal mass of the mediating virtual quantum-relaxational boson [Eqs. (1.1) and (1.2)]. By contrast, in the usual Fermi liquid case [46, 47, 52], one typically assumes short-ranged spin-exchange interactions; these give rise to a spin-triplet diffuson hydrodynamic mode that is prevented by the SU(2) Ward identity from acquiring a thermal mass. The form in Eq. (1.4) neglects the effects of dynamical screening, which only play an important role at low temperatures $t \lesssim \bar{g}^2/N$. In the $t \rightarrow 0$ limit, $1/t$ is replaced by $\log^2(t)$, analogous to that of the zero-bias anomaly in disordered metals [21, 53].

We emphasize that the AA correction arises here due to the fact that SU(N) symmetry is *preserved in every realization of disorder*, and therefore flavor polarization forms a slow hydrodynamic mode that survives on time and length scales larger than those set by the impurity scattering. Technically, this manifests through SU(N) flavor degrees of freedom that appear in the matrix field of the sigma model. If instead we were to include random flavor-dependent Yukawa couplings (as in SYK-type models [16, 32–38]), the SU(N) mode and associated AA correction would be suppressed by the interflavor-impurity scattering rate [40, 44, 47, 54, 55].

The overall resistivity $\rho(t)$ [Eq. (1.4)] is plotted in Fig. 1 for different values of the dimensionless parameters \bar{g}^2 and $\bar{\rho}\mathcal{G}_{AA}$. Without the AA correction, the resistivity increases linearly with temperature, as expected from the MFL phenomenology [1]. It saturates at the Drude resistivity ρ_{Drude} instead of zero at $T = 0$ due to impurity scattering [38]. However, with the AA correction, $\rho(t)$ is instead driven all the way towards zero as $t \rightarrow 0$. Interestingly, the AA correction effectively shifts the resistivity curve downward and thus continues the MFL phenomenology to very low temperatures $t \ll 1$. Our work therefore suggests that the combined effects of forces mediated by quantum-relaxational bosons and spatial quantum coherence in the particle-hole channel can induce strange metal behavior, offering a possible microscopic origin for MFL phenomenology.

B. A brief survey of strange-metal theory

There have been a number of theoretical frameworks proposed to understand strange-metal behavior. In the cuprates, an early attempt was to employ MFL phenomenology in which quasiparticles are only marginally defined [1]. However, the underlying microscopic origin

remains unclear, despite recent developments (see e.g. Refs. [34, 36, 38]). On the other hand, it has been suspected that the strange-metal physics is associated with an underlying QCP [56, 57]. Models with N flavors of fermions coupled to quantum-critical bosons, which represent critical order-parameter fields, have been extensively studied in the large- N limit and are known to result in a critical Fermi surface without well-defined quasiparticles (see e.g. Refs. [26, 58–72] for recent developments). Lee [67] showed that these models cannot however be controlled by large- N and remain strongly coupled in 2D, due to an extra enhancement factor of N in higher-loop diagrams. An alternative approach is to consider the matrix large- N limit, in which N fermion flavors are coupled to $N \times N$ matrix bosons, as recently proposed by Damia *et al.* [39] and employed in this work. It was shown that this model yields a tractable large- N limit and gives the same non-analytical form of self-energies as in the vector-boson model. Nevertheless, a fully quantum treatment of the transport properties in these models remains elusive given the complication in satisfying the Ward identity [73, 74]. Linear- T resistivity has been observed in quantum Monte Carlo simulations of an fermions undergoing an Ising-nematic transition [75].

Another playground for exploring systems without quasiparticles is offered by the Sachdev-Ye-Kitaev (SYK) class of models [16, 32–38, 76–82]. The SYK model is an exactly solvable (0+1) dimensional model involving a large number of fermions coupled via randomized all-to-all interactions [77, 79]. Upon averaging over the randomness, the system exhibits a number of appealing features, such as emergent conformal invariance and NFL behavior. In particular, transport properties have been investigated in higher-dimensional generalizations of the SYK model [15, 16, 32, 78, 80]. For example, linear- T resistivity and anomalous Lorenz number are obtained in lattice models of SYK quantum dots with random intersite hopping [32]. Translationally invariant versions of the lattice model have also been considered and found to display local quantum critically and MFL behaviors in a certain temperature range [36].

The idea of systematically controlling models of strongly correlated systems with random interaction couplings has ignited new theories for realizing linear- T resistivity by revisiting more conventional physical systems [33–35, 37, 38, 41]. In Refs. [34, 38], a model with a critical Fermi surface with random Yukawa-like couplings was constructed. Specifically, when the couplings are random in both flavor and position space, the system demonstrates Planckian transport. On the other hand, in Ref. [35], an effective theory of heavy fermions with random couplings in the flavor space near the critical point was studied and found to realize robust MFL behavior at the strong-coupling metallic fixed point. Pairing instabilities in these kinds of models have also been explored recently [33–35, 37]. Since these models often assume Gaussian distributed random flavor couplings with zero mean, consensus on the applicability of them to real ma-

materials is yet to be reached. Nevertheless, they successfully capture some signatures of the strange metal phase.

Recently a model-independent theory for the origin of strange metals was proposed [83]. It was shown that linear- T resistivity down to zero temperature in a clean and translationally invariant metal requires a divergent susceptibility for an observable that is odd under inversion/time reversal symmetries, and has zero crystal momentum.

C. Disordered, interacting Fermi liquids

The long-standing problem of disordered and interacting electrons in Fermi liquids has been well-studied over the past 4 decades [17, 43, 44, 47, 48]. Both electron-electron interactions and quenched disorder can be crucial in describing low-temperature metal-insulator transitions (MITs). The effect of interactions is nontrivial, contributing both indirectly and directly to quantum corrections to the dc electrical conductivity. Interactions dephase pure quantum interference corrections such as weak (anti)localization (WL, WAL), and separately induce additional AA corrections (logarithmic in 2D). An AA correction can appear with sign opposite to that of WL or WAL, and can therefore alter the localization physics relative to the single-particle problem [17, 21, 22, 53, 84]. Disorder can also enhance interaction matrix elements, through the combination of wave-function multifractality and Chalker scaling [27–30, 85, 86], and this can induce or augment interaction-driven instabilities relative to the clean Fermi liquid [47, 48, 54, 55].

In experiments, a MIT was observed in semiconductor inversion layers [87], challenging the conventional view from the noninteracting picture that all states localize in 2D. Theoretically analyzing systems with both interactions and disorder in a controlled manner is typically challenging. The standard tool for summing quantum corrections to transport that can incorporate all of the aforementioned effects of interactions is the Finkel’stein nonlinear sigma model [44, 46–48, 54, 55]. This enabled a scaling theory for the MIT with interactions, using the renormalization group. In work designed to address the 2D MIT, the sigma model was combined with a large- N analysis in order to cope with a potential magnetic instability [52, 88].

The problem studied in this paper of fermions with a Fermi surface, interacting through critical collective modes in 2D and subject to quenched disorder, has recently attracted significant attention [34, 38, 40, 89, 90]. Unlike the Fermi liquid case, in which the interactions are dynamically screened and thus effectively short-ranged, interactions mediated by critical bosons are manifestly long-ranged in proximity to the QCP. In particular, the stability of the zero-temperature conducting phase of the model studied in this paper was addressed in Ref. [40], where a modified sigma model incorporating true non-

Fermi liquid exponents was considered. Our focus here is instead on finite-temperature physics that gives rise to the MFL phenomenology discussed above in Sec. I A.

D. Technical approach of this work

We employ the G - Σ - D -II formalism [36, 77] to derive a set of saddle-point equations governing the Green’s functions and self-energies for large N , incorporating both disorder and interactions on the same footing. The saddle point solutions yield the quantum-relaxational propagator for the bosons and the MFL self-energy for the fermions in Eqs. (1.1) and (1.3), above.

We then examine fluctuations around the saddle points to derive the Finkel’stein nonlinear sigma model (FNLsM) — a field theory describing a system of interacting diffusons. We restrict our attention in this paper to the particle-hole channel, formally assuming unitary (class A [18]) symmetry, as in Refs. [40, 46]. The derivation is carried out in the Keldysh framework [43, 44, 46, 91–96], which naturally avoids the subtlety of analytical continuation from imaginary time and allows extension to explore dephasing [44, 97–99] and nonequilibrium phenomena [43, 44, 91].

Armed with this powerful analytical tool, we evaluate the density (linear) response function and demonstrate how the Ward identity for particle conservation can be satisfied at both semiclassical and quantum levels. We assume that the bosons are at thermal equilibrium and therefore neglect their kinetics. Satisfying the Ward identity in this system is a nontrivial task because of the anomalous diffuson propagator that originates from the MFL self-energy. We show that it is necessary to incorporate a new term in the sigma model action, describing the interaction ladder [49, 50], which is absent in ordinary Fermi liquid case [43, 44, 46, 91]. This term introduces new vertex corrections for the Feynman diagrams contributing to the density response, necessary to ensure particle conservation.

We derive the lowest-order quantum AA correction, taking into account various vertex corrections and the effects of the boson thermal mass [Eq. (1.2)] and dynamical screening. Upon summing over all Feynman diagrams to leading order in the dimensionless Drude resistivity per channel $\bar{\rho}$ and $1/N$, we recover particle conservation. The final formula for the AA correction is relatively simple and can be reduced to the one for disordered metals in an appropriate limit [22, 43, 53, 84], see Sec. VII D.

E. Outline

The rest of the paper is organized as follows. In Sec. II, we present the ingredients of our model and our convention for the Keldysh path integral. We then introduce disorder and perform disorder averaging in Sec. III, and

we derive a set of saddle-point equations for the self-energies in Sec. IV. In Sec. V, we consider the effects of fluctuations around the saddle point and derive the FNLsM. Using the FNLsM, we compute the semiclassical result and the AA correction to the density response function in Secs. VI and VII, respectively. Finally, we discuss and conclude our results in Sec. VIII. Various technical details are relegated to the appendices.

II. THE MODEL

We consider a system of fermions ψ at finite density with N flavors coupled to critical $SU(N)$ matrix bosons

$\hat{\phi}$. For simplicity, we assume time-reversal symmetry is broken so that the system belongs to unitary class A according to the ten-fold classification scheme [100–102], as in the early seminal work by Finkel’stein [46]. We study this system using the finite-temperature Keldysh formalism [43, 44, 95, 103–106]. In the presence of external source field V , the generating function for the closed Keldysh contour going from $t = -\infty$ to $t = \infty$ and then back to $t = -\infty$ is given by

$$Z[V] = \int \mathcal{D}\bar{\psi} \mathcal{D}\psi \mathcal{D}\hat{\phi} \exp \left\{ i \int_{\omega, \mathbf{x}, \mathbf{x}'} \bar{\psi}_i^a(\omega, \mathbf{x}) G_{0,ab}^{-1}(\omega; \mathbf{x}, \mathbf{x}') \psi_i^b(\omega, \mathbf{x}') + i \frac{1}{2} \int_{t, \mathbf{x}} \phi_{ij}^a(t, \mathbf{x}) [(i\partial_t)^2 + c^2 \partial_x^2] \phi_{ji}^a(t, \mathbf{x}) \tau_{a,a}^3 \right. \\ \left. + i \frac{g}{\sqrt{N}} \int_{t, \mathbf{x}} \tau_{a,a}^3 \phi_{jk}^a(t, \mathbf{x}) \bar{\psi}_j^a(t, \mathbf{x}) \psi_k^a(t, \mathbf{x}) - i \frac{\lambda_\phi}{2N^2} \int_{t, \mathbf{x}} [\phi_{ij}^a(t, \mathbf{x}) \phi_{ji}^a(t, \mathbf{x})]^2 \tau_{a,a}^3 \right. \\ \left. - i \int_{t, \mathbf{x}} \frac{1}{\sqrt{N}} u(\mathbf{x}) \bar{\psi}_i^a(t, \mathbf{x}) \psi_i^a(t, \mathbf{x}) \tau_{a,a}^3 - i \int_{t, \mathbf{x}} V^a(t, \mathbf{x}) \bar{\psi}^a(t, \mathbf{x}) \psi^a(t, \mathbf{x}) \tau_{a,a}^3 \right\}, \quad (2.1)$$

where c is the speed of the bosons, g is the “Yukawa” coupling constant, λ_ϕ is the coupling constant for quartic boson-boson interactions, and $u(\mathbf{x})$ is the onsite impurity potential. Meanwhile, $i = 1, 2, \dots, N$ is the $SU(N)$ flavor index, $a = 1, 2$ (which corresponds to forward or backward time-ordering) is the Keldysh label, and τ^a are the Pauli matrices acting in the Keldysh space. We also introduced the shorthand $\int_{t, \mathbf{x}} = \int dt \int d^2\mathbf{x}$. Throughout this paper, summation over repeated indices is assumed unless otherwise specified and we work with the unit $\hbar = k_B = c = 1$, where \hbar is the Planck constant and k_B is the Boltzmann constant. The fermionic field ψ_i^a transforms in the defining representation of $SU(N)$, while the matrix bosonic field $\hat{\phi} \rightarrow \phi_{ij}^a$ transforms in the adjoint representation. The quartic bosonic interaction is symmetry-allowed and analogous to the biquadratic spin-spin interaction $\sim (\mathbf{S}_{\text{site } A} \cdot \mathbf{S}_{\text{site } B})^2$ in lattice systems. The source field V is incorporated to facilitate the calculation of the density response function.

Our Keldysh conventions and approach mainly follow Refs. [44, 104, 105]. Detailed reviews on the Keldysh formalism can be found in (e.g.) Refs. [42, 43, 103].

The clean, non-interacting Green’s function for the fermions and bosons are respectively denoted by \hat{G}_0 and \hat{D}_0 . In the space-time basis, they are given respectively by

$$i\hat{G}_0(t, t'; \mathbf{x}, \mathbf{x}') = \begin{bmatrix} i\hat{G}_{0, \top} & i\hat{G}_{0, <} \\ i\hat{G}_{0, >} & i\hat{G}_{0, \bar{\top}} \end{bmatrix} = \begin{bmatrix} \langle \top \psi_i(\mathbf{x}, t) \bar{\psi}_i(\mathbf{x}', t') \rangle_0 & -\langle \bar{\psi}_i(\mathbf{x}', t') \psi_i(\mathbf{x}, t) \rangle_0 \\ \langle \psi_i(\mathbf{x}, t) \bar{\psi}_i(\mathbf{x}', t') \rangle_0 & \langle \bar{\top} \psi_i(\mathbf{x}, t) \bar{\psi}_i(\mathbf{x}', t') \rangle_0 \end{bmatrix}, \quad (2.2)$$

where i is not summed over, and

$$i\hat{D}_0(t, t'; \mathbf{x}, \mathbf{x}') = \begin{bmatrix} i\hat{D}_{0, \top} & i\hat{D}_{0, <} \\ i\hat{D}_{0, >} & i\hat{D}_{0, \bar{\top}} \end{bmatrix} = \begin{bmatrix} \langle \top \phi_{ij}(\mathbf{x}, t) \phi_{ji}(\mathbf{x}', t') \rangle_0 & \langle \phi_{ij}(\mathbf{x}', t') \phi_{ji}(\mathbf{x}, t) \rangle_0 \\ \langle \phi_{ij}(\mathbf{x}, t) \phi_{ji}(\mathbf{x}', t') \rangle_0 & \langle \bar{\top} \phi_{ij}(\mathbf{x}, t) \phi_{ji}(\mathbf{x}', t') \rangle_0 \end{bmatrix}, \quad (2.3)$$

where i, j are not summed. The symbol \top ($\bar{\top}$) denotes the time-ordering (anti-time-ordering) operator.

We now decouple the quartic bosonic interaction with the Hubbard-Stratonovich (H.S.) fields $X_{1,2}$ and express

$$e^{-i \frac{\lambda_\phi}{2N^2} \int_{t, \mathbf{x}} \tau_{a,a}^3 [\phi_{ij}^a(t, \mathbf{x}) \phi_{ji}^a(t, \mathbf{x})]^2} = \int \mathcal{D}X e^{-\int_{t, \mathbf{x}} \left\{ \frac{N^2}{2\tau\lambda_\phi} (X_1^2 + X_2^2) + i\text{Tr}[(\hat{\phi}^1)^2]X_1 + \text{Tr}[(\hat{\phi}^2)^2]X_2 \right\}}, \quad (2.4)$$

where $\int \mathcal{D}X = \int \mathcal{D}X_1 \mathcal{D}X_2$. We further introduce the classical component V_{cl} and quantum component V_{q} of

the external scalar potential. They are related to the

forward (backward) component V_1 (V_2) by

$$V_{\text{cl}} = \frac{1}{2}(V_1 + V_2), \quad V_{\text{q}} = \frac{1}{2}(V_1 - V_2). \quad (2.5)$$

The coupling between the density and the external potential [the last term in the exponent of Eq. (2.1)] can then be written as

$$-i \int_{t,\mathbf{x}} [V^{\text{cl}} \bar{\psi}_i \hat{\tau}^3 \psi_i + V^{\text{q}} \bar{\psi}_i \psi_i]. \quad (2.6)$$

Similarly, we introduce

$$\hat{\phi}^{\text{cl}} = \frac{1}{2}(\hat{\phi}^1 + \hat{\phi}^2), \quad \hat{\phi}^{\text{q}} = \frac{1}{2}(\hat{\phi}^1 - \hat{\phi}^2), \quad (2.7)$$

so that the free bosonic action [second term in the exponent of Eq. (2.1)] becomes

$$\begin{aligned} & \frac{i}{2} \int_{t,\mathbf{x}} \phi_{ij}^\alpha [D_0^{-1}]^{\alpha\beta} \phi_{ji}^\beta \\ & \equiv \frac{i}{2} \int_{t,\mathbf{x}} \begin{bmatrix} \phi_{ij}^{\text{cl}} & \phi_{ij}^{\text{q}} \end{bmatrix} \begin{bmatrix} 0 & (D_0^{\text{A}})^{-1} \\ (D_0^{\text{R}})^{-1} & (D_0^{\text{K}})^{-1} \end{bmatrix} \begin{bmatrix} \phi_{ji}^{\text{cl}} \\ \phi_{ji}^{\text{q}} \end{bmatrix}, \end{aligned} \quad (2.8)$$

where the retarded (R), advanced (A) and Keldysh (K) components of the bosonic propagator respectively take the following form in Fourier space

$$D_0^{R/A}(\Omega, \mathbf{q}) = \frac{1}{2} \frac{1}{(\Omega \pm i\eta)^2 - \mathbf{q}^2}, \quad (2.9)$$

$$D_0^K(\Omega, \mathbf{q}) = [D_0^R(\Omega, \mathbf{q}) - D_0^A(\Omega, \mathbf{q})] F_B(\Omega), \quad (2.10)$$

where $\eta \rightarrow 0^+$ and $F_B(\varepsilon) = \coth(\varepsilon/2T)$ is the generalized Bose distribution function at temperature T . By defining

$$\tilde{X}_1 = X_1 - iX_2, \quad \tilde{X}_2 = X_1 + iX_2, \quad (2.11)$$

Eq. (2.4) can be rewritten as

$$\begin{aligned} & e^{-i \frac{\lambda_\phi}{2N^2} \int_{t,\mathbf{x}} \tau_{a,a}^3 \phi_{ij}^a(t,\mathbf{x}) \phi_{ji}^a(t,\mathbf{x})} \\ & = \int \mathcal{D}\tilde{X} \exp \left\{ \begin{aligned} & -i \int_{t,\mathbf{x}} \begin{bmatrix} \phi_{ij}^{\text{cl}} & \phi_{ij}^{\text{q}} \end{bmatrix} \begin{bmatrix} \tilde{X}_1 & \tilde{X}_2 \\ \tilde{X}_2 & \tilde{X}_1 \end{bmatrix} \begin{bmatrix} \phi_{ji}^{\text{cl}} \\ \phi_{ji}^{\text{q}} \end{bmatrix} \\ & - \int_{t,\mathbf{x}} \frac{N^2}{2i\lambda_\phi} (\tilde{X}_1 \tilde{X}_2) \end{aligned} \right\}, \end{aligned} \quad (2.12)$$

where $\int \mathcal{D}\tilde{X} = \int \mathcal{D}\tilde{X}_1 \mathcal{D}\tilde{X}_2$.

For the fermions, we switch to the physical representation via the following non-unitary transformation

$$\psi \rightarrow \hat{\tau}^3 \hat{U}_{\text{LO}} \psi, \quad \bar{\psi} \rightarrow \bar{\psi} \hat{U}_{\text{LO}}^\dagger, \quad (2.13)$$

where

$$\hat{U}_{\text{LO}} = \frac{1}{\sqrt{2}}(1 + i\hat{\tau}^2). \quad (2.14)$$

The fermionic Green's function then turns into

$$\hat{G}_0 \rightarrow \hat{U}_{\text{LO}}^\dagger \hat{\tau}^3 \hat{G}_0 \hat{U}_{\text{LO}} = \begin{bmatrix} G_0^{\text{R}} & G_0^{\text{K}} \\ 0 & G_0^{\text{A}} \end{bmatrix}_\tau, \quad (2.15)$$

where the retarded (R), advanced (A) and Keldysh (K) components are respectively given by

$$G_0^{R/A}(\omega, \mathbf{k}) = \frac{1}{\omega \pm i\eta - \tilde{\varepsilon}_{\mathbf{k}}}, \quad (2.16)$$

$$G_0^K(\omega, \mathbf{k}) = [G_0^R(\omega, \mathbf{k}) - G_0^A(\omega, \mathbf{k})] F(\omega), \quad (2.17)$$

$$\tilde{\varepsilon}_{\mathbf{k}} = \frac{\mathbf{k}^2}{2m} - \mu. \quad (2.18)$$

Here, m is the mass of fermions, μ is the chemical potential, and $F(\omega) = \tanh(\omega/2T)$ is the generalized Fermi distribution function at temperature T . The subscript τ indicates that the matrix is expressed in the Keldysh space. We further perform a thermal rotation

$$\psi \rightarrow \hat{M}_F \psi, \quad \bar{\psi} \rightarrow \bar{\psi} \hat{M}_F, \quad (2.19)$$

where

$$\hat{M}_F(\hat{\omega}) = \begin{bmatrix} 1 & F(\hat{\omega}) \\ 0 & -1 \end{bmatrix}_\tau = \hat{M}_F^{-1}(\hat{\omega}). \quad (2.20)$$

Under this transformation, the fermionic Green's function acquires a diagonal form

$$\hat{G}_0 \rightarrow \begin{bmatrix} G_0^{\text{R}} & 0 \\ 0 & G_0^{\text{A}} \end{bmatrix}_\tau, \quad (2.21)$$

which is convenient for subsequent analysis.

After the above transformations, the partition function and action can be expressed as

$$Z = \int \mathcal{D}\bar{\psi} \mathcal{D}\psi \mathcal{D}\hat{\phi} \mathcal{D}\tilde{X} e^{-S}, \quad (2.22)$$

$$S = S_\psi + S_\phi + S_{\psi\phi} + S_{\phi X} + S_{\psi V} + S_{\text{dis}} + S_X, \quad (2.23)$$

where

$$S_\psi = -i \int_{\omega, \mathbf{k}} \bar{\psi}_i(\omega, \mathbf{k}) \hat{G}_0^{-1}(\omega, \mathbf{k}) \psi_i(\omega, \mathbf{k}), \quad (2.24)$$

$$S_\phi = -\frac{i}{2} \int_{\Omega, \mathbf{q}} \text{Tr} [\hat{\phi}(\Omega, \mathbf{q}) \hat{D}_0^{-1}(\Omega, \mathbf{q}) \hat{\phi}(-\Omega, -\mathbf{q})], \quad (2.25)$$

$$S_{\psi\phi} = -i \frac{g}{\sqrt{N}} \int_{\omega, \omega', \mathbf{x}} \bar{\psi}_i(\omega, \mathbf{x}) \hat{\Phi}_{ij}(\omega, \omega', \mathbf{x}) \psi_j(\omega', \mathbf{x}), \quad (2.26)$$

$$S_{\phi X} = i \int_{t, \mathbf{x}} \text{Tr} \left\{ \hat{\phi}(t, \mathbf{x}) \left[\tilde{X}_1(t, \mathbf{x}) + \tilde{X}_2(t, \mathbf{x}) \hat{\tau}^1 \right] \hat{\phi}(t, \mathbf{x}) \right\}, \quad \text{shorthand notations} \quad (2.27)$$

$$\hat{\mathcal{V}}(\omega, \omega', \mathbf{x}) = \sum_{s=\text{cl}, \mathbf{q}} \hat{\gamma}_{\omega, \omega'}^s V_{\omega - \omega'}^s(\mathbf{x}), \quad (2.31)$$

$$S_{\psi V} = i \int_{\omega, \omega', \mathbf{x}} \bar{\psi}_i(\omega, \mathbf{x}) \hat{\mathcal{V}}(\omega, \omega', \mathbf{x}) \psi_i(\omega', \mathbf{x}), \quad (2.28)$$

$$\hat{\Phi}_{ij}(\omega, \omega', \mathbf{x}) = \sum_{s=\text{cl}, \mathbf{q}} \hat{\gamma}_{\omega, \omega'}^s \phi_{ij, \omega - \omega'}^s(\mathbf{x}), \quad (2.32)$$

$$S_{\text{dis}} = i \int_{t, \mathbf{x}} \frac{1}{\sqrt{N}} u(\mathbf{x}) \bar{\psi}_i(t, \mathbf{x}) \psi_i(t, \mathbf{x}), \quad (2.29) \quad \text{with}$$

$$\hat{\gamma}_{\omega, \omega'}^{\text{cl}} = \hat{M}_F(\omega) \hat{M}_F(\omega'), \quad \hat{\gamma}_{\omega, \omega'}^{\mathbf{q}} = \hat{M}_F(\omega) \hat{\tau}^1 \hat{M}_F(\omega'). \quad (2.33)$$

$$S_X = \int_{t, \mathbf{x}} \frac{N^2}{2i\lambda_\phi} \tilde{X}_1(t, \mathbf{x}) \tilde{X}_2(t, \mathbf{x}), \quad (2.30)$$

and where $\int_\omega = \int \frac{d\omega}{2\pi}$, $\int_{\mathbf{k}} = \int \frac{d^2\mathbf{k}}{(2\pi)^2}$. Here, we defined the

Now the fermion distribution function appears only in the coupling matrices $\hat{\gamma}_{\omega, \omega'}$. This convention allows a clear separation between purely virtual quantum-interference modes on one hand, and on the other hydrodynamic fluctuations of conserved currents [44].

III. DISORDER AVERAGING

Assume the impurity potential $u(\mathbf{x})$ is described by a Gaussian distribution function $P[u]$ given by

$$P[u] = e^{-\pi\nu_0\tau_{\text{el}} \int_{\mathbf{x}} u^2(\mathbf{x})}, \quad (3.1)$$

where τ_{el} is the elastic scattering time due to impurities. We perform disorder averaging by integrating out the potential $u(\mathbf{x})$

$$\begin{aligned} \int \mathcal{D}u P[u] e^{-S_{\text{dis}}} &= \int \mathcal{D}u e^{-\pi\nu_0\tau_{\text{el}} \int_{\mathbf{x}} u^2(\mathbf{x})} e^{i \int_{t, \mathbf{x}} \frac{1}{\sqrt{N}} u(\mathbf{x}) \bar{\psi}_i^a(t, \mathbf{x}) \psi_i^a(t, \mathbf{x})} = e^{\frac{1}{4N\pi\nu_0\tau_{\text{el}}} \int_{t, t', \mathbf{x}} \bar{\psi}_i^a(t, \mathbf{x}) \psi_j^b(t', \mathbf{x}) \bar{\psi}_j^b(t', \mathbf{x}) \psi_i^a(t, \mathbf{x})} \\ &= \int \mathcal{D}\hat{q} e^{-\frac{\pi\nu_0}{4\tau_{\text{el}}N} \int_{\mathbf{x}} \text{Tr} [\hat{q}^2(\mathbf{x})] - \frac{1}{2\tau_{\text{el}}N} \int_{t, t', \mathbf{x}} q_{ij; tt'}^{ab}(\mathbf{x}) \bar{\psi}_i^a(t, \mathbf{x}) \psi_j^b(t', \mathbf{x})}. \end{aligned} \quad (3.2)$$

In the last step, we decoupled the disordered induced four-fermion interaction using the H.S. field, $\hat{q}(\mathbf{x}) \rightarrow q_{ij; tt'}^{ab}(\mathbf{x})$, which is a Hermitian matrix containing time indices t, t' , flavor indices i, j , and Keldysh indices a, b . In this work, we focus on the unitary class A in which time-reversal symmetry (TRS) is broken (e.g. by a weak external magnetic field), so that the Cooperon contribution to transport is suppressed [43, 44]. Hence, we restrict our attention to the particle-hole channel in the above decoupling. We note, however, that restoring TRS is essential for exploring the interplay of dephasing and weak localization [17, 43, 44], as well as pairing instabilities to superconductivity. We leave these for a separate study.

IV. BILOCAL FIELD FORMULATION

In this section, we derive a set of saddle-point equations governing fermionic and bosonic self-energies arising due to disorder and interactions in the large- N limit. Analogous to the treatment for the SYK model [36, 77], we introduce the bilocal auxiliary fields \hat{G} and \hat{D} defined by

$$G_{ij}^{ab}(x', x) = -i\psi_i^a(x') \bar{\psi}_j^b(x), \quad (4.1)$$

$$D^{ss'}(x', x) = -\frac{i}{N^2} \sum_{ij} \phi_{ji}^s(x') \phi_{ij}^{s'}(x), \quad (4.2)$$

where $x = (t, \mathbf{x})$, $a, b \in \{R, A\}$ (retarded, advanced) are fermion Keldysh indices, and $s, s' \in \{\text{cl}, \mathbf{q}\}$ (classical, quantum) are boson Keldysh indices. [Recall that the bare fermion Green's function is diagonal after the transformation in Eq. (2.19), possessing only retarded and advanced nonzero components, Eq. (2.21)]. We impose the constraints in

Eqs. (4.1) and (4.2) using the identities

$$1 = \int \mathcal{D}\hat{G} \delta [G_{ji}^{ba}(x', x) - i\bar{\psi}_i^a(x)\psi_j^b(x')] = \int \mathcal{D}\hat{G} \mathcal{D}\hat{\Sigma} e^{\sum_{ij} \int_{x, x'} \Sigma_{ij}^{ab}(x, x') [G_{ji}^{ba}(x', x) - i\bar{\psi}_i^a(x)\psi_j^b(x')]}, \quad (4.3)$$

$$1 = \int \mathcal{D}\hat{D} \delta \left[D^{s's}(x', x) + \frac{i}{N^2} \sum_{ij} \phi_{ij}^s(x) \phi_{ji}^{s'}(x') \right] = \int \mathcal{D}\hat{D} \mathcal{D}\hat{\Pi} e^{-\frac{1}{2} \int_{x, x'} \Pi^{ss'}(x, x') \left[N^2 D^{s's}(x', x) + i \sum_{ij} \phi_{ij}^s(x) \phi_{ji}^{s'}(x') \right]}. \quad (4.4)$$

Physically, the Lagrange multipliers $\hat{\Sigma}$ and $\hat{\Pi}$ describe respectively the fermionic and bosonic self-energies due to the Yukawa interaction.

Upon integrating out the fermions and bosons, we obtain the following disorder-averaged large- N partition function for the \hat{q} matrix field (bilocal in time, but local in position), the boson-boson interaction-mediating Hubbard-Stratonovich field \tilde{X} , and the spacetime bilocal fields \hat{G} , $\hat{\Sigma}$, \hat{D} , and $\hat{\Pi}$:

$$Z = \int \mathcal{D}\hat{q} \mathcal{D}\tilde{X} \mathcal{D}\hat{G} \mathcal{D}\hat{\Sigma} \mathcal{D}\hat{D} \mathcal{D}\hat{\Pi} e^{-S}, \quad (4.5)$$

where the effective action is

$$\begin{aligned} S = & \frac{N^2}{2} \text{Tr} \ln \left(\hat{D}_0^{-1} - \hat{\Pi} - 2\tilde{X}_1 - 2\tilde{X}_2 \hat{\tau}^1 \right) - \text{Tr} \ln \left(\hat{G}_0^{-1} - \hat{V} - \hat{\Sigma} + \frac{i}{2\tau_{\text{el}} N} \hat{q} \right) - \text{Tr} [\hat{\Sigma} \hat{G}] + \frac{N^2}{2} \text{Tr} [\hat{\Pi} \hat{D}] \\ & + i \frac{g^2}{2N} \int_{\omega_1, \omega_2, \omega_3, \omega_4, \mathbf{x}, \mathbf{x}'} [\hat{\gamma}_{\omega_1, \omega_2}^s]^{ab} [\hat{\gamma}_{\omega_3, \omega_4}^{s'}]^{cd} G_{jj}^{bc}(\omega_2, \mathbf{x}; \omega_3, \mathbf{x}') G_{ii}^{da}(\omega_4, \mathbf{x}'; \omega_1, \mathbf{x}) D^{ss'}(\omega_1 - \omega_2, \mathbf{x}; \omega_3 - \omega_4, \mathbf{x}') \\ & + \frac{\pi\nu_0}{4\tau_{\text{el}} N} \int_{\mathbf{x}} \text{Tr} [\hat{q}(\mathbf{x})^2] + \int_{t, \mathbf{x}} \frac{N^2}{2i\lambda_\phi} \tilde{X}_1(t, \mathbf{x}) \tilde{X}_2(t, \mathbf{x}). \end{aligned} \quad (4.6)$$

In the second last line, we performed a second-order cumulant expansion to write

$$\begin{aligned} & e^{i \frac{g}{\sqrt{N}} \int_{\omega, \omega', \mathbf{x}} \bar{\psi}_i(\omega, \mathbf{x}) \hat{\Phi}_{ij}(\mathbf{x}, \omega, \omega') \psi_j(\omega', \mathbf{x})} \\ \rightarrow & e^{-i \frac{g^2}{2N} \int_{\omega_1, \omega_2, \omega_3, \omega_4, \mathbf{x}, \mathbf{x}'} [\hat{\gamma}_{\omega_1, \omega_2}^s]^{ab} [\hat{\gamma}_{\omega_3, \omega_4}^{s'}]^{cd} (-i) \psi_j^b(\omega_2, \mathbf{x}) \bar{\psi}_i^c(\omega_3, \mathbf{x}') (-i) \psi_m^d(\omega_4, \mathbf{x}') \bar{\psi}_i^a(\omega_1, \mathbf{x}) (-i) \phi_{ij}^s(\omega_1 - \omega_2, \mathbf{x}) \phi_{im}^{s'}(\omega_3 - \omega_4, \mathbf{x}')} \\ = & e^{-i \frac{g^2}{2N} \int_{\omega_1, \omega_2, \omega_3, \omega_4, \mathbf{x}, \mathbf{x}'} [\hat{\gamma}_{\omega_1, \omega_2}^s]^{ab} [\hat{\gamma}_{\omega_3, \omega_4}^{s'}]^{cd} G_{jj}^{bc}(\omega_2, \mathbf{x}; \omega_3, \mathbf{x}') G_{ii}^{da}(\omega_4, \mathbf{x}'; \omega_1, \mathbf{x}) D^{ss'}(\omega_1 - \omega_2, \mathbf{x}; \omega_3 - \omega_4, \mathbf{x}')}, \end{aligned} \quad (4.7)$$

where we used the definitions in Eqs. (4.1) and (4.2) in the last step.

A. Saddle-point equations

We now look for spacetime-translationally invariant and flavor-space $\text{SU}(N)$ -invariant saddle-point solutions. In particular, we let the saddle points of \hat{G} and $\hat{\Sigma}$ to be respectively $\hat{G}_{\text{sp}} \otimes \hat{1}_{\text{SU}(N)}$ and $\hat{\Sigma}_{\text{sp}} \otimes \hat{1}_{\text{SU}(N)}$, where $\hat{1}_{\text{SU}(N)}$ is the identity matrix of size $N \times N$ in the flavor space. Also, we assume that the saddle points for \tilde{X}_1 , \tilde{X}_2 and \hat{q}_{sp} are spatially uniform and time-independent. Setting the external source fields $V^{\text{cl}}, V^{\text{q}}$ to zero and minimizing with respect to $\{\hat{\Sigma}, \hat{\Pi}, \hat{G}, \hat{D}, \tilde{X}_1, \tilde{X}_2, \hat{q}\}$, we obtain the following set of saddle-point equations:

$$\hat{G}_{\text{sp}}^{-1} = \hat{G}_0^{-1} - \hat{\Sigma}_{\text{sp}} + i\gamma_{\text{el}} \hat{q}_{\text{sp}}, \quad (4.8)$$

$$\hat{D}_{\text{sp}}^{-1} = \hat{D}_0^{-1} - \hat{\Pi}_{\text{sp}} - 2\tilde{X}_{1, \text{sp}} - 2\tilde{X}_{2, \text{sp}} \hat{\tau}^1, \quad (4.9)$$

$$\Sigma_{\text{sp}}^{ab}(\omega, \mathbf{k}) = ig^2 \int_{\Omega, \mathbf{q}} \left[\hat{\gamma}_{\omega, \Omega}^{s'} \hat{G}_{\text{sp}}(\Omega, \mathbf{q}) \hat{\gamma}_{\Omega, \omega}^s \right]^{ab} D_{\text{sp}}^{ss'}(\Omega - \omega, \mathbf{q} - \mathbf{k}), \quad (4.10)$$

$$\Pi_{\text{sp}}^{ss'}(\Omega, \mathbf{q}) = -i \frac{g^2}{N} \int_{\omega, \mathbf{k}} \text{Tr} \left[\hat{\gamma}_{\omega, \omega-\Omega}^{s'} \hat{G}_{\text{sp}}(\omega - \Omega, \mathbf{k}) \hat{\gamma}_{\omega-\Omega, \omega}^s \hat{G}_{\text{sp}}(\omega, \mathbf{k} + \mathbf{q}) \right], \quad (4.11)$$

$$\tilde{X}_{1, \text{sp}} = 2i\lambda_\phi \int_{\Omega, \mathbf{q}} \text{Tr} \left[\hat{D}_{\text{sp}}(\Omega, \mathbf{q}) \hat{\tau}^1 \right], \quad (4.12)$$

$$\tilde{X}_{2, \text{sp}} = 2i\lambda_\phi \int_{\Omega, \mathbf{q}} \text{Tr} \left[\hat{D}_{\text{sp}}(\Omega, \mathbf{q}) \right], \quad (4.13)$$

and

$$\hat{q}_{\text{sp}} = \frac{i}{\pi\nu_0} \int_{\mathbf{k}} \frac{1}{\hat{G}_0^{-1}(\omega, \mathbf{k}) - \hat{\Sigma}_{\text{sp}}(\omega, \mathbf{k}) + i\gamma_{\text{el}} \hat{q}_{\text{sp}}}. \quad (4.14)$$

Here, $x = (t, \mathbf{x})$, $a, b \in \{R, A\}$ and $s, s' \in \{\text{cl}, \mathbf{q}\}$ are Keldysh labels, and

$$\gamma_{\text{el}} \equiv \frac{1}{2N\tau_{\text{el}}} \quad (4.15)$$

is the elastic scattering rate for fermions in each flavor channel. Our approach automatically generates the Schwinger-Dyson equations for the self-energies $\hat{\Sigma}_{\text{sp}}$ and $\hat{\Pi}_{\text{sp}}$. Note that interaction-vertex corrections to the bosonic self-energy are absent due to large- N suppression. The last equation (4.14) means that disorder is treated under the self-consistent Born approximation at the saddle-point level.

The self-energies in Eqs. (4.10)–(4.14) are diagrammatically depicted in Fig. 2. We use straight, wavy and dotted lines to respectively represent fermionic, bosonic, and disorder propagators. The saddle-point propagators are denoted by bold lines. The advantage of the current approach is that disorder and interactions are treated under equal footing self-consistently. In the absence of disorder and boson self-interactions, the above set of equations agrees with the Schwinger-Dyson equations in Refs. [39, 40].

We now solve the saddle-point equations. For the \hat{q} matrix, we assume that the elastic scattering rate γ_{el} due to the disorder is the largest energy scale, relative to the other symmetry-breaking terms (the frequency ω or the fermion self-energy $\hat{\Sigma}_{\text{sp}}$). We find the following time-translational invariant and spatially homogeneous saddle point solution:

$$\hat{q}_{\text{sp}} = \hat{\tau}^3 \otimes \hat{1}_{\text{SU}(N)}. \quad (4.16)$$

The causality structure is consistent with the infinitesimal “ η prescription” in the clean, noninteracting fermionic Green’s function [Eq. (2.16)].

For the bosonic and fermionic self-energies generated by the Yukawa interaction [Eqs. (4.10) and (4.11)], their retarded component in Fourier space can be expressed

respectively as

$$\Pi_{\text{sp}}^R(\Omega, \mathbf{q}) = -i \frac{g^2}{N} \int_{\omega, \mathbf{k}} \left[G_{\text{sp}}^R(\omega + \Omega, \mathbf{k} + \mathbf{q}) G_{\text{sp}}^K(\omega, \mathbf{k}) + G_{\text{sp}}^K(\omega + \Omega, \mathbf{k} + \mathbf{q}) G_{\text{sp}}^A(\omega, \mathbf{k}) \right] \quad (4.17)$$

and

$$\Sigma_{\text{sp}}^R(\omega, \mathbf{k}) = ig^2 \int_{\Omega, \mathbf{q}} \left[D_{\text{sp}}^K(\Omega, \mathbf{q}) G_{\text{sp}}^R(\omega + \Omega, \mathbf{k} + \mathbf{q}) + D_{\text{sp}}^A(\Omega, \mathbf{q}) G_{\text{sp}}^K(\omega + \Omega, \mathbf{k} + \mathbf{q}) \right]. \quad (4.18)$$

By linearizing the dispersion of the fermions around the Fermi surface as $\tilde{\varepsilon}_{\mathbf{k}} \simeq v_F \delta k$, where $\delta \mathbf{k} = \mathbf{k} - \mathbf{k}_F$ and $v_F = k_F/m$ is the Fermi velocity, Eq. (4.17) can be written as

$$\begin{aligned} \Pi_{\text{sp}}^R(\Omega, \mathbf{q}) = & -i \frac{g^2}{N} \int_{-\infty}^{\infty} \frac{d\omega}{2\pi} \int_{-\infty}^{\infty} \frac{k_F d\delta k}{2\pi} \int_0^{2\pi} \frac{d\theta}{2\pi} \\ & \times \frac{1}{\tilde{\Sigma}_{\omega+\Omega}^R + i\gamma_{\text{el}} - v_F(\delta k + q \cos \theta)} \\ & \times \frac{1}{\tilde{\Sigma}_{\omega}^A - i\gamma_{\text{el}} - v_F \delta k} (F_{\omega+\Omega} - F_{\omega}), \end{aligned} \quad (4.19)$$

where $\tilde{\Sigma}_{\omega}^{R/A} = \omega - \Sigma_{\text{sp}}^{R/A}(\omega)$ and θ is the angle between \mathbf{k}_F and \mathbf{q} . We assumed for the fermionic self-energy $\Sigma_{\text{sp}}^R(\omega, \mathbf{k}) \simeq \Sigma_{\text{sp}}^R(\omega, \mathbf{k}_F) \equiv \Sigma_{\text{sp}, \omega}^R$. Throughout this work, we use $\Sigma_{\text{sp}, \omega}^R$ and $\Sigma_{\text{sp}}^R(\omega)$ interchangeably. Performing the momentum and angular integral, we have

$$\begin{aligned} \Pi_{\text{sp}}^R(\Omega, \mathbf{q}) = & -i \frac{mg^2}{2\pi N} \int_{-\infty}^{\infty} d\omega \\ & \times \frac{F_{\omega+\Omega} - F_{\omega}}{\sqrt{(v_F q)^2 - (\tilde{\Sigma}_{\omega+\Omega}^R - \tilde{\Sigma}_{\omega}^A + 2i\gamma_{\text{el}})^2}}. \end{aligned} \quad (4.20)$$

To leading order in $1/\gamma_{\text{el}}$, this evaluates to

$$\Pi_{\text{sp}}^R(\Omega, \mathbf{q}) \simeq -2i\alpha\Omega, \quad \alpha \equiv \frac{g^2\nu_0}{2N\gamma_{\text{el}}}, \quad (4.21)$$

where $\nu_0 = m/2\pi$ is the bare density of states per fermion flavor. The parameter α carries units of inverse diffusion constant, is independent of temperature, and gives rise to diffusive dynamics at zero-temperature for the quantum-critical bosons. In evaluating Eq. (4.21), we have neglected the fermion-fermion contribution to the boson mass m_b^2 [Eq. (1.1)], which is negative, proportional to ν_0 , and independent of temperature to leading order. We assume that the bosons are tuned to a zero-temperature QCP, with paramagnetic critical fluctuations at $T > 0$.

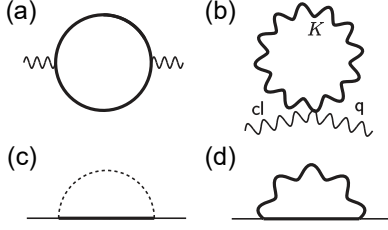


FIG. 2. Diagrams for the saddle-point solution to (a) the bosonic self-energy $\hat{\Pi}_{\text{sp}}$ due to the Yukawa interaction, (b) the bosonic thermal mass m_b^2 due to the quartic bosonic (\tilde{X} -mediated) interaction, (c) the q -matrix \hat{q}_{sp} , and (d) the fermionic self-energy $\hat{\Sigma}_{\text{sp}}$ due to the Yukawa interaction. Straight, wavy and dotted lines respectively represent fermions, bosons and disorder. The propagator lines in bold are fully dressed at the saddle-point level. Vertex corrections due to interactions are suppressed by $1/N$. In diagram (b), the symbol K labels the Keldysh component of the bosonic propagator, while cl and q label respectively the classical and quantum component of the external legs.

These generically induce a positive m_b^2 ; we consider an explicit calculation next.

We examine the saddle-point equations for $\tilde{X}_{1,2,\text{sp}}$ [Eqs. (4.12) and (4.13)]. Since $\tilde{X}_{1,\text{sp}}$ is proportional to an integral over purely retarded or advanced components of the bosonic propagator, it vanishes

$$\tilde{X}_{1,\text{sp}} = 0. \quad (4.22)$$

This is consistent with the Keldysh structure of \hat{D}_{sp} . For $\tilde{X}_{2,\text{sp}}$, we have

$$\tilde{X}_{2,\text{sp}} = 2i\lambda_\phi \int_{\Omega, \mathbf{q}} D_{\text{sp}}^K(\Omega, \mathbf{q}). \quad (4.23)$$

By performing the frequency Ω integral, followed by the

momentum \mathbf{q} integral as outlined in Appendix A, we find

$$\tilde{X}_{2,\text{sp}} \equiv m_b^2 = \alpha_m T, \quad (4.24)$$

where α_m is a constant depending on α and λ_ϕ . It can be determined by self-consistently solving Eq. (A6). In contrast to clean case, in which the thermal mass term is proportional to $T \ln T$ [45, 107], our leading result is not modified by the logarithm. The bosonic propagator at saddle-point level is then

$$D_{\text{sp}}^R(\Omega, \mathbf{q}) = -\frac{1}{2} \frac{1}{\mathbf{q}^2 + m_b^2 - i\alpha\Omega}. \quad (4.25)$$

Physically, m_b^2 represents the thermal mass induced by the quartic bosonic interaction. The Yukawa interaction mediated by the quantum-critical bosons is therefore screened at any finite temperature. The thermal mass m_b^2 serves as the phase relaxation rate for the bosons, crucial for describing the dynamics in the quantum relaxational regime [24–26]. The proportionality of the relaxation rate to T is not surprising, since it is the only relevant energy scale.

Compared to the zero-temperature bosonic self-energy in the clean limit [39, 40],

$$\Pi_{\text{clean}}^R(\Omega, \mathbf{q}) = M_D^2 \left(\frac{-i\Omega}{q} \right), \quad (4.26)$$

where the Landau damping scale $M_D^2 = \frac{1}{N} \frac{g^2 \nu_0}{v_F}$, the singularity $\sim \Omega/q$ at $q \rightarrow 0$ is neutralized, rendering the bosons diffusive in Eq. (4.25) [19]. In fact, this form of the bosonic propagator is quite generic and not unexpected—it is the simplest possible form allowed by symmetry in the quantum-relaxational regime, when non-analyticities are smeared out by disorder.

To evaluate the fermionic self-energy due to the Yukawa interaction, we feed Eq. (4.25) back to Eq. (4.18). By performing the momentum integral up to a cutoff q_{max} below which Eq. (4.21) is justified, we obtain

$$\Sigma_{\text{sp}}^R(\omega) = \frac{g^2}{(2\pi)^2 \gamma_{\text{el}}} \int_{-\infty}^{\infty} d\Omega \left\{ \frac{i}{2} \tan^{-1} \left(\frac{\alpha\Omega}{m_b^2} \right) \left[\tanh \left(\frac{\Omega + \omega}{2T} \right) - \coth \left(\frac{\Omega}{2T} \right) \right] - \frac{1}{4} \ln \left[\frac{q_{\text{max}}^4}{(\alpha\Omega)^2 + m_b^4} \right] \tanh \left(\frac{\Omega + \omega}{2T} \right) \right\}. \quad (4.27)$$

Using the expression for m_b^2 in Eq. (4.24), we find, up to logarithmic accuracy, that

$$\Sigma_{\text{sp}}^R(\omega) = -\bar{g}^2 \left[\omega \ln \left(\frac{\omega_c}{x} \right) + i \frac{\pi}{2} x \right], \quad (4.28)$$

$$x \equiv \max(|\omega|, JT),$$

which is the expression shown at the beginning [Eq. (1.3)]. Here $\bar{g}^2 = g^2/(4\pi^2 \gamma_{\text{el}})$ is the dimensionless square of the reduced Yukawa coupling and $\omega_c > 0$ is a cutoff below which the MFL form holds. The dimen-

sionless temperature coefficient J is determined by the thermal mass coefficient; it is expressed as the integral

$$J(A) = \frac{4}{\pi} \int_0^{\infty} dy \tan^{-1}(Ay) (\coth y - \tanh y), \quad (4.29)$$

where $A \equiv 2\alpha/\alpha_m$, with α and α_m respectively defined via Eqs. (4.21) and (4.24). A plot of J as a function of $2\alpha/\alpha_m$ is shown in Fig. 3; it has the asymptotic behav-

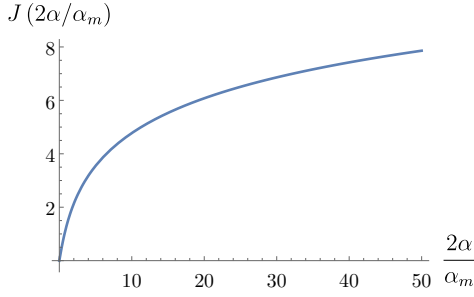


FIG. 3. Plot of the dimensionless coefficient J that determines the temperature dependence of the MFL fermion self-energy in Eq. (4.28). The integral defining J is given by Eq. (4.29); the argument $2\alpha/\alpha_m$ is the ratio of the inverse-diffusion constant [Eq. (4.21)] and the temperature coefficient of the thermal mass [Eq. (4.24)] for the quantum-relaxational bosons.

iors

$$J(A \rightarrow 0) \simeq \pi A/2, \quad J(A \rightarrow \infty) \simeq 2 \ln(A). \quad (4.30)$$

The form of Σ_{sp}^R in Eq. (4.28) is reminiscent of the fermionic self-energy in the MFL phenomenology developed for the cuprates [1]. Our calculations suggest the combined effect of disorder and interaction with critical collective modes serve as a possible origin for the MFL behavior. The expression for Σ_{sp}^R is in sharp contrast with the clean case, in which the fermionic self-energy acquires a NFL form [39, 40] as

$$\Sigma_{\text{clean}}^R(\omega) = -\frac{g^2}{2\pi\sqrt{3}v_F} \frac{1}{M_D^{2/3}} (-i\omega)^{2/3}. \quad (4.31)$$

The MFL form in Eq. (4.28) behaves in a less singular manner; this a physical consequence of disorder broadening.

More importantly, the temperature-dependence of the MFL self-energy in Eq. (4.28) is only stabilized for a nonzero bosonic thermal mass $\alpha_m > 0$ [Eq. (4.24)]. Eq. (4.30) shows that the temperature coefficient J diverges logarithmically in the limit $\alpha_m \rightarrow 0$.

B. Marginal Fermi liquid dc resistivity at the saddle-point level

The marginal Fermi liquid form of fermionic self-energy in Eq. (4.28) gives rise to a linear- T resistivity on top of the zero-temperature Drude result due to impurity scattering. The one-loop retarded current-current correlation function is given by [43, 105]

$$\begin{aligned} \chi^R(\Omega \rightarrow 0, \mathbf{q} = 0) &= \frac{e^2}{2i} \frac{Nv_F^2}{d} \int_{\omega, \mathbf{k}} G_{\text{sp}}^R(\omega, \mathbf{k}) G_{\text{sp}}^A(\omega, \mathbf{k}) (F_\omega - F_{\omega+\Omega}), \end{aligned} \quad (4.32)$$

where $d = 2$ is the spatial dimension and the prefactor N is due to N flavors of fermions. Here, we assume that quantum relaxational bosons remain in equilibrium, and the temperature dependence of the resistivity reflects the real absorption and emission of bosons by the MFL fermions. This ignores the possibility of boson-fermion drag [51]. Vertex corrections can be ignored, because the thermal mass renders the quantum relaxational bosons short-ranged.

At low temperature, Eq. (4.32) can be expressed as

$$\begin{aligned} \chi^R(\Omega \rightarrow 0, \mathbf{q} = 0) &= -\frac{e^2}{2i} \frac{Nv_F^2}{d} \int_{\omega, \mathbf{k}} G_{\text{sp}}^R(\omega, \mathbf{k}) G_{\text{sp}}^A(\omega, \mathbf{k}) \frac{\Omega}{2T} \text{sech}^2 \frac{\omega}{2T} \\ &\simeq -\frac{e^2}{2i} \frac{Nv_F^2}{d} \int_{\omega} \frac{\pi\nu_0}{\gamma_{\text{el}} + \frac{\pi}{2}\bar{g}^2 \max(|\omega|, JT)} \frac{\Omega}{2T} \text{sech}^2 \frac{\omega}{2T}. \end{aligned} \quad (4.33)$$

The dc conductivity is related to the current-current correlation function via

$$\sigma_{\text{MFL}}(T) = \frac{1}{i\Omega} \chi^R(\Omega \rightarrow 0, \mathbf{q} = 0) = \sigma_{\text{Drude}} \mathcal{F}\left(t, \frac{J}{2}\right), \quad (4.34)$$

where $\sigma_{\text{Drude}} = Ne^2\nu_0 D$ is the Drude conductivity,

$$\mathcal{F}(t, x) \equiv \int_0^\infty dy \frac{\text{sech}^2 y}{1 + \bar{g}^2 \pi t \max(y, x)}, \quad t = \frac{T}{\gamma_{\text{el}}}, \quad (4.35)$$

and

$$D = \frac{v_F^2}{4\gamma_{\text{el}}} \quad (4.36)$$

is the diffusion constant in 2D. As illustrated in Appendix B, $\mathcal{F}(t, x)$ can be well-approximated by

$$\mathcal{F}(t, x) = \frac{1}{1 + \mathcal{S}(x) \bar{g}^2 t}, \quad (4.37)$$

where

$$\mathcal{S}(x) \simeq \pi \sqrt{x^2 + r^2}, \quad r \simeq 0.41. \quad (4.38)$$

Hence, at the saddle point level and low temperature, we expect linear- T resistivity according to

$$\frac{\rho_{\text{MFL}}(T)}{\rho_{\text{Drude}}} = 1 + \mathcal{S}(J/2) \bar{g}^2 t, \quad (4.39)$$

where $\rho_{\text{Drude}} = \sigma_{\text{Drude}}^{-1}$. Due to impurity scattering, the above expression approaches ρ_{Drude} instead of zero at $T = 0$. This accounts for the first term in the square brackets of our final result quoted in Eq. (1.4).

In the next section, we explore the effects of quantum interference corrections to the density response function. As we will demonstrate below, the conductivity eventually gets dominated by an interaction-mediated

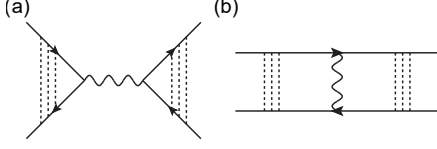


FIG. 4. Diagrammatic representation for the matrix-boson mediated interactions terms (a) $S_{\text{int I}}$ and (b) $S_{\text{int II}}$, in the action of the MFL-FNLsM in Eqs. (5.3), (5.7), and (5.8). Solid lines and wavy lines correspond respectively to \hat{G}_{sp} and \hat{D}_{sp} . The dotted-line ladder represents lowest-order quantum (diffuson) fluctuations of the constrained matrix field \hat{q} .

Altshuler-Aronov correction at low enough temperature.

V. NON-LINEAR SIGMA MODEL (“MFL-FNLsM”)

We now consider fluctuations around the saddle points obtained in Sec. IV A, which leads to an effective \hat{q} -matrix field theory [46] that we dub the “marginal-Fermi liquid Finkel’stein nonlinear sigma model” (MFL-FNLsM). Specifically, we only allow \hat{G} , $\hat{\Sigma}$ and \hat{q} to fluctuate, while freezing the bosonic fields \hat{D} , $\hat{\Pi}$, and \hat{X} at their saddle-point values. We do this since our primary interest here is in fermion charge transport; in this paper, we do not consider the conduction of the conserved $\text{SU}(N)$ “spin.” We also note that fluctuations in the bosonic sector are expected to be suppressed by $1/N$, and that the saddle-point boson propagator [Eq. (4.25)] is already damped by the thermal mass in the quantum relaxational regime.

As usual in a matrix sigma model for quantum (de)localization [18, 42, 44, 46, 47], we ignore the massive fluctuations of \hat{q} and focus on the Goldstone modes, which can be parametrized as

$$\hat{q} = \hat{U}^\dagger \hat{q}_{\text{sp}} \hat{U}, \quad (5.1)$$

where \hat{U} is a unitary rotation matrix acting upon the composite space of frequencies $\otimes \{\text{retarded, advanced}\} \otimes \text{SU}(N)$ flavors; the saddle-point \hat{q}_{sp} is given by Eq. (4.16). The massless modes correspond to diffusons, quantum two-particle diffusion modes in the particle-hole channel.

In this work, we focus on the diffusive regime in which $\gamma_{\text{el}} \gg \omega, v_F k$, where k is a fermion rendered from the Fermi surface. To derive an effective action involving only \hat{q} , we integrate out the fluctuation $\delta\hat{G}$, followed by $\delta\hat{\Sigma}$. We then perform a gradient expansion to obtain the FNLsM, following the standard procedures [43, 44, 46, 91–95]. Leaving the technical details for the derivation in Appendix C, we state the resulting action below:

$$Z[V] = \int \mathcal{D}\hat{q} e^{-S[\hat{q}]}, \quad (5.2)$$

$$S[\hat{q}] = S_D + S_{\text{int I}} + S_{\text{int II}} + S_{qV} + S_V, \quad (5.3)$$

where the \hat{q} matrix is subjected to the constraints

$$\hat{q}^2 = \hat{1}, \quad \text{Tr}[\hat{q}] = 0, \quad \hat{q} = \hat{q}^\dagger, \quad (5.4)$$

which follow from Eq. (5.1). The matrix $\hat{q} \rightarrow q_{ij;\omega\omega'}^{ab}$ with frequency $\{\omega, \omega'\}$, $\text{SU}(N)$ flavor $\{i, j\}$, and Keldysh $\{a, b\}$ indices displayed.

The first term in the action is

$$S_D = \frac{1}{2\lambda} \int_{\mathbf{x}} \text{Tr} [\nabla \hat{q} \cdot \nabla \hat{q}] + 2ih \int_{\mathbf{x}} \text{Tr} [(\hat{\omega} + i\eta \hat{\tau}^3 - \hat{\Sigma}_{\text{sp}}) \hat{q}], \quad (5.5)$$

where

$$1/\lambda = Dh, \quad h = \pi\nu_0/2, \quad (5.6)$$

with D the semiclassical diffusion constant in Eq. (4.36). In Eq. (5.5) and what follows, matrix traces $\text{Tr}(\dots)$ run over all indices not explicitly displayed. We focus on the weak-disorder limit in which $\gamma_{\text{el}} \ll \mu$ (μ is the chemical potential) so that λ , proportional to the inverse conductance, can be treated as a small parameter. The only difference from the usual unitary-class sigma model in Eq. (5.5) is the MFL fermion self-energy $\hat{\Sigma}_{\text{sp}} = \text{diag} \{ \hat{\Sigma}_{\text{sp}}^R, \hat{\Sigma}_{\text{sp}}^A \}_\tau$ [Eq. (4.28)].

Meanwhile, interparticle interactions mediated by the quantum-relaxational bosons via the Yukawa coupling give rise to the terms

$$S_{\text{int I}} = \Gamma_1 \int_{1-4, \mathbf{k}} \delta_{1+3, 2+4} \text{Tr} [\hat{q}_{ij;1,2}(-\mathbf{k}) \hat{\gamma}_{2,1}^s D_{\text{sp}, 2-1}^{ss'}(\mathbf{k}) \text{Tr} [\hat{\gamma}_{4,3}^{s'} \hat{q}_{ji;3,4}(\mathbf{k})]], \quad (5.7)$$

$$S_{\text{int II}} = -\Gamma_2 \int_{1-4, \mathbf{k}} \delta_{1+3, 2+4} \text{Tr} [\hat{q}_{ii;1,2}(-\mathbf{k}) \hat{\gamma}_{2,3}^s \hat{q}_{jj;3,4}(\mathbf{k}) \hat{\gamma}_{4,1}^{s'}] \int_{\mathbf{k}'} D_{\text{sp}, 1-4}^{ss'}(\mathbf{k}'), \quad (5.8)$$

where the coupling constants

$$\Gamma_1 \equiv i \frac{2h^2 g^2}{N}, \quad \Gamma_2 \equiv i \frac{hg^2}{\gamma_{\text{el}} N}. \quad (5.9)$$

Here, we defined the shorthands $\int_{1-4} = \int_{1,2,3,4}$, $\{1, 2, 3, 4\} \equiv \{\omega_1, \omega_2, \omega_3, \omega_4\}$ and the energy-conserving Dirac- δ function $\delta_{1+3,2+4} = 2\pi\delta(\omega_1 + \omega_3 - \omega_2 - \omega_4)$. The numerical subscripts thus stand for the corresponding frequency labels. In addition, $s, s' \in \{\text{cl}, \text{q}\}$ are boson Keldysh indices, while the traces run over the fermion Keldysh space $a \in \{R, A\}$.

The interactions are depicted diagrammatically in Fig. 4. The first one [S_{intI} , Fig. 4(a)] is the usual interaction term appearing in the FNLsM. The second one [S_{intII} , Fig. 4(b)], which involves a vertical interaction line, is not considered in the original paper by Finkel'stein [46]. However, in the case of the MFL-FNLsM, this term is essential for fixing the Ward identity for physical response functions. In the context of disordered d -wave superconductors, interaction terms similar to S_{intII} were also taken into account in the derivation of the sigma model [49, 50].

Finally, the terms in the action [Eq. (5.3)] involving the source field are

$$S_{qV} = -2ih \int_{t,\mathbf{x}} \text{Tr} \left\{ \hat{q}_{t,t}(\mathbf{x}) [V^{\text{cl}}(t, \mathbf{x}) \hat{\gamma}^{\text{cl}} + V^{\text{q}}(t, \mathbf{x}) \hat{\gamma}^{\text{q}}] \right\} \quad (5.10)$$

and

$$S_V = -2iN\nu_0 \int_{t,\mathbf{x}} V^{\text{q}}(t, \mathbf{x}) V^{\text{cl}}(t, \mathbf{x}). \quad (5.11)$$

The second term arises from the integration involving products of retarded-retarded and advanced-advanced fermionic Green's functions in the second-order gradient expansion [43, 44]. It gives the static-compressibility component of the density response function.

A. π - σ parametrization

We employ the “ π - σ ” parametrization for the \hat{q} matrix

$$\hat{q} = \begin{bmatrix} \sqrt{\hat{1} - \hat{W}\hat{W}^\dagger} & \hat{W} \\ \hat{W}^\dagger & -\sqrt{\hat{1} - \hat{W}^\dagger\hat{W}} \end{bmatrix}_\tau \quad (5.12)$$

$$\equiv \hat{q}^{(0)} + \hat{q}^{(1)} + \hat{q}^{(2)} + \dots$$

where

$$\hat{q}^{(0)} = \begin{bmatrix} \hat{1} & 0 \\ 0 & -\hat{1} \end{bmatrix}_\tau, \quad (5.13)$$

$$\hat{q}^{(1)} = \begin{bmatrix} 0 & \hat{W} \\ \hat{W}^\dagger & 0 \end{bmatrix}_\tau, \quad (5.14)$$

$$\hat{q}^{(2)} = -\frac{1}{2} \begin{bmatrix} \hat{W}\hat{W}^\dagger & 0 \\ 0 & -\hat{W}^\dagger\hat{W} \end{bmatrix}_\tau, \quad (5.15)$$

$$\hat{q}^{(3)} = 0, \quad (5.16)$$

$$\hat{q}^{(4)} = -\frac{1}{8} \begin{bmatrix} (\hat{W}\hat{W}^\dagger)^2 & 0 \\ 0 & -(\hat{W}^\dagger\hat{W})^2 \end{bmatrix}_\tau, \quad (5.17)$$

and $\hat{W} \rightarrow W_{ij;\omega_1,\omega_2}$ is a matrix field containing flavor indices i, j and frequency labels ω_1, ω_2 . In the following, we expand the action in Eq. (5.3) up to quartic order in \hat{W} . After the expansion, we will rescale $\hat{W} \rightarrow \sqrt{\lambda}\hat{W}$, $\hat{W}^\dagger \rightarrow \sqrt{\lambda}\hat{W}^\dagger$ to facilitate the perturbative calculation in λ .

1. Diffusion term

By plugging Eqs. (5.12)–(5.17) into S_D [Eq. (5.5)], we have

$$S_D^{(2)}[W, W^\dagger] = \int_{1,2,\mathbf{q}} \left[\mathbf{q}^2 - ih\lambda(\omega_2 - \hat{\Sigma}_2^R - \omega_1 + \hat{\Sigma}_1^A) \right] \text{Tr} \left[\hat{W}_{12}^\dagger(\mathbf{q}) \hat{W}_{21}(\mathbf{q}) \right] \quad (5.18)$$

and

$$S_D^{(4)}[W, W^\dagger] = \lambda \int_{1-4,\mathbf{q}_i} \square_{1,2,3,4}^{\mathbf{q}_1,\mathbf{q}_2,\mathbf{q}_3,\mathbf{q}_4} \delta_{\mathbf{q}_1+\mathbf{q}_3,\mathbf{q}_2+\mathbf{q}_4} \text{Tr} \left[\hat{W}_{12}^\dagger(\mathbf{q}_1) \hat{W}_{23}(\mathbf{q}_2) \hat{W}_{34}^\dagger(\mathbf{q}_3) \hat{W}_{41}(\mathbf{q}_4) \right]. \quad (5.19)$$

Here, $\int_{\mathbf{q}_i} \equiv \int_{\mathbf{q}_1,\mathbf{q}_2,\mathbf{q}_3,\mathbf{q}_4}$, the trace runs over the Keldysh space and we defined

$$\square_{1,2,3,4}^{\mathbf{q}_1,\mathbf{q}_2,\mathbf{q}_3,\mathbf{q}_4} = \frac{1}{2^3} \left[-2(\mathbf{q}_1 \cdot \mathbf{q}_3 + \mathbf{q}_2 \cdot \mathbf{q}_4) + (\mathbf{q}_1 + \mathbf{q}_3) \cdot (\mathbf{q}_2 + \mathbf{q}_4) \right. \\ \left. - ih\lambda(\omega_2 + \omega_4 - \omega_1 - \omega_3) + ih\lambda(\Sigma_{\text{sp},2}^R + \Sigma_{\text{sp},4}^R - \Sigma_{\text{sp},1}^A - \Sigma_{\text{sp},3}^A) \right]. \quad (5.20)$$

2. Interaction terms

By substituting Eqs. (5.13)–(5.17) into $S_{\text{int I}}$ [Eq. (5.7)], we obtain the corresponding quadratic, cubic, and quartic interaction terms, which are respectively given by

$$S_{\text{int I}}^{(2)} = -2\lambda\Gamma_1 \int_{1-4, \mathbf{q}} (F_1 - F_2) W_{ij;1,2}^\dagger(\mathbf{q}) W_{ji;3,4}(\mathbf{q}) D_{\text{sp},2-1}^R(\mathbf{q}) \delta_{1+3,2+4}, \quad (5.21)$$

$$S_{\text{int I}}^{(3)} = -\lambda^{3/2}\Gamma_1 \int_{1-5, \mathbf{p}, \mathbf{q}} \left\{ \begin{aligned} &W_{ij;1,2}^\dagger(\mathbf{q}) \hat{W}_{jk;3,5}(\mathbf{p} + \mathbf{q}) W_{ki;5,4}^\dagger(\mathbf{p}) D_{\text{sp},2-1}^R(\mathbf{q}) \left[(F_1 - F_2) \left(\frac{1}{F_{3-4}} + F_4 \right) \right] \\ &+ W_{ij;1,2}^\dagger(\mathbf{q}) \hat{W}_{jk;3,5}^\dagger(\mathbf{p}) W_{ki;5,4}(\mathbf{p} + \mathbf{q}) D_{\text{sp},2-1}^R(\mathbf{q}) \left[(F_1 - F_2) \left(F_3 - \frac{1}{F_{3-4}} \right) \right] \\ &- W_{ij;1,2}(\mathbf{q}) \left[W_{jk;3,5}(\mathbf{p}) W_{ki;5,4}^\dagger(\mathbf{p} + \mathbf{q}) - W_{jk;3,5}^\dagger(\mathbf{p} + \mathbf{q}) W_{ki;5,4}(\mathbf{p}) \right] D_{\text{sp},2-1}^A(-\mathbf{q}) \end{aligned} \right\} \delta_{1+3,2+4}, \quad (5.22)$$

and

$$S_{\text{int I}}^{(4)} = \frac{\lambda^2}{2} \Gamma_1 \int_{1-6, \mathbf{k}, \mathbf{p}, \mathbf{q}} \left[\begin{aligned} &W_{ik;1,5}(\mathbf{p}) W_{kj;5,2}^\dagger(\mathbf{p} + \mathbf{q}) W_{jl;3,6}(\mathbf{k}) W_{li;6,4}^\dagger(\mathbf{k} - \mathbf{q}) \left(\frac{1}{F_{3-4}} + F_4 \right) \\ &+ W_{ik;1,5}(\mathbf{p}) W_{kj;5,2}^\dagger(\mathbf{p} + \mathbf{q}) W_{jl;3,6}^\dagger(\mathbf{k} - \mathbf{q}) W_{li;6,4}(\mathbf{k}) \left(-\frac{1}{F_{3-4}} + F_3 \right) \\ &+ W_{ik;1,5}^\dagger(\mathbf{p} + \mathbf{q}) W_{kj;5,2}(\mathbf{p}) W_{jl;3,6}(\mathbf{k}) W_{li;6,4}^\dagger(\mathbf{k} - \mathbf{q}) \left(-\frac{1}{F_{3-4}} - F_4 \right) \\ &+ W_{ik;1,5}^\dagger(\mathbf{p} + \mathbf{q}) W_{kj;5,2}(\mathbf{p}) W_{jl;3,6}^\dagger(\mathbf{k} - \mathbf{q}) W_{li;6,4}(\mathbf{k}) \left(\frac{1}{F_{3-4}} - F_3 \right) \end{aligned} \right] D_{\text{sp},2-1}^R(\mathbf{q}) \delta_{1+3,2+4}, \quad (5.23)$$

where $F_\omega \equiv F(\omega)$.

Repeating the above procedures for $S_{\text{int II}}$ [Eq. (5.8)], we obtain the type II interaction terms

$$S_{\text{int II}}^{(2)} = -2\lambda\Gamma_2 \int_{1-4, \mathbf{k}, \mathbf{q}} W_{ii;1,2}^\dagger(\mathbf{q}) W_{jj;3,4}(\mathbf{q}) \left[D_{\text{sp},1-4}^K(\mathbf{k}) - F_1 D_{\text{sp},1-4}^R(\mathbf{k}) + F_2 D_{\text{sp},1-4}^A(\mathbf{k}) \right] \delta_{1+3,2+4}, \quad (5.24)$$

and

$$S_{\text{int II}}^{(3)} = \lambda^{3/2}\Gamma_2 \int_{1-4, \mathbf{k}, \mathbf{p}, \mathbf{q}} \delta_{1+3,2+4} \times \left\{ \begin{aligned} &-W_{jk;3,5}(\mathbf{p}) W_{kj;5,4}^\dagger(\mathbf{p} + \mathbf{q}) W_{ii;1,2}(\mathbf{q}) D_{\text{sp},1-4}^A(\mathbf{k}) \\ &+ W_{jk;3,5}^\dagger(\mathbf{p} + \mathbf{q}) W_{kj;5,4}(\mathbf{p}) W_{ii;1,2}(\mathbf{q}) D_{\text{sp},1-4}^R(\mathbf{k}) \\ &+ W_{jk;3,5}(\mathbf{p} + \mathbf{q}) W_{kj;5,4}^\dagger(\mathbf{p}) W_{ii;1,2}^\dagger(\mathbf{q}) \left[(F_1 - F_4) F_2 D_{\text{sp},1-4}^A(\mathbf{k}) - (1 - F_1 F_4) D_{\text{sp},1-4}^R(\mathbf{k}) + (F_1 - F_4) D_{\text{sp},1-4}^K(\mathbf{k}) \right] \\ &- W_{jk;3,5}^\dagger(\mathbf{p}) W_{kj;5,4}(\mathbf{p} + \mathbf{q}) W_{ii;1,2}^\dagger(\mathbf{q}) \left[-(1 - F_2 F_3) D_{\text{sp},1-4}^A(\mathbf{k}) - F_1 (F_3 - F_2) D_{\text{sp},1-4}^R(\mathbf{k}) + (F_3 - F_2) D_{\text{sp},1-4}^K(\mathbf{k}) \right] \end{aligned} \right\}. \quad (5.25)$$

The contribution of the quartic terms from $S_{\text{int II}}$ to the density correlation function is subleading and thus omitted here.

3. Source field term

Similarly, the S_{qV} [Eq. (5.10)] becomes

$$S_{qV} = -2ih \int_{1-3, \mathbf{p}, \mathbf{q}} \left\{ \begin{aligned} &\sqrt{\lambda} V_{2-1}^{\text{cl}}(\mathbf{q}) (F_1 - F_2) W_{ii;1,2}^\dagger(\mathbf{q}) \delta_{\mathbf{p}, \mathbf{q}} \delta_{2,3} \\ &+ \sqrt{\lambda} \left[-W_{ii;1,2}(\mathbf{q}) V_{2-1}^{\text{q}}(-\mathbf{q}) \delta_{\mathbf{p}, \mathbf{q}} - (1 - F_1 F_2) W_{ii;1,2}^\dagger(\mathbf{q}) V_{2-1}^{\text{q}}(\mathbf{q}) \delta_{\mathbf{p}, \mathbf{q}} \right] \delta_{2,3} \\ &- \frac{\lambda}{2} \left[V_{2-1}^{\text{cl}}(\mathbf{q}) W_{ij;1,3}(\mathbf{p}) W_{ji;3,2}^\dagger(\mathbf{p} + \mathbf{q}) - V_{2-1}^{\text{cl}}(\mathbf{q}) W_{ij;1,3}^\dagger(\mathbf{p} + \mathbf{q}) W_{ji;3,2}(\mathbf{p}) \right] \\ &- \frac{\lambda}{2} \left[V_{2-1}^{\text{q}}(\mathbf{q}) W_{ij;1,3}(\mathbf{p}) W_{ji;3,2}^\dagger(\mathbf{q} + \mathbf{k}) F_2 + V_{2-1}^{\text{q}}(\mathbf{q}) W_{ij;1,3}^\dagger(\mathbf{p} + \mathbf{q}) W_{ji;3,2}(\mathbf{p}) F_1 \right] \end{aligned} \right\}. \quad (5.26)$$

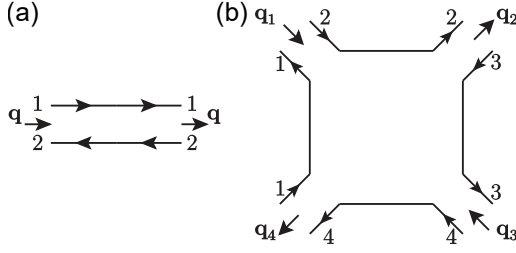


FIG. 5. (a) The bare propagator and (b) quartic vertex generated from S_D .

B. Feynman rules

1. Bare propagator

From Eq. (5.18), we can read off the bare diffuson propagator to be

$$\begin{aligned} \Delta_{1,2}^R(\mathbf{q})\delta_{1,4}\delta_{2,3} &\equiv \left\langle W_{ij;1,2}(\mathbf{q})W_{ji;3,4}^\dagger(\mathbf{q}) \right\rangle_0 \\ &= \frac{\delta_{1,4}\delta_{2,3}}{\mathbf{q}^2 - ih\lambda(\omega_1 - \omega_2) - ih\lambda[\Sigma_{\text{sp}}^A(\omega_2) - \Sigma_{\text{sp}}^R(\omega_1)]}. \end{aligned} \quad (5.27)$$

This is in contrast with the diffuson propagator in the Fermi liquid case [42–44, 46, 91, 92],

$$\Delta_{\text{FL};1,2}^R(\mathbf{q}) = \Delta_{\text{FL};1,-2}^R(\mathbf{q}) = \frac{1}{\mathbf{q}^2 - ih\lambda(\omega_1 - \omega_2)}, \quad (5.28)$$

which explicitly conserves particles. Our diffuson in Eq. (5.27) is now anomalous due to the appearance of the MFL fermionic self-energy $\Sigma_{\text{sp}}^{R/A}(\omega)$.

The anomalous diffuson propagator is represented diagrammatically in Fig. 5(a) by two black solid lines with arrows pointing in the opposite directions. The frequency indices of the matrix fields \hat{W} and \hat{W}^\dagger are labeled by the numbers. The flavor indices are implicit. Along a solid line, the frequency label and flavor index remain unchanged. The momentum flowing through the diffuson is labeled by an arrow in the middle of the two black solid lines. The momentum arrow points inwards (outwards) for the field \hat{W} (\hat{W}^\dagger).

2. Interaction vertices

Fig. 5(b) and Figs. 6–8 illustrate the interaction vertices. In particular, the amplitudes of the terms linear in \hat{W} are

$$\text{Fig. 8(a)(i)} = 2ih\sqrt{\lambda}(F_1 - F_2)V_{2-1}^{\text{cl}}(\mathbf{q}), \quad (5.29)$$

$$\text{Fig. 8(a)(ii)} = -2ih\sqrt{\lambda}V_{2-1}^{\text{q}}(-\mathbf{q}), \quad (5.30)$$

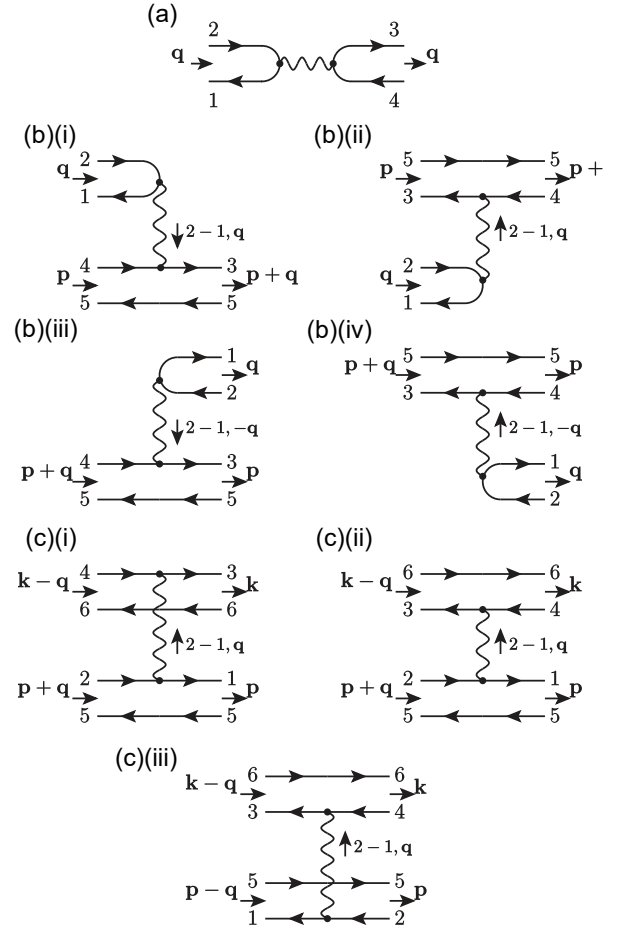


FIG. 6. The set of vertices due to S_{int} . Diagram (a) represents the quadratic vertex, (b) represents the cubic interaction vertices, and (c) represents the quartic interaction vertices.

$$\text{Fig. 8(a)(iii)} = -2ih\sqrt{\lambda}(1 - F_1F_2)V_{2-1}^{\text{q}}(\mathbf{q}). \quad (5.31)$$

Those quadratic in \hat{W} are

$$\text{Fig. 6(a)} = 2\lambda\Gamma_1(F_1 - F_2)D_{\text{sp},2-1}^R(\mathbf{q})\delta_{1+3,2+4}, \quad (5.32)$$

$$\text{Fig. 7(a)} = 2\lambda\Gamma_2\delta_{1+3,2+4}$$

$$\times \int_{\mathbf{k}} \left[D_{\text{sp},1-4}^K(\mathbf{k}) - F_1 D_{\text{sp},1-4}^R(\mathbf{k}) + F_2 D_{\text{sp},1-4}^A(\mathbf{k}) \right], \quad (5.33)$$

$$\text{Fig. 8(b)(i)} = -ih\lambda V_{2-1}^{\text{cl}}(\mathbf{q}), \quad (5.34)$$

$$\text{Fig. 8(b)(ii)} = ih\lambda V_{2-1}^{\text{cl}}(\mathbf{q}), \quad (5.35)$$

$$\text{Fig. 8(b)(iii)} = -ih\lambda V_{2-1}^{\text{q}}(\mathbf{q})F_2, \quad (5.36)$$

$$\text{Fig. 8(b)(iv)} = -ih\lambda V_{2-1}^{\text{q}}(\mathbf{q})F_1. \quad (5.37)$$

The cubic ones are

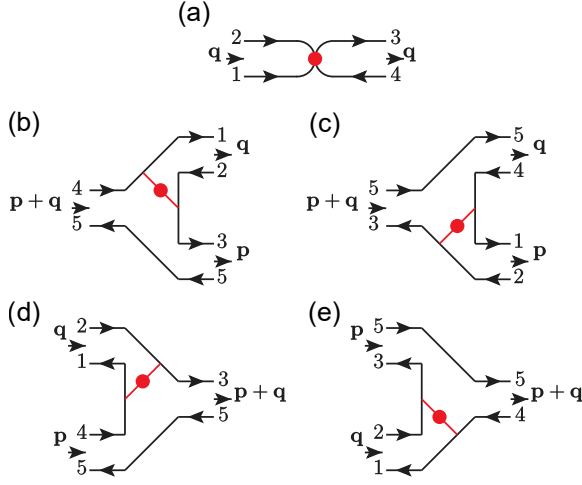


FIG. 7. The set of vertices due to S_{intII} . Diagram (a) represents the quadratic vertex and (b)–(e) represent the cubic vertices.

Fig. 6(b)(i)

$$= \lambda^{3/2} \Gamma_1 \delta_{1+3,2+4} D_{\text{sp},2-1}^R(\mathbf{q}) (F_1 - F_2) \left(\frac{1}{F_{3-4}} + F_4 \right), \quad (5.38)$$

Fig. 6(b)(ii)

$$= \lambda^{3/2} \Gamma_1 \delta_{1+3,2+4} D_{\text{sp},2-1}^R(\mathbf{q}) (F_1 - F_2) \left(F_3 - \frac{1}{F_{3-4}} \right), \quad (5.39)$$

$$\text{Fig. 6(b)(iii)} = -\lambda^{3/2} \Gamma_1 \delta_{1+3,2+4} D_{\text{sp},2-1}^A(-\mathbf{q}), \quad (5.40)$$

$$\text{Fig. 6(b)(iv)} = \lambda^{3/2} \Gamma_1 \delta_{1+3,2+4} D_{\text{sp},2-1}^A(-\mathbf{q}), \quad (5.41)$$

$$\text{Fig. 7(b)} = \lambda^{3/2} \Gamma_2 \delta_{1+3,2+4} \int_{\mathbf{k}} D_{\text{sp},1-4}^A(\mathbf{k}), \quad (5.42)$$

$$\text{Fig. 7(c)} = -\lambda^{3/2} \Gamma_2 \delta_{1+3,2+4} \int_{\mathbf{k}} D_{\text{sp},1-4}^R(\mathbf{k}), \quad (5.43)$$

$$\begin{aligned} \text{Fig. 7(d)} &= -\lambda^{3/2} \Gamma_2 \delta_{1+3,2+4} \\ &\times \int_{\mathbf{k}} \left[\begin{aligned} &(F_1 - F_4) F_2 D_{\text{sp},1-4}^A(\mathbf{k}) \\ &-(1 - F_1 F_4) D_{\text{sp},1-4}^R(\mathbf{k}) \\ &+(F_1 - F_4) D_{\text{sp},1-4}^K(\mathbf{k}) \end{aligned} \right], \end{aligned} \quad (5.44)$$

$$\begin{aligned} \text{Fig. 7(e)} &= -\lambda^{3/2} \Gamma_2 \delta_{1+3,2+4} \\ &\times \int_{\mathbf{k}} \left[\begin{aligned} &(1 - F_2 F_3) D_{\text{sp},1-4}^A(\mathbf{k}) \\ &+F_1 (F_3 - F_2) D_{\text{sp},1-4}^R(\mathbf{k}) \\ &-(F_3 - F_2) D_{\text{sp},1-4}^K(\mathbf{k}) \end{aligned} \right]. \end{aligned} \quad (5.45)$$

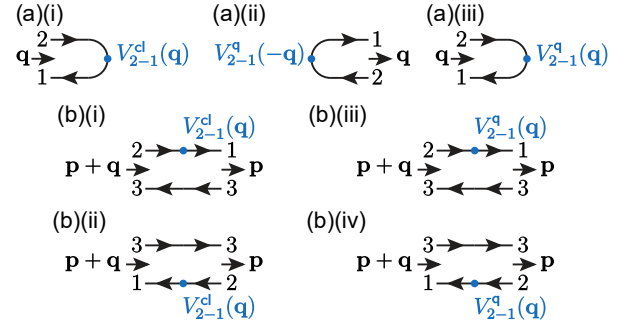


FIG. 8. The set of vertices due to S_{qV} . Diagram (a) shows the coupling between $V^{\text{cl/q}}$ and $\hat{q}^{(1)}$ while (b) shows the coupling between $V^{\text{cl/q}}$ and $\hat{q}^{(2)}$.

The quartic ones are

$$\text{Fig. 5(b)} = -2\lambda \square_{1,2,3,4}^{\mathbf{q}_1, \mathbf{q}_2, \mathbf{q}_3, \mathbf{q}_4} \delta_{\mathbf{q}_1 + \mathbf{q}_3, \mathbf{q}_2 + \mathbf{q}_4}, \quad (5.46)$$

Fig. 6(c)(i)

$$= -\frac{\lambda^2}{2} \Gamma_1 \delta_{1+3,2+4} D_{\text{sp},2-1}^R(\mathbf{q}) \left(\frac{1}{F_{3-4}} + F_4 \right), \quad (5.47)$$

Fig. 6(c)(ii)

$$= -\frac{\lambda^2}{2} \Gamma_1 \delta_{1+3,2+4} \left[\begin{aligned} &D_{\text{sp},2-1}^R(\mathbf{q}) \left(-\frac{1}{F_{3-4}} + F_3 \right) \\ &-D_{\text{sp},4-3}^R(\mathbf{q}) \left(\frac{1}{F_{1-2}} + F_2 \right) \end{aligned} \right], \quad (5.48)$$

Fig. 6(c)(iii)

$$= -\frac{\lambda^2}{2} \Gamma_1 \delta_{1+3,2+4} D_{\text{sp},2-1}^R(\mathbf{q}) \left(\frac{1}{F_{3-4}} - F_3 \right), \quad (5.49)$$

where $\square_{1,2,3,4}^{\mathbf{q}_1, \mathbf{q}_2, \mathbf{q}_3, \mathbf{q}_4}$ is defined in Eq. (5.20). In Eq. (5.46), we included a symmetry factor of 2. We also made use of the fact that $D_{\text{sp},\Omega}^R(\mathbf{q}) = D_{\text{sp},\Omega}^R(-\mathbf{q})$.

VI. SEMICLASSICAL RESULT FOR THE DENSITY RESPONSE FUNCTION

We now evaluate the density linear response function using the NLsM derived above. Under the Keldysh response theory, the retarded density-density correlation function is defined as

$$\pi^R(\Omega, \mathbf{q}) = -\frac{1}{2i} \frac{\delta^2 Z[V]}{\delta V_{\Omega}^{\text{cl}}(\mathbf{q}) \delta V_{-\Omega}^{\text{q}}(-\mathbf{q})} \Big|_{V^{\text{cl}}=V^{\text{q}}=0}. \quad (6.1)$$



FIG. 9. Diagrammatic representation for $\pi_{\text{dyn}}^R(\Omega, \mathbf{q}) = \sum_{n=0}^{\infty} \pi_{\text{dyn}}^{R(n)}(\Omega, \mathbf{q})$ [Eq. (6.7)]. The n th term on the right hand side is denoted by $\pi_{\text{dyn}}^{R(n)}$, which contains n red dot(s) defined in Fig. 7(a). The blue dots are scalar potential vertices defined in Fig. 8(a).

Using the partition function in Eq. (5.2), we have

$$\pi^R(\Omega, \mathbf{q}) = -N\nu_0 + \pi_{\text{dyn}}^R(\Omega, \mathbf{q}), \quad (6.2)$$

where the first term is the static contribution and the second one is the dynamical contribution given by

$$\begin{aligned} \pi_{\text{dyn}}^R(\Omega, \mathbf{q}) &= i \frac{(2h)^2}{2} \int_{1,2} (F_1 - F_{1+\Omega}) \\ &\times \left\langle W_{ii;2+\Omega,2}(\mathbf{q}) W_{jj;1,1+\Omega}^\dagger(\mathbf{q}) \right\rangle. \end{aligned} \quad (6.3)$$

The appearance of N in the static term is due to N flavors of fermions.

In this section, we consider the semiclassical contribution to the density response function to leading order of $1/N$, i.e. we only perform the calculation at the Gaussian level. If we ignore interaction corrections and just make use of the bare diffuson propagator in Eq. (5.27), the dynamical density response function is

$$\pi_{\text{dyn}}^{R(0)}(\Omega, \mathbf{q}) \simeq N\nu_0 \frac{-ih\lambda\Omega}{\mathbf{q}^2 - ih\lambda\Omega - ih\lambda r_\Omega}, \quad (6.4)$$

where we can approximate to logarithmic accuracy that

$$\Delta_{2+\Omega,2}^R(\mathbf{q}) \simeq \frac{1}{\mathbf{q}^2 - ih\lambda\Omega - ih\lambda r_\Omega} \equiv \Delta_\Omega^R(\mathbf{q}), \quad (6.5)$$

with

$$r_\Omega = \bar{g}^2 \Omega \ln \frac{2\omega_c}{|\Omega|}. \quad (6.6)$$

Due to the presence of the fermionic self-energy in the free propagator [Eq. (5.27)], the full density response function in Eq. (6.2) does not go to zero at $\mathbf{q} \rightarrow 0$, violating particle conservation. To rectify this, one must take $S_{\text{int II}}^{(2)}$ into account and consider the series of diagrams shown in Fig. 9. We note that a similar set of diagrams have to be summed in order to satisfy particle conservation in the context of clean non-Fermi and marginal Fermi liquids [23, 73, 74, 108].

Denote the n th term in the series as $\pi_{\text{dyn}}^{R(n)}(\Omega, \mathbf{q})$, which contains n interaction vertices due to $S_{\text{int II}}^{(2)}$. The dynamical part of the density response function is then

ical part of the density response function is then

$$\pi_{\text{dyn}}^R(\Omega, \mathbf{q}) = \sum_{n=0}^{\infty} \pi_{\text{dyn}}^{R(n)}(\Omega, \mathbf{q}). \quad (6.7)$$

The $n = 1$ term (second term on the RHS of Fig. 9) is

$$\begin{aligned} \pi_{\text{dyn}}^{R(1)}(\Omega, \mathbf{q}) &= 2iN^2\lambda h^2 (2\lambda\Gamma_2) \\ &\times \int_{1,2,\mathbf{k}} \Delta_{1+\Omega,1}^R(\mathbf{q}) \Delta_{2+\Omega,2}^R(\mathbf{q}) (F_1 - F_{1+\Omega}) \\ &\times [D_{\text{sp},2-1}^K(\mathbf{k}) + F_{2+\Omega} D_{\text{sp},2-1}^A(\mathbf{k}) - F_2 D_{\text{sp},2-1}^R(\mathbf{k})]. \end{aligned} \quad (6.8)$$

Performing frequency integrals and focusing on the $T = 0$ limit, we have

$$\begin{aligned} \pi_{\text{dyn}}^{R(1)}(\Omega, \mathbf{q}) &\simeq 2iN^2\lambda h^2 (2\lambda\Gamma_2) [\Delta_\Omega^R(\mathbf{q})]^2 \\ &\times \int_1 (F_1 - F_{\Omega+1}) \int_0^{q_{\text{max}}} \frac{dx}{4\pi} \left(-\frac{1}{2\pi} \frac{2}{i\alpha} \right) \ln \left(\frac{x}{x - i\alpha\Omega/2} \right) \\ &\simeq 2iN\lambda^2 h^2 [\Delta_\Omega^R(\mathbf{q})]^2 \int_1 (F_1 - F_{1+\Omega}) (-ihr_\Omega), \end{aligned} \quad (6.9)$$

For $n > 1$, the diagrams can be evaluated in a similar fashion, resulting in the following geometric series

$$\begin{aligned} \pi_{\text{dyn}}^R(\Omega, \mathbf{q}) &= 2iN\lambda h^2 \int_1 (F_1 - F_{1+\Omega}) \Delta_\Omega^R(\mathbf{q}) [1 - ih\lambda r_\Omega \Delta_\Omega^R(\mathbf{q}) + \dots] \\ &= 2iN\lambda h^2 \int_1 (F_1 - F_{1+\Omega}) \Delta_{\text{FL},\Omega}^R(\mathbf{q}) \\ &= \nu_0 N \frac{-ih\lambda\Omega}{\mathbf{q}^2 - ih\lambda\Omega}. \end{aligned} \quad (6.10)$$

where $\Delta_{\text{FL},\Omega}$ is defined in Eq. (5.28). The dynamical term cancels the static one at $\mathbf{q} = 0$ in Eq. (6.2), as required by the Ward identity. *Despite the strongly dissipative MFL self-energy, the semiclassical density-density response is purely diffusive, with the usual semiclassical diffusion constant defined via Eq. (4.36).*

The conductivity can be obtained via the continuity relation

$$\sigma^R = \lim_{\mathbf{q} \rightarrow 0} e^2 \frac{i\Omega}{\mathbf{q}^2} \pi^R(\Omega, \mathbf{q}) = e^2 N D \nu_0. \quad (6.11)$$

We thus recover the semiclassical Drude conductivity at zero temperature, consistent with Eq. (4.39).

VII. QUANTUM INTERACTION CORRECTIONS TO THE DENSITY RESPONSE FUNCTION

We now examine the interaction correction due to quantum interference to the density response function, analogous to the AA correction in disordered metals [17, 22, 52, 53, 84, 109]. In the following, we first discuss the vertex correction to the $q^{(2)}-V$ vertices shown in Fig. 8(b). We then study the effect of dynamical screening on the interaction. Finally, we present the Feynman diagrams responsible for the correction of density

response, by taking into account both vertex corrections and the effect of dynamical screening.

A. Vertex corrections to the $q^{(2)}-V$ coupling

We now consider vertex corrections to the $q^{(2)}-V$ (matrix field-source) coupling, due to interactions. The bare vertices are captured by the last two lines of S_{qV} in Eq. (5.26). Suppose the modified vertices are described by the following action

$$S_{q^{(2)}V}^{\text{eff}} = ih\lambda \int_{1-3, \Omega, \mathbf{p}, \mathbf{q}} \left\{ V_{\Omega}^{\text{cl}}(\mathbf{q}) \begin{bmatrix} (1 + \delta\Gamma_{V^{\text{cl}}}^{(1)})W_{ij;1,2}(\mathbf{p})W_{ji;2,1+\Omega}^{\dagger}(\mathbf{p} + \mathbf{q}) \\ -(1 + \delta\Gamma_{V^{\text{cl}}}^{(2)})W_{ij;1,2}^{\dagger}(\mathbf{p} + \mathbf{q})W_{ji;2,1+\Omega}(\mathbf{p}) \end{bmatrix} \right. \\ \left. + V_{-\Omega}^{\text{q}}(-\mathbf{q}) \begin{bmatrix} (1 + \delta\Gamma_{V^{\text{q}}}^{(1)})W_{ij;1+\Omega,2}(\mathbf{p} + \mathbf{q})W_{ji;2,1}^{\dagger}(\mathbf{p})F_1 \\ +(1 + \delta\Gamma_{V^{\text{q}}}^{(2)})W_{ij;1+\Omega,2}^{\dagger}(\mathbf{p})W_{ji;2,1}(\mathbf{p} + \mathbf{q})F_{1+\Omega} \end{bmatrix} \right\}, \quad (7.1)$$

where $\delta\Gamma_{V^{\text{cl/q}}}^{(i)}$ are vertex corrections that we are going to evaluate below. To facilitate the calculation of the density correlation function in the next subsection, we explicitly define the frequency passing through $V^{\text{cl/q}}$ as $\pm\Omega$.

We only consider the corrections originated from S_{intII} , since they are not suppressed by $1/N$. The corresponding Feynman diagrams are shown in Fig. 10. In each panel, the first term on the right-hand-side is the bare coupling term [see Fig. 8(b)] and the subsequent term is the corresponding vertex correction $\delta\Gamma_{V^{\text{cl/q}}}^{(i)}$. The shaded box in the diagrams denotes the vertex correction demonstrated in Fig. 9.

1. Vertex correction $\delta\Gamma_{V^{\text{cl}}}^{(i)}$

The diagrams responsible for $\delta\Gamma_{V^{\text{cl}}}^{(i)}$ are shown on the right-hand-side of Fig. 10(a). They are constructed using the vertices shown in Figs. 7(a) and (b). Using the corresponding Feynman rules, we find the leading order correction to be

$$\begin{aligned} \delta\Gamma_{V^{\text{cl}}}^{(1)} &= -2N\Gamma_2\lambda \int_{\varepsilon, \mathbf{k}} D_{\text{sp}, \varepsilon-1}^A(\mathbf{k})(F_{\varepsilon} - F_{\varepsilon+\Omega})\Delta_{\text{FL}, \varepsilon+\Omega, \varepsilon}^R(\mathbf{q}) \\ &= -2N\Gamma_2\lambda \int_{\varepsilon} \frac{-1}{8\pi} \ln \frac{\omega_c}{i(\varepsilon - \omega_1)} (F_{\varepsilon} - F_{\varepsilon+\Omega})\Delta_{\text{FL}, \Omega}^R(\mathbf{q}) \\ &\simeq -ih\lambda\bar{g}^2\Omega \ln \frac{\omega_c}{|\Omega/2 + \omega_1|} \Delta_{\text{FL}, \Omega}^R(\mathbf{q}) + \dots, \end{aligned} \quad (7.2)$$

where ... are subleading terms. Here, we have made use of the result in Eq. (6.10). The modified coupling is thus

$$1 + \delta\Gamma_{V^{\text{cl}}}^{(1)} \simeq \left(\mathbf{q}^2 - ih\lambda\Omega - ih\lambda\bar{g}^2\Omega \ln \frac{\omega_c}{|\omega_1|} \right) \Delta_{\text{FL}, \Omega}^R(\mathbf{q}). \quad (7.3)$$

The correction $\delta\Gamma_{V^{\text{cl}}}^{(2)}$ can be computed in a similar fashion by considering the Feynman diagrams shown in Fig. 10 (b), which involve the vertices shown in Figs. 7(a)

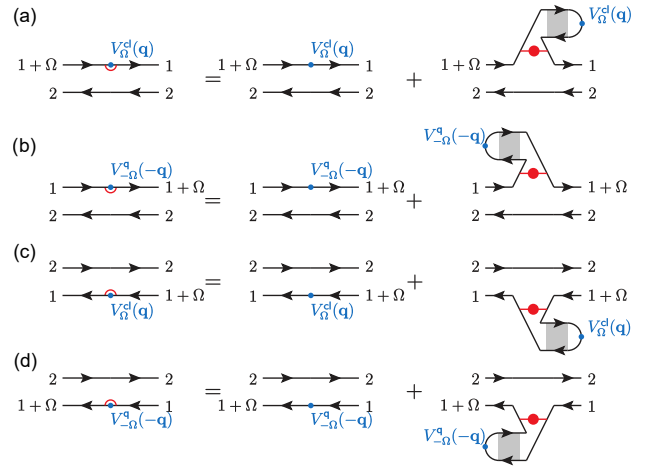


FIG. 10. The effective coupling between $q^{(2)}$ and V [Eq. (7.1)]. The blue dot represents external scalar potential $V^{\text{cl/q}}$. The dressed vertex is indicated by an additional red semicircle. In each subfigure, the first term on the right hand side is the bare coupling and the subsequent diagram is the vertex correction for (a) $\delta\Gamma_{V^{\text{cl}}}^{(1)}$, (b) $\delta\Gamma_{V^{\text{q}}}^{(1)}$, (c) $\delta\Gamma_{V^{\text{cl}}}^{(2)}$, and (d) $\delta\Gamma_{V^{\text{q}}}^{(2)}$. The shaded box denotes the vertex correction demonstrated in Fig. 9.

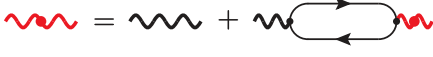


FIG. 11. Diagrammatic representation of the dynamically screened bosonic propagator D_{scr}^R under random phase approximation (RPA). The black wavy line (red wavy line with a dot) represents the interaction without (with) dynamical screening.

and (c). Following the lines of calculations as above, we find that

$$\delta\Gamma_{V^{\text{cl}}}^{(2)} = \delta\Gamma_{V^{\text{cl}}}^{(1)}, \quad (7.4)$$

as expected.

2. Vertex correction $\delta\Gamma_{V^{\text{q}}}^{(i)}$

Next, we consider the correction $\delta\Gamma_{V^{\text{q}}}^{(1)}$, which is diagrammatically described in Figs. 10(b). The diagrams are constructed using the vertices shown in Figs. 7(a) and (d). By restricting our attention to terms with the same thermal factor (F_1) as the bare coupling, we find

$$\begin{aligned} \delta\Gamma_{V^{\text{q}}}^{(1)} &= -2N\Gamma_2\lambda \int_{\epsilon, \mathbf{k}} \Delta_{\text{FL}, \epsilon+\Omega, \epsilon}^R(\mathbf{q}) \\ &\times \left[-F_{\epsilon+\Omega} D_{\text{sp}, \epsilon-1}^A(\mathbf{k}) + F_{\epsilon} D_{\text{sp}, \epsilon-1}^R(\mathbf{k}) \right] \\ &= -2N\Gamma_2\lambda \int_{\epsilon} \frac{-1}{8\pi} \ln \frac{\omega_c}{|\epsilon - \omega_1|} (F_{\epsilon} - F_{\epsilon+\Omega}) \Delta_{\text{FL}, \Omega}^R(\mathbf{q}) + \dots \\ &\simeq -ih\lambda\bar{g}^2\Omega \ln \frac{\omega_c}{|\Omega/2 + \omega_1|} \Delta_{\text{FL}, \Omega}^R(\mathbf{q}). \end{aligned} \quad (7.5)$$

Hence, the modified coupling is again

$$1 + \delta\Gamma_{V^{\text{q}}}^{(1)} \simeq \left(\mathbf{q}^2 - ih\lambda\Omega - ih\lambda\bar{g}^2\Omega \ln \frac{\omega_c}{|\omega_1|} \right) \Delta_{\text{FL}, \Omega}^R(\mathbf{q}). \quad (7.6)$$

Lastly, for $\delta\Gamma_{V^{\text{q}}}^{(2)}$, we have to consider a similar set of diagrams shown in Fig. 10(d) which are constructed with the vertices in Figs. 7(a) and (e). This time, we focus on terms with thermal factor $F_{1+\Omega}$, as in the bare coupling. Evaluating the diagrams explicitly, we find

$$\delta\Gamma_{V^{\text{q}}}^{(2)} = \delta\Gamma_{V^{\text{q}}}^{(1)}, \quad (7.7)$$

which is again what we expect.

B. Dynamical screening

As in the case of disordered Fermi liquid, dynamical screening is crucial for evaluating the interaction correction to the density response and conductivity [43, 44, 53,

84, 91], particularly in the temperature $T \rightarrow 0$ limit. In the following, we treat dynamical screening under the random phase approximation (RPA). The dynamically screened bosonic propagator is represented by a red wavy line in Fig. 11. This effectively modifies the bosonic propagator in the quartic vertices in Fig. 6(c). Such vertex corrections can alternatively be obtained by joining the cubic and quadratic vertices in Figs. 6(a)–(b). Since the bosons are quantum critical, mass terms in the self-energy can be fine-tuned to zero at $T = 0$. We therefore throw away the constant term $\sim \nu_0$, which is generated from terms $\sim G^R G^R + G^A G^A$ during the gradient expansion [43, 44], in the polarization bubble [as already discussed at the saddle-point level, below Eq. (4.21)].

Explicitly, the retarded bosonic self-energy due to dynamical screening at $T = 0$ is

$$\begin{aligned} \Pi_{\text{scr}}^R(\Omega, \mathbf{q}) &= \Gamma_1\lambda \int_1 \Delta_{1+\Omega, 1}^R(\mathbf{q})(F_1 - F_{1+\Omega}) \\ &\simeq -\frac{2i}{\pi N} \frac{h^2 g^2 \lambda \Omega}{\mathbf{q}^2 - ih\lambda\Omega - ih\lambda r_{\Omega}}. \end{aligned} \quad (7.8)$$

The retarded component of the screened bosonic propagator under RPA is then

$$\begin{aligned} D_{\text{scr}}^R(\Omega, \mathbf{q}) &= [(D_{\text{sp}}^R)^{-1}(\Omega, \mathbf{q}) - \Pi_{\text{scr}}^R(\Omega, \mathbf{q})]^{-1} \\ &= -\frac{1}{2(\mathbf{q}^2 + m_b^2 - i\alpha\Omega) + \Pi_{\text{scr}}^R(\Omega, \mathbf{q})}. \end{aligned} \quad (7.9)$$

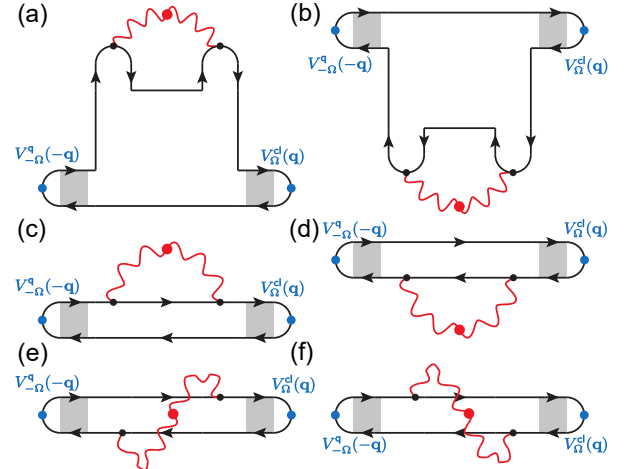


FIG. 12. The set of type-A diagrams contributing to the interaction correction of the density response function to leading order of $1/N$ and λ . The blue dots are vertices between the diffuson and scalar potential. The red wavy line is the dynamically screened interaction [Fig. 11]. The gray box represents the vertex correction shown in Fig. 9.

C. Feynman diagrams for the interaction correction

We divide the leading order (in λ and $1/N$) interaction correction to the retarded density response into two types, A and B,

$$\delta\pi^R(\Omega, \mathbf{q}) = \delta\pi_{\text{type A}}^R(\Omega, \mathbf{q}) + \delta\pi_{\text{type B}}^R(\Omega, \mathbf{q}), \quad (7.10)$$

which are diagrammatically depicted in Figs. 12–14. The type-A diagrams [Fig. 12] involve contributions from the self-energy correction of the diffuson. Meanwhile, the type-B diagrams [Fig. 13] are analogous to the wavefunction renormalization correction in the context of the disordered FL [44]. They are obtained by considering the vertices in Figs. 8(a)–(b).

In both the type A and B diagrams, vertex corrections and the effect of dynamical screening have been taken into account. In particular, the red wavy line represents the dynamically screened interaction in Fig. 11. On the other hand, the shaded diffuson denotes the vertex correction shown in Fig. 9, while the scalar potential vertices with a red semicircle are the vertex corrections considered in Fig. 10. Note, however, that two of the diffusons in Figs. 12(a)–(b) and the diffusons in the middle of the interaction line in Figs. 12(c)–(f) and 13 are not shaded since those corrections are suppressed by $1/N$.

Finally, there is an additional set of diagrams [Fig. 14] formed with the purely quadratic vertices in Fig. 8(b). However, they are summed to zero and thus we do not discuss them further. These “donut” diagrams are important in non-standard universality classes [44].

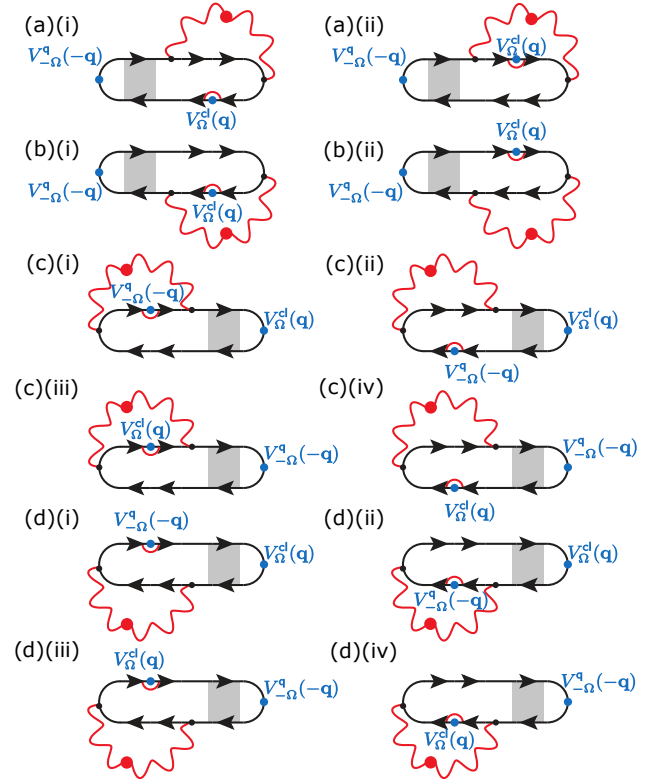


FIG. 13. The set of type-B diagrams contributing to the interaction correction of the density response function to leading order of $1/N$ and λ . The convention here is the same as Fig. 12. The red semicircle denotes the vertex corrections shown in Fig. 10.

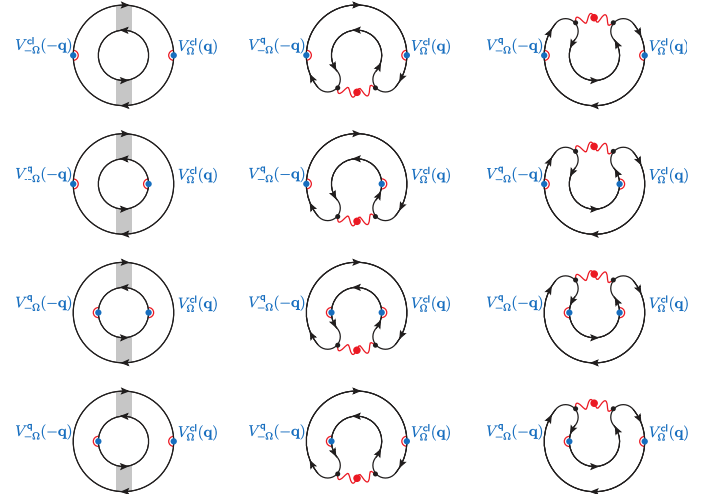


FIG. 14. The set of type-C diagrams for the interaction correction of the density response function to leading order of $1/N$ and λ . They are summed to zero.

1. Type-A diagrams

After summing the diagrams in Fig. 12 and using the definition in Eq. (6.1), we find

$$\delta\pi_{\text{type A}}^R(\Omega, \mathbf{q}) = -\frac{(2h)^2\lambda}{2i} \int_{\omega} (F_{\omega} - F_{\omega+\Omega}) [\Delta_{\text{FL};\Omega}^R(\mathbf{q})]^2 \left\{ \sum_{t=a,b,c,d} [\Sigma_{W;i,j;j,i}^{12(t)}(\mathbf{q})]_{\omega+\Omega,\omega;\omega,\omega+\Omega} \delta_{ij} \right. \\ \left. + \sum_{t=e,f} [\Sigma_{W;i,i;j,j}^{12(t)}(\mathbf{q})]_{\omega+\Omega+\xi,\omega+\xi;\omega,\omega+\Omega} \right\}, \quad (7.11)$$

where $\Delta_{\text{FL};\Omega}^R(\mathbf{q})$ is given by Eq. (5.28) and Σ_W represents the self-energy of the matrix field \hat{W} . The subscripts in Σ_W indicate the flavor indices and the external frequencies. Meanwhile, the superscript in it indicates the correspondence to the diagrams in Fig. 12. In particular, the frequency-diagonal self-energies are given by

$$[\Sigma_{W;i,j;j,i}^{12(a)}(\mathbf{q})]_{\omega+\Omega,\omega;\omega,\omega+\Omega} = -\frac{\lambda^2}{2} N\Gamma_1 \int_{\xi,\mathbf{k}} (F_{\omega+\Omega-\xi} - F_{\omega+\Omega}) D_{\text{scr},\xi}^R(\mathbf{k}) \left\{ [\Delta_{\omega+\Omega,\omega}^R(\mathbf{q})]^{-1} [\Delta_{\omega+\Omega,\omega+\Omega-\xi}^R(\mathbf{k})]^2 \right. \\ \left. + \Delta_{\omega+\Omega,\omega+\Omega-\xi}^R(\mathbf{k}) \right\}, \quad (7.12)$$

$$[\Sigma_{W;i,j;j,i}^{12(b)}(\mathbf{q})]_{\omega+\Omega,\omega;\omega,\omega+\Omega} = -\frac{\lambda^2}{2} N\Gamma_1 \int_{\xi,\mathbf{k}} (F_{\omega} - F_{\omega+\xi}) D_{\text{scr},\xi}^R(\mathbf{k}) \left\{ [\Delta_{\omega+\Omega,\omega}^R(\mathbf{q})]^{-1} [\Delta_{\omega+\xi,\omega}^R(\mathbf{k})]^2 \right. \\ \left. + \Delta_{\omega+\xi,\omega}^R(\mathbf{k}) \right\}, \quad (7.13)$$

$$[\Sigma_{W;i,j;j,i}^{12(c)}(\mathbf{q})]_{\omega+\Omega,\omega;\omega,\omega+\Omega} = -\frac{\lambda^2}{2} N\Gamma_1 \int_{\xi,\mathbf{k}} \Delta_{\omega+\Omega+\xi,\omega}^R(\mathbf{k} + \mathbf{q}) \left[D_{\text{scr},\xi}^R(\mathbf{k}) \left(\frac{1}{F_{\xi}} + F_{\omega+\Omega} \right) \right. \\ \left. + D_{\text{scr},\xi}^A(\mathbf{k}) \left(-\frac{1}{F_{\xi}} + F_{\omega+\Omega+\xi} \right) \right], \quad (7.14)$$

and

$$[\Sigma_{W;i,j;j,i}^{12(d)}(\mathbf{q})]_{\omega+\Omega,\omega;\omega,\omega+\Omega} = -\frac{\lambda^2}{2} N\Gamma_1 \int_{\xi,\mathbf{k}} \Delta_{\omega+\Omega,\omega-\xi}^R(\mathbf{k} + \mathbf{q}) \left[D_{\text{scr},\xi}^R(\mathbf{k}) \left(\frac{1}{F_{\xi}} - F_{\omega} \right) \right. \\ \left. + D_{\text{scr},\xi}^A(\mathbf{k}) \left(-\frac{1}{F_{\xi}} + F_{\xi-\omega} \right) \right]. \quad (7.15)$$

On the other hand, the frequency-off-diagonal self-energies are

$$[\Sigma_{W;i,i;j,j}^{12(e)}(\mathbf{q})]_{\omega+\Omega+\xi,\omega+\xi;\omega,\omega+\Omega} = -\frac{\lambda^2}{2} \Gamma_1 \int_{\xi,\mathbf{k}} \Delta_{\omega+\Omega,\omega-\xi}^R(\mathbf{k} + \mathbf{q}) \left[D_{\text{scr},\xi}^R(\mathbf{k}) \left(-\frac{1}{F_{\xi}} - F_{\omega+\Omega-\xi} \right) \right. \\ \left. + D_{\text{scr},\xi}^A(\mathbf{k}) \left(\frac{1}{F_{\xi}} - F_{\xi-\omega} \right) \right] \quad (7.16)$$

and

$$[\Sigma_{W;i,i;j,j}^{12(f)}(\mathbf{q})]_{\omega+\Omega+\xi,\omega+\xi;\omega,\omega+\Omega} = -\frac{\lambda^2}{2} \Gamma_1 \int_{\xi,\mathbf{k}} \Delta_{\omega+\Omega+\xi,\omega}^R(\mathbf{k} + \mathbf{q}) \left[D_{\text{scr},\xi}^R(\mathbf{k}) \left(-\frac{1}{F_{\xi}} + F_{\omega+\xi} \right) \right. \\ \left. + D_{\text{scr},\xi}^A(\mathbf{k}) \left(\frac{1}{F_{\xi}} - F_{\omega+\Omega+\xi} \right) \right]. \quad (7.17)$$

Here, the momentum (\mathbf{k}) integrals are performed over the whole space and the frequency (ξ) integrals are bounded in the ultraviolet by $\Lambda = \gamma_{\text{el}}$. We will perform integrals to logarithmic accuracy in the ultraviolet cutoff Λ by expanding in the external frequency Ω and momentum \mathbf{q} .

2. Type-B diagrams

The evaluation of the type-B diagrams in Fig. 13 is straightforward yet tedious. We leave the detailed expressions of the diagrams to Appendix D. In the large- N limit, the total contribution of the type-B diagrams to the density

response can be approximated as

$$\delta\pi_{\text{type B}}^R(\Omega, \mathbf{q}) = -\frac{C}{2i} \int_{\xi, \omega, \mathbf{k}} \Delta_{\text{FL};\Omega}^R(\mathbf{q}) [\Delta_{\xi,0}^R(\mathbf{k})]^2 D_{\text{scr},\xi}^R(\mathbf{k}) \left[\frac{(F_{\omega+\xi} + F_{\omega+\Omega} - F_{\omega} - F_{\omega+\Omega-\xi})(F_{\omega} - F_{\omega+\Omega}) \Phi_1}{+ (-F_{\omega+\xi-\Omega} + F_{\omega+\xi} + F_{\omega+\Omega} - F_{\omega})(F_{\omega} - F_{\omega+\xi}) \Phi_2} \right] \quad (7.18)$$

where $C = -2h^2\lambda^3\Gamma_1 N^2 = -4iNh^4g^2\lambda^3$,

$$\Phi_1(\Omega, \xi, \mathbf{q}) = \left(\mathbf{q}^2 - ih\lambda\Omega - ih\lambda\bar{g}^2\Omega \ln \frac{\omega_c}{|\xi|} \right) \Delta_{\text{FL};\Omega}^R(\mathbf{q}), \quad (7.19)$$

and

$$\Phi_2(\Omega, \mathbf{q}) = \left(\mathbf{q}^2 - ih\lambda\Omega - ih\lambda\bar{g}^2\Omega \ln \frac{\omega_c}{|\Omega/2|} \right) \Delta_{\text{FL};\Omega}^R(\mathbf{q}). \quad (7.20)$$

The factor Φ_i is due to the vertex corrections discussed in Sec. VII A. The first line in the big square parenthesis is originated from the diagrams in Figs. 13(a)–(b), while the second line in it is originated from the diagrams in Figs. 13(c)–(d). Here, we only retain terms in leading order of external frequency Ω and momentum \mathbf{q} .

3. Total contribution

After summing the expressions in Eqs. (7.11) and (7.18) in leading order of \mathbf{q} and Ω , we have

$$\delta\pi^R(\Omega, \mathbf{q}) = \frac{4C}{2i} \mathbf{q}^2 [\Delta_{\text{FL};\Omega}^R(\mathbf{q})]^2 \int_{\xi, \mathbf{k}} (-B_{\xi-\Omega} + B_{\xi}) \mathbf{k}^2 [\Delta_{\xi,0}^R(\mathbf{k})]^3 D_{\text{scr},\xi}^R(\mathbf{k}), \quad (7.21)$$

where

$$B_{\omega} = \frac{\omega}{\pi} \coth \frac{\omega}{2T} = \int_{\omega'} (1 - F_{\omega+\omega'} F_{\omega'}). \quad (7.22)$$

Note that $\delta\pi^R(\Omega, \mathbf{q} \rightarrow 0) = 0$, as required by the Ward identity. This is further supported with our numerics in Appendix E. This shows that the vertex corrections we considered are essential for obtaining the correct density response function, due to the anomalous MFL self-energy term in the bare diffuson, which arises from the interplay between disorder and interactions with the quantum-critical collective modes. Without such corrections, particle conservation would be violated.

The interaction correction to conductivity can be found using the continuity relation

$$\sigma_{\text{AA}}(\Omega) = \lim_{\mathbf{q} \rightarrow 0} e^2 \frac{i\Omega}{\mathbf{q}^2} \delta\pi^R(\Omega, \mathbf{q}). \quad (7.23)$$

In the dc limit $\Omega \rightarrow 0$, we find

$$\sigma_{\text{AA},\text{dc}} = 2ie^2g^2\lambda(2h)^2N \int_{\xi, \mathbf{k}} \frac{\partial}{\partial \xi} \left(\frac{\xi}{\pi} \coth \frac{\xi}{2T} \right) \mathbf{k}^2 [\Delta_{\xi,0}^R(\mathbf{k})]^3 D_{\text{scr},\xi}^R(\mathbf{k}). \quad (7.24)$$

This is the main result of this section. In the FL limit, Eq. (7.24) reduces to the well-known formula for the AA correction when the anomalous diffuson propagator is replaced by the normal one [22, 43, 53, 84].

D. Evaluation of the AA correction

1. Finite temperature, dc limit

Here we compute the AA correction in Eq. (7.24). At temperatures $T \gtrsim g^2/N$, we can ignore the effects of dynamical screening in the boson propagator $D_{\text{scr},\xi}^R(\mathbf{k})$. Then Eq. (7.24) takes the form

$$\sigma_{\text{AA},\text{dc}} = -\frac{Ni\lambda(2ehg)^2}{\pi} \int_{\xi} \tilde{F}(\xi) \int_0^{\infty} \frac{dx}{4\pi} \frac{x}{\{x - ih\lambda[\xi - \Sigma_{\text{sp}}^R(\xi)]\}^3 \{x - i\alpha\xi + m_{\text{b}}^2\}}, \quad (7.25)$$

where we have changed variables to $x \equiv k^2$, $\Sigma_{\text{sp}}^R(\xi)$ is the retarded MFL fermion self-energy at finite temperature [Eqs. (1.3) and (4.28)], and the thermal factor is

$$\tilde{F}(\xi) = \frac{\partial}{\partial \xi} \left[\xi \coth \left(\frac{\xi}{2T} \right) \right] \simeq \tanh \left(\frac{\xi}{3T} \right). \quad (7.26)$$

Performing the squared-momentum x -integral in Eq. (7.25), we can cast the AA correction as follows:

$$\sigma_{\text{AA},\text{dc}} = \frac{Ne^2}{2\pi^2} \left(\frac{g^2}{T} \right) \mathcal{G}_{\text{AA}}, \quad T \gtrsim g^2/N, \quad (7.27)$$

where

$$\mathcal{G}_{\text{AA}} = \left(\frac{h}{\pi\alpha_m} \right) \mathcal{I}_1 \left[D\alpha_m, D\alpha, \bar{g}^2, \log \left(\frac{\omega_c}{T} \right) \right], \quad (7.28)$$

and the full expression for the kernel \mathcal{I}_1 is given by Eq. (F1) in Appendix F. This kernel depends on dimensionless combinations of the semiclassical diffusion constant D [Eq. (4.36)], the boson inverse-diffusion constant α [Eqs. (4.21) and (4.25)], and the boson thermal mass coefficient α_m [Eq. (4.24)]. Through the MFL self-energy [Eq. (4.28)], it also depends separately on \bar{g}^2 and the temperature (via the logarithm). Eq. (7.27) gives the second term in the square brackets in Eq. (1.4) in the Introduction.

A simple limiting case takes $\alpha = 0$ (static, massive boson) and $\bar{g}^2 = 0$ (the Fermi liquid case, ignoring the MFL self-energy). Then

$$\mathcal{I}_1(D\alpha_m) = \int_0^{\infty} dy \tanh \left(\frac{yD\alpha_m}{3} \right) \left[\frac{(1-3y^2)(y^2+1-\pi y) + 2y(y^3-3y)\ln(y)}{y(y^2+1)^3} \right]. \quad (7.29)$$

This kernel is independent of N and temperature T . The integration is finite, with a result that is logarithmic in $D\alpha_m$ for values of this parameter much larger than one. This is the usual logarithm associated to AA corrections in 2D [20, 21]. Here there is no explicit dependence on a UV cutoff, because we have retained the formally irrelevant k^2 momentum-dependence of the boson propagator [Eq. (4.25) with $\alpha = 0$].

In the general case with nonzero α , retaining the MFL self-energy, the kernel \mathcal{I}_1 exhibits weak temperature dependence. In Figs. 15–17 we plot $\mathcal{G}_{\text{AA}} = \mathcal{I}_1$ (with $h/\pi\alpha_m \rightarrow 1$), comparing the result to the static, Fermi liquid case in Eq. (7.29).

So far we have ignored the effects of dynamical screening in the bosonic propagator. The latter becomes important at very low temperatures, or to determine the frequency-dependent ac conductivity at zero temperature. The bosonic propagator in Eq. (7.9) can be approximated as

$$D_{\text{scr}}^R(\xi, \mathbf{k}) \simeq -\frac{1}{2} \frac{\mathbf{k}^2 - i\mathbf{a}}{\mathbf{k}^4 + (m_{\text{b}}^2 - i\mathbf{a})\mathbf{k}^2 - i\mathbf{b}}, \quad (7.30)$$

where we have defined

$$\mathbf{a}(\xi) = h\lambda\xi \left(1 + \bar{g}^2 \ln \frac{\omega_c}{|\xi|} \right), \quad (7.31)$$

$$\mathbf{b}(\xi) = b\xi, \quad b = \frac{h^2 g^2 \lambda}{\pi N}. \quad (7.32)$$

The AA conductivity correction can be written as

$$\sigma_{\text{AA},\text{dc}} = \frac{2e^2 \lambda (2h)^2 g^2 N}{8\pi^3} \int_0^{\infty} d\xi \tilde{F}(\xi) \mathcal{M}(\mathbf{a}, \mathbf{b}, m_{\text{b}}^2), \quad (7.33)$$

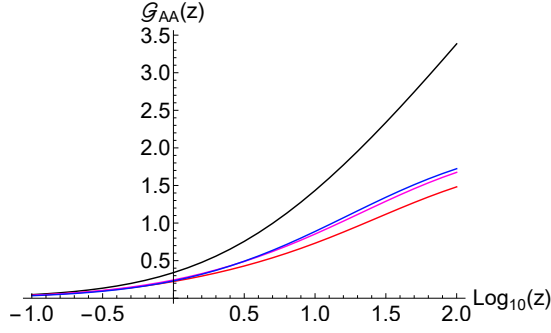


FIG. 15. Linear-log plot of the coefficient \mathcal{G}_{AA} that determines the AA correction [Eq. (7.27), (7.28) and (F1)], as a function of the variable $z \equiv D\alpha_m \equiv f D\alpha$, for fixed f and \bar{g}^2 and variable T/ω_c . Here $f = 0.1$ and $\bar{g}^2 = 0.5$. The curves have $T/\omega_c = \{0.25, 0.5, 0.75\}$ (blue to red, top to bottom). For comparison, the black curve is the $\alpha = 0$, $\bar{g}^2 = 0$ (static boson, Fermi-liquid electron) case [Eq. (7.29)]. We set the prefactor $h/\pi\alpha_m = 1$ in Eq. (7.28).

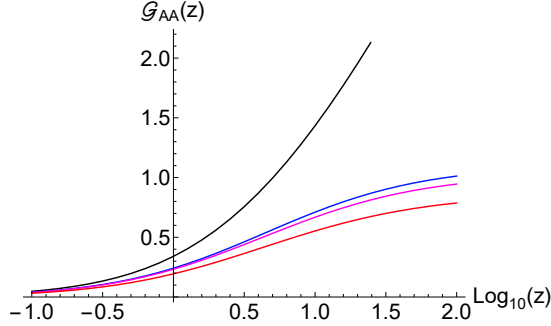


FIG. 16. Same as Fig. 15, but for $f = 0.5$ and $\bar{g}^2 = 0.5$. The curves have $T/\omega_c = \{0.25, 0.5, 0.75\}$ (blue to red, top to bottom). For comparison, the black curve is the $\alpha = 0$, $\bar{g}^2 = 0$ (static boson, Fermi-liquid electron) case [Eq. (7.29)].

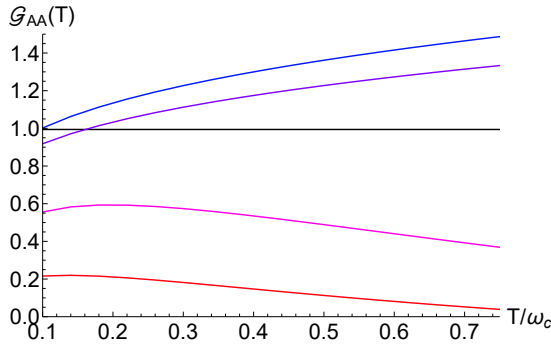


FIG. 17. Plot of the coefficient \mathcal{G}_{AA} that determines the AA correction [Eq. (7.27), (7.28) and (F1)], as a function of the temperature T , for fixed $D\alpha_m$ and variable $D\alpha$, \bar{g}^2 . All curves have $D\alpha_m = 5$. The horizontal black curve is the $\alpha = 0$, $\bar{g}^2 = 0$ (static boson, Fermi-liquid electron) case [Eq. (7.29)]. The general results have $\{D\alpha, \bar{g}^2\} = \{\{0.01, 0.1\}, \{0.1, 0.1\}, \{0.1, 0.5\}, \{0.5, 1\}\}$ (blue to red, top to bottom). We set the prefactor $h/\pi\alpha_m = 1$ in Eq. (7.28).

where the kernel

$$\mathcal{M}(\mathbf{a}, \mathbf{b}, m_b^2) = \text{Im} \int_0^\infty dx \frac{x}{(x - i\mathbf{a})^2 [x^2 + (m_b^2 - i\mathbf{a})x - i\mathbf{b}]}. \quad (7.34)$$

The x -integral in $\mathcal{M}(\mathbf{a}, \mathbf{b}, m_b^2)$ can be done exactly, with the detailed expression given in Appendix F. To make further analytical progress, we approximate the thermal factor as

$$\tilde{F}(\xi) \simeq \frac{\xi}{3T} \theta(3T - \xi) + \theta(\xi - 3T), \quad \xi > 0, \quad (7.35)$$

where $\theta(x)$ is the Heaviside step function. We assume a large cutoff ω_c such that we can approximate

$$\mathbf{a}(\xi) \simeq h\lambda\xi \left(1 + \bar{g}^2 \ln \frac{\omega_c}{T}\right) \equiv a\xi. \quad (7.36)$$

With above approximations, the frequency integral can be performed exactly and we obtain

$$\sigma_{AA,dc}(T) \simeq \frac{2e^2\lambda(2h)^2g^2N}{8\pi^3} \mathcal{I}_2(a, b, m_b^2, T), \quad (7.37)$$

where the full expression of kernel \mathcal{I}_2 is given by Eq. (F5) in Appendix F.

The low-temperature behavior ($T \ll \gamma_{el}$) of the kernel \mathcal{I}_2 is governed by the relative strength between the thermal mass m_b^2 and dynamical the dynamical screening coupling $\sim g^2/N$. Specifically, we have

$$\mathcal{I}_2(a, b, m_b^2, T) \simeq \begin{cases} \frac{\pi}{24a^2T}, & T \gg g^2/N, \\ \frac{1}{4b} \ln^2\left(\frac{a^2T}{b}\right), & T \ll g^2/N. \end{cases} \quad (7.38)$$

Hence, at low temperatures the AA correction acquires the following simple asymptotic form

$$\sigma_{AA,dc} \simeq \frac{N^2e^2}{4\pi^2} \ln^2\left(\frac{N\lambda}{4\pi} \bar{g}^2 t\right), \quad T \ll g^2/N, \quad (7.39)$$

where $t \equiv T/\gamma_{el}$, as in Eq. (1.4).

In the $T \gtrsim g^2/N$ regime, the quantum relaxational thermal mass is the major screening mechanism for the interaction, leading to the AA correction quoted in Eqs. (1.4) and (7.27). On the other hand, for $T \ll g^2/N$, thermal screening is no longer effective and dynamical screening becomes important. In both cases, the AA correction is positive, indicating its antilocalizing nature. At low temperature, the semiclassical MFL contribution [Eq. (4.34)] is insufficient to fully describe the electric transport and one must take the AA correction into account.

Our low-temperature result in Eq. (7.39) should be compared with the AA conductance correction in a disordered Fermi liquid subjected to $SU(N)$ ferromagnetic

spin-spin interactions

$$\sigma_{\text{AA,dc}}^{\text{FL}}(T) \propto \frac{N^2 e^2}{2\pi^2} \ln\left(\frac{\gamma_{\text{el}}}{T}\right), \quad (7.40)$$

valid to leading order in N . Eq. (7.40) is proportional to N^2 due to the exchange carrier-carrier scattering among fermions with different flavors; in this case, the AA correction diverges as log instead of squared-log [47, 52].

2. Zero temperature limit with finite external frequency

At $T = 0$ with finite external frequency Ω , we evaluate the AA correction by making use of Eqs. (7.21) and (7.23). For small Ω , we have

$$\begin{aligned} \sigma_{\text{AA}}(\Omega) &\simeq \frac{2e^2 \lambda (2h)^2 g^2}{8\pi^3} \\ &\times \int_0^\infty d\xi \left[\frac{2\xi}{\Omega} \theta(\Omega/2 - \xi) + \theta(\xi - \Omega/2) \right] \mathcal{M}_0(\mathbf{a}, \mathbf{b}) \end{aligned} \quad (7.41)$$

where $\theta(x)$ is the Heaviside step function and the kernel

$$\mathcal{M}_0(\mathbf{a}, \mathbf{b}) = \mathcal{M}(\mathbf{a}, \mathbf{b}, 0) = \frac{1}{4\mathbf{b}} R\left(\frac{\mathbf{a}^2}{\mathbf{b}}\right), \quad (7.42)$$

with

$$\begin{aligned} R(x) &= -\pi x - 2 \ln(e^2 x) \\ &+ 2 \operatorname{Im} \left[\frac{x - 3i}{\sqrt{1 - 4i/x}} \ln \frac{1 - \sqrt{1 - 4i/x}}{1 + \sqrt{1 - 4i/x}} \right]. \end{aligned} \quad (7.43)$$

By making the same approximation as in Eq. (7.36), we can perform the remaining frequency integral exactly, resulting in

$$\sigma_{\text{AA}}(\Omega) \simeq \frac{2e^2 \lambda (2h)^2 g^2 N}{8\pi^3} \frac{1}{4} \mathcal{R}(a, b, \Omega), \quad (7.44)$$

where

$$\mathcal{R}(a, b, \Omega) = \mathcal{R}_1(a, b, \Omega) + \mathcal{R}_2(a, b, \Omega) \quad (7.45)$$

with

$$\begin{aligned} \mathcal{R}_1(a, b, \Omega) &= \frac{2}{a^2 \Omega} \int_0^{x_0} dx R(x) \\ &= -\frac{x_0}{a^2 \Omega} \left[4 + \pi x_0 + 4 \ln x_0 - 2x_0 \operatorname{Im} \left(\varphi \ln \frac{1 - \varphi}{1 + \varphi} \right) \right] \end{aligned} \quad (7.46)$$

and

$$\begin{aligned} \mathcal{R}_2(a, b, \Omega) &= \frac{1}{b} \int_{x_0}^\infty dx \frac{1}{x} R(x) \\ &= \frac{1}{b} \left\{ 4 - \frac{\pi^2}{4} + \pi x_0 + 4 \ln x_0 + \ln^2 x_0 \right. \\ &\quad \left. + 4x_0 \operatorname{Im} [\varphi \tanh^{-1} \varphi] - 4 \operatorname{Re} (\tanh^{-1} \varphi)^2 \right\}. \end{aligned} \quad (7.47)$$

In the above expressions, we defined

$$\varphi = \sqrt{\frac{x_0 - 4i}{x_0}}, \quad x_0 = \frac{a^2 \Omega}{2b}. \quad (7.48)$$

In the small Ω limit, we find

$$\sigma_{\text{AA}}(\Omega) \sim N^2 \ln^2 \Omega. \quad (7.49)$$

VIII. DISCUSSION AND OUTLOOK

In this paper, we have investigated the combined effects of disorder and quantum-critical interactions on the dc electric transport by incorporating both the semiclassical contribution and the Altshuler-Aronov (AA) quantum correction. Through self-consistently solving the saddle-point equations in the large- N limit at finite temperature, we uncovered the quantum relaxational nature of the bosons and a MFL self-energy for the fermions, signaling a breakdown of the quasiparticle picture. We showed that such MFL self-energy results in a linear- T resistivity, in addition to the Drude contribution due to semiclassical impurity scattering. Even though the concept of quasiparticle is no longer well-defined, we argued that the hydrodynamic modes corresponding to the diffusive motion of electrons can remain quantum coherent. We demonstrated that the quantum interference among these hydrodynamic modes results in an antilocalizing AA correction, which depends on temperature T as (i) N/T when thermal screening for the interaction dominates, and (ii) $N^2 \ln^2 T$ when dynamical screening for the interaction becomes important at very low temperatures. We found that the AA correction effectively shifts the resistivity curve downward and continues the MFL phenomenology to low temperature, as shown in Fig. 1. As temperature approaches zero, the resistivity is driven to zero by the singularity in the AA correction.

We have also elucidated how the Ward identity for particle conservation can be satisfied by introducing a new interaction term in the MFL-FNLsM, which also includes the MFL fermion self-energy. By incorporating various vertex corrections, we showed in leading order of disorder and $1/N$ that our density response function fulfills the Ward identity at both the classical and quantum levels at $T = 0$. The fulfillment by the quantum correction is further supported by numerics.

We comment on a few differences between the present work and some of the existing ones. First, instead of starting with the clean NFL fixed point [40], the self-energies for the fermions and bosons are dictated by a set of finite-temperature saddle-point equations. These capture the effects of disorder, Yukawa interactions, and thermal screening. Second, the randomness of our model enters through the impurity potential instead of the Yukawa coupling [34, 38]. Our model is thus manifestly $\text{SU}(N)$ invariant for a fixed realization of disorder. As a consequence, the $\text{SU}(N)$ flavor polarization forms a slow

hydrodynamic mode that survives on time and length scales larger than those set by the impurity scattering. These slow flavor degrees of freedom are responsible for the AA correction in Eq. (1.4).

Our results are potentially applicable to physical systems with fermions coupled to magnetic fluctuations near a the QCP, although N is practically 2 in reality. For instance, the Ising nematic transition (ferromagnetic QCP) and linear- T resistivity have indeed been observed in iron-based superconductors [3, 4] (some heavy fermion compounds [12, 13]). Recently, linear- T resistivity has also been reported in a non-superconducting iron-pnictide $\text{Ba}(\text{Fe}_{1/3}\text{Co}_{1/3}\text{Ni}_{1/3})_2\text{As}_2$, which possesses a ferromagnetic QCP at zero temperature and magnetic field [110]. Intriguingly, at zero field, the linear- T resistivity demonstrates a downturn at low temperature which is in qualitative agreement with the AA quantum correction discussed in this work, (*cf.* Fig. 1). Our calculations are also potentially relevant for Si metal-oxide-semiconductor field-effect transistors, in which formation of spin droplets was reported in the insulating phase [111, 112]. In particular, linear- T resistivity was reported in the low-temperature regime for samples with low carrier densities [112]. It would be interesting to look into the resistivity at even lower temperature in these compounds to verify the quantum correction.

We close by mentioning a couple of interesting avenues and open questions that warrant further investigations. (i) It is desirable to carry out an RG analysis of our MFL-FNLsM and clarify the stability of the interaction term. Specifically, a key question is whether there is *multifractal enhancement* for the interaction [27–30, 85, 86]. Based on our quantum correction in Eq. (7.39), we expect to have double-logarithmic terms in the RG equations. While double-logarithmic divergences are not common in conventional field theories

[113], they have been reported in the studies of zero-bias anomaly in disordered metals [46, 53] and bilayer graphene [114], and can arise due to subtle variations in the infrared structure of the quantum-loop propagators. A systematic RG analysis for the MFL-FNLsM, incorporating higher-loop contributions, might be conveniently performed with the background field method [92]. (ii) It would be interesting to extend our MFL-FNLsM to other symmetry classes. In particular, the current work assumes weakly broken time-reversal symmetry, and neglects the contribution of Cooperons which give rise to the weak-localization correction [17, 43, 44, 97–99]. A crucial question is how would these corrections affect the electric transport and (especially) the BCS pairing instability [33, 37, 63, 72, 81, 82, 115–120]. (iii) Various mesoscopic effects, such as level statistics and zero-bias anomaly [43, 96], can in principle be derived using the MFL-FNLsM. (iv) While the concept of a quasiparticle is not well-defined in our system due to the MFL self-energy, the kinetic equation governing the distribution functions can still be formally applied [43, 121, 122]. Determining the nonequilibrium distribution allows one to go beyond linear response theory and study phenomena such as shot noise [43, 123] and transport due to out-of-equilibrium bosons [51].

IX. ACKNOWLEDGMENT

We thank Alexander Altland, Alex Levchenko, and Aavishkar A. Patel for useful discussions. This work was supported by the Welch Foundation Grant No. C-1809 (T.C.W. and M.S.F.), and by the Simons Foundation “Ultra-Quantum Matter” Research Collaboration (Y.L.).

Appendix A: Evaluation of the thermal mass m_b^2

In the following, we derive the thermal mass result shown in Eq. (4.24). Consider the saddle-point equation

$$m_b^2 = 2i\lambda_\phi \int_{\Omega, \mathbf{q}} D_{\text{sp}}^K(\Omega, \mathbf{q}) = 2\lambda_\phi \int_{\Omega, \mathbf{q}} \frac{\alpha\Omega}{(\mathbf{q}^2 + m_b^2)^2 + (\alpha\Omega)^2} \coth\left(\frac{\Omega}{2T}\right). \quad (\text{A1})$$

Since the model is tuned to a QCP, we have to subtract off the zero-temperature contribution such that

$$\begin{aligned} m_b^2 &\rightarrow \frac{\lambda_\phi}{2\pi^2} \int_0^\infty d\Omega \int_0^\infty dx \left[\frac{\alpha\Omega}{(x + m_b^2)^2 + (\alpha\Omega)^2} \coth\left(\frac{\Omega}{2T}\right) - \frac{\alpha\Omega}{x^2 + (\alpha\Omega)^2} \right] \\ &= \frac{\lambda_\phi}{2\pi^2} \int_0^{\omega_c} d\Omega \left\{ \left[\frac{\pi}{2} - \tan^{-1}\left(\frac{m_b^2}{\alpha\Omega}\right) \right] \coth\left(\frac{\Omega}{2T}\right) - \frac{\pi}{2} \right\}, \end{aligned} \quad (\text{A2})$$

which ensures that $m_b^2(T=0)=0$. On the second line in Eq. (A2), we have restricted the frequency integral below the UV cutoff ω_c ; this integral is still logarithmically divergent. We isolate the divergence by writing

$$\begin{aligned} m_b^2 &= \frac{\lambda_\phi}{2\pi^2} \left\{ (2T) \int_0^\infty dy [\coth(y) - 1] \left[\frac{\pi}{2} - \tan^{-1} \left(\frac{m_b^2}{2\alpha T y} \right) \right] - \int_0^{\omega_c} d\Omega \tan^{-1} \left(\frac{m_b^2}{\alpha \Omega} \right) \right\} \\ &\simeq \frac{\lambda_\phi T}{2\pi^2} \left[I \left(\frac{\alpha_m}{2\alpha} \right) - \left(\frac{\alpha_m}{\alpha} \right) \ln \left(\frac{e\alpha\omega_c}{\alpha_m T} \right) \right], \end{aligned} \quad (\text{A3})$$

valid to logarithmic accuracy, and where

$$I(z) \equiv 2 \int_0^\infty dy [\coth(y) - 1] \left[\frac{\pi}{2} - \tan^{-1} \left(\frac{z}{y} \right) \right]. \quad (\text{A4})$$

In Eq. (A3), we have parametrized $m_b^2 \equiv \alpha_m T$. The function $I(z)$ has the asymptotic behaviors

$$I(z \rightarrow 0) \simeq -\pi \ln(2z), \quad I(z \rightarrow \infty) \simeq \frac{\pi^2}{6z}. \quad (\text{A5})$$

Therefore for $(\alpha_m/\alpha) \lesssim 1$, we can neglect the second term in the square brackets on the right-hand side of Eq. (A3), and approximate

$$\alpha_m \simeq \frac{\lambda_\phi}{2\pi^2} I \left(\frac{\alpha_m}{2\alpha} \right). \quad (\text{A6})$$

The T -independent coefficient α_m can be obtained by solving Eq. (A6).

Appendix B: Evaluation of $\mathcal{F}(t, x)$

In this appendix, we demonstrate how $\mathcal{F}(t, x)$ in Eq. (4.35) implies linear- T resistivity. We denote $t' \equiv \bar{g}^2 \pi t$ and express $\mathcal{F}(t, x)$ as

$$\mathcal{F}(t, x) = \int_0^\infty dy \frac{\text{sech}^2 y}{1 + t' \max(y, x)} = 1 + \sum_{n=1}^\infty \int_0^\infty dy \text{sech}^2 y [-t' \max(y, x)]^n. \quad (\text{B1})$$

One can then evaluate the integrals term by term as follows:

$$\int_0^\infty dy \text{sech}^2 y \max(y, x) = \ln(2 \cosh x), \quad (\text{B2})$$

$$\int_0^\infty dy \text{sech}^2 y \max(y, x)^2 = x^2 + 2x \ln(1 + e^{-2x}) - \text{Li}_2(-e^{-2x}), \quad (\text{B3})$$

$$\int_0^\infty dy \text{sech}^2 y \max(y, x)^3 = x^3 + 3x^2 \ln(1 + e^{-2x}) - 3x \text{Li}_2(-e^{-2x}) - \frac{3}{2} x^2 \ln(1 + e^{-2x}), \quad (\text{B4})$$

and so on, where $\text{Li}_2(x)$ is the dilogarithm function. For $x \gtrsim 1$, we can approximate $\mathcal{F}(t, x)$ by dropping the exponentially suppressed terms such that

$$\mathcal{F}(t, x) \simeq 1 + \sum_{n=1}^\infty (-t' x)^n = \frac{1}{1 + t' x}. \quad (\text{B5})$$

For $x \gtrsim 1$, this agrees with Eq. (4.37) in the main text.

Appendix C: Derivation of the MFL-FNLsM

In this appendix, we provide some technical details for the derivation of the FNLsM from Eq. (4.6). The FNLsM is derived by considering fluctuations around the saddle points discussed in Sec. IV A. By dropping the fluctuations

of $\{\hat{D}, \hat{\Pi}, \tilde{X}_1, \tilde{X}_2\}$ and keeping only fluctuations in the fermionic sector, we write

$$\hat{G} = \hat{G}_{\text{sp}} \otimes \hat{1}_{\text{SU}(N)} + \delta\hat{G}, \quad \hat{\Sigma} = \hat{\Sigma}_{\text{sp}} \otimes \hat{1}_{\text{SU}(N)} + \delta\hat{\Sigma}, \quad \hat{q} = \hat{q}_{\text{sp}} + \delta\hat{q}, \quad (\text{C1})$$

where the saddle points \hat{G}_{sp} , $\hat{\Sigma}_{\text{sp}}$ and \hat{q}_{sp} can be found in Sec. IV A. Here, $\delta\hat{G} \rightarrow \delta G_{ij}^{ab}(x, x')$ and $\delta\hat{\Sigma} \rightarrow \delta\Sigma_{ij}^{ab}(x, x')$ are bilocal matrix fields containing flavor indices i, j , Keldysh indices a, b and spacetime $x = (t, \mathbf{x})$. Meanwhile, $\delta\hat{q} \rightarrow \delta q_{ij;t,t'}^{ab}(\mathbf{x})$ is a matrix field that is bilocal in time but local in space. Plugging Eq. (C1) into Eq. (4.6), we obtain the action for the fluctuating matrix fields

$$\begin{aligned} \delta S = & -\text{Tr} \ln[\hat{1} - \hat{G}_{\text{sp}} \delta\hat{\Sigma} + i\gamma_{\text{el}} \hat{G}_{\text{sp}} \delta\hat{q} - \hat{G}_{\text{sp}} \hat{\mathcal{V}} \otimes \hat{1}_{\text{SU}(N)}] \\ & + \int_{x,x'} \delta\Sigma_{ij}^{ab}(x, x') \delta G_{ji}^{ba}(x', x) + i \frac{g^2}{2N} \int_{x,x'} \delta G_{ii}^{b'a}(x', x) \gamma_{ab}^s D_{\text{sp}}^{ss'}(x, x') \gamma_{a'b'}^{s'} \delta G_{jj}^{ba'}(x, x') \\ & + \frac{\pi\nu_0\gamma_{\text{el}}}{2} \int_{\mathbf{x}} \text{Tr} [\hat{q}(\mathbf{x})^2], \end{aligned} \quad (\text{C2})$$

where we dropped unimportant constant terms and omitted terms linear in $\delta\hat{\Sigma}$ and $\delta\hat{G}$ that will be canceled with the corresponding terms in the $\text{Tr} \ln[\dots]$, owing to the saddle point conditions discussed in Sec. IV A. Here, $\int_x = \int_{t,\mathbf{x}} = \int dt d^2\mathbf{x}$.

By expanding the $\text{Tr} \ln[\dots]$ in δS [Eq. (C2)] up to quartic order, we have

$$\begin{aligned} & -\text{Tr} \ln[\hat{1} - \hat{G}_{\text{sp}} \delta\hat{\Sigma} + i\gamma_{\text{el}} \hat{G}_{\text{sp}} \delta\hat{q} - \hat{G}_{\text{sp}} \hat{\mathcal{V}} \otimes \hat{1}_{\text{SU}(N)}] \\ & = \frac{1}{2} \text{Tr} [-\hat{G}_{\text{sp}} \delta\hat{\Sigma} + i\gamma_{\text{el}} \hat{G}_{\text{sp}} \delta\hat{q} - \hat{G}_{\text{sp}} \hat{\mathcal{V}} \otimes \hat{1}_{\text{SU}(N)}]^2 - \frac{1}{3} \text{Tr} [-\hat{G}_{\text{sp}} \delta\hat{\Sigma} + i\gamma_{\text{el}} \hat{G}_{\text{sp}} \delta\hat{q} - \hat{G}_{\text{sp}} \hat{\mathcal{V}} \otimes \hat{1}_{\text{SU}(N)}]^3 \\ & + \frac{1}{4} \text{Tr} [-\hat{G}_{\text{sp}} \delta\hat{\Sigma} + i\gamma_{\text{el}} \hat{G}_{\text{sp}} \delta\hat{q} - \hat{G}_{\text{sp}} \hat{\mathcal{V}} \otimes \hat{1}_{\text{SU}(N)}]^4 + \dots \\ & = -\frac{\gamma_{\text{el}}^2}{2} \text{Tr} [\hat{G}_{\text{sp}} \delta\hat{q} \hat{G}_{\text{sp}} \delta\hat{q}] - i\gamma_{\text{el}} \text{Tr} [\hat{G}_{\text{sp}} \delta\hat{q} \hat{G}_{\text{sp}} \hat{\mathcal{V}}] + \frac{N}{2} \text{Tr} [\hat{G}_{\text{sp}} \hat{\mathcal{V}} \hat{G}_{\text{sp}} \hat{\mathcal{V}}] \\ & + \frac{1}{2} \text{Tr} [\hat{G}_{\text{sp}} \delta\hat{\Sigma} \hat{G}_{\text{sp}} \delta\hat{\Sigma}] - i\gamma_{\text{el}} \text{Tr} [\hat{G}_{\text{sp}} \delta\hat{\Sigma} \hat{G}_{\text{sp}} \delta\hat{q}] - \frac{\gamma_{\text{el}}^2}{2} \text{Tr} [\hat{G}_{\text{sp}} \delta\hat{\Sigma} \hat{G}_{\text{sp}} \delta\hat{q} \hat{G}_{\text{sp}} \delta\hat{\Sigma} \hat{G}_{\text{sp}} \delta\hat{q}] + \dots \end{aligned} \quad (\text{C3})$$

In the second line, we again dropped the linear terms due to the saddle point conditions. In the last step, we neglected the cubic terms which generate interaction terms that are less important. As we are going to show below, the terms in the first line give rise to S_D [Eq. (5.5)], S_{qV} [Eq. (5.10)] and S_V [Eq. (5.11)], respectively, while those in the second line give rise to S_{intI} [Eq. (5.7)] and S_{intII} [Eq. (5.8)].

1. Derivation for S_D , S_{qV} and S_V

The diffusive part of the FNLsM, S_D in Eq. (5.5), can be derived following the standard gradient expansion. The Keldysh-space-diagonal components of $\delta\hat{q}$ correspond to the massive fluctuations around the saddle point, while the off-diagonal components correspond to massless Goldstone modes that are important for the quantum transport. By ignoring the diagonal components, we can write

$$\begin{aligned} & -\frac{\gamma_{\text{el}}^2}{2} \text{Tr} [\hat{G}_{\text{sp}} \delta\hat{q} \hat{G}_{\text{sp}} \delta\hat{q}] \\ & = -\frac{\gamma_{\text{el}}^2}{2} \int_{\omega_1, \omega_2, \mathbf{q}} \delta q_{\omega_1, \omega_2; ij}^{ab}(-\mathbf{q}) \left[\int_{\mathbf{p}} G_{\text{sp}}^{aa}(\omega_1, \mathbf{p}) G_{\text{sp}}^{bb}(\omega_2, \mathbf{p} + \mathbf{q}) \right] \delta q_{\omega_2, \omega_1; ji}^{ba}(\mathbf{q}) \\ & \simeq \frac{1}{2} \int_{\omega_1, \omega_2, \mathbf{q}} \delta q_{\omega_1, \omega_2; ij}^{ab}(-\mathbf{q}) \left\{ -\pi\nu_0\gamma_{\text{el}} + \frac{1}{\lambda} \mathbf{q}^2 - ih \{ (\omega_2 - \Sigma_{\text{sp}, \omega_2}^{bb}) [\hat{\tau}^3]^{bb} + (\omega_1 - \Sigma_{\text{sp}, \omega_1}^{aa}) [\hat{\tau}^3]^{aa} \} \right\} \delta q_{\omega_2, \omega_1; ji}^{ba}(\mathbf{q}), \end{aligned} \quad (\text{C4})$$

where λ and h are given in Eq. (5.6). The first term exactly cancels with the last term in Eq. (C2) when the latter is expanded to second order in $\delta\hat{q}$, indicating the off-diagonal fluctuations are indeed soft modes of the system. By

further making use of the constraint $\hat{q}^2 = (\hat{q}_{\text{sp}} + \delta\hat{q})^2 = \hat{1}$ and going back to real space, we have

$$S_D = \frac{1}{2\lambda} \int_{\mathbf{x}} \text{Tr} [\nabla\hat{q} \cdot \nabla\hat{q}] + 2ih \int_{\mathbf{x}} \text{Tr} [(\hat{\omega} + i\eta\hat{\tau}^3 - \hat{\Sigma}_{\text{sp}})\hat{q}]. \quad (\text{C5})$$

On the other hand, the coupling term between $\delta\hat{q}$ and the source field V is

$$\begin{aligned} -i\gamma_{\text{el}} \text{Tr} [\hat{G}_{\text{sp}} \delta\hat{q} \hat{G}_{\text{sp}} \hat{\mathcal{V}}] &= -i\gamma_{\text{el}} \int_{\omega_1, \omega_2, \mathbf{q}} \delta q_{ii; \omega_1, \omega_2}^{\text{ab}}(\mathbf{q}) \left[\int_{\mathbf{p}} G_{\text{sp}}^{aa}(\omega_1, \mathbf{p} + \mathbf{q}) G_{\text{sp}}^{bb}(\omega_2, \mathbf{p}) \right] \mathcal{V}_{\omega_2, \omega_1}^{ba}(-\mathbf{q}) \\ &\simeq -i\pi\nu_0 \int_{\omega_1, \omega_2, \mathbf{q}} \delta q_{ii; \omega_1, \omega_2}^{\text{ab}}(\mathbf{q}) \mathcal{V}_{\omega_2, \omega_1}^{ba}(-\mathbf{q}). \end{aligned} \quad (\text{C6})$$

In real space, this can be written as

$$S_{qV} = -2ih \int_{t, \mathbf{x}} \text{Tr} [\hat{q}_{t, t}(\mathbf{x}) (V^{\text{cl}}(t, \mathbf{x}) \hat{\gamma}^{\text{cl}} + V^{\text{q}}(t, \mathbf{x}) \hat{\gamma}^{\text{q}})], \quad (\text{C7})$$

which is Eq. (5.10).

Lastly, for the source field term, one has to be careful when handling the integral involving retarded-retarded and advanced-advanced combinations of Green's function components:

$$\begin{aligned} S_V &= \frac{N}{2} \text{Tr} [\hat{G}_{\text{sp}} \hat{\mathcal{V}} \hat{G}_{\text{sp}} \hat{\mathcal{V}}] \\ &= \frac{N}{2} \int_{\omega, \Omega, \mathbf{p}, \mathbf{q}} G_{\text{sp}}^{aa}(\omega + \Omega, \mathbf{p} + \mathbf{q}) \mathcal{V}_{\omega + \Omega, \omega}^{ab}(\mathbf{q}) G_{\text{sp}}^{bb}(\omega, \mathbf{p}) \mathcal{V}_{\omega, \omega + \Omega}^{ba}(-\mathbf{q}) \\ &\simeq N \int_{\Omega, \mathbf{q}} \left\{ \int_{\omega, \mathbf{p}} F_{\omega} [G_{\text{sp}}^R(\omega, \mathbf{p}) G_{\text{sp}}^R(\omega, \mathbf{p}) - G_{\text{sp}}^A(\omega, \mathbf{p}) G_{\text{sp}}^A(\omega, \mathbf{p})] \right\} V^{\text{cl}}(\Omega, \mathbf{q}) V^{\text{q}}(-\Omega, -\mathbf{q}) \\ &\simeq -2iN\nu_0 \int_{t, \mathbf{x}} V^{\text{cl}}(t, \mathbf{x}) V^{\text{q}}(t, \mathbf{x}), \end{aligned} \quad (\text{C8})$$

which is Eq. (5.11).

2. Derivation for $S_{\text{int I}}$ and $S_{\text{int II}}$

We now show that $S_{\text{int I}}$ and $S_{\text{int II}}$ can be derived from the last two terms of Eq. (C3). To obtain the interaction terms $S_{\text{int I}}$ and $S_{\text{int II}}$, we have to first derive the contraction rule for $\delta\hat{\Sigma}$. To do so, we combine the second line of Eq. (C2) and the first term in the last line of Eq. (C3) such that

$$\delta S_{\delta\Sigma} = \frac{1}{2} \text{Tr} \left[\left(\hat{G}_{\text{sp}} \delta\hat{\Sigma} \right)^2 \right] + \int_{x, x'} \delta\Sigma_{ij}^{ab}(x, x') \delta G_{ji}^{ba}(x', x) + \frac{1}{2} \int_{x, x'} \delta G_{ij}^{ab}(x, x') \mathcal{T}_{ji; lk}^{ba; dc}(x, x') \delta G_{kl}^{cd}(x', x), \quad (\text{C9})$$

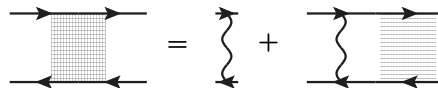


FIG. 18. Diagrammatic depiction of the propagator of $\delta\hat{\Sigma}$. Contraction of a pair of $\delta\hat{\Sigma}$ effectively inserts the interaction ladder.

where we defined the kernel

$$\mathcal{T}_{ji;lk}^{ba;dc}(x, x') = i \frac{g^2}{N} \gamma_{bc}^s D_{\text{sp}}^{ss'}(x, x') \gamma_{da}^{s'} \delta_{ij} \delta_{kl}. \quad (\text{C10})$$

Integrating out δG , we have

$$\begin{aligned} \delta S_{\delta\Sigma} &= \frac{1}{2} \text{Tr} \left[\hat{G}_{\text{sp}} \delta \hat{\Sigma}_{ij} \hat{G}_{\text{sp}} \delta \hat{\Sigma}_{ji} \right] - \int_{x_1, \dots, x_4} \delta \Sigma_{ij}^{ab}(x_1, x_2) [\mathcal{T}^{-1}]_{ji;lk}^{ba;dc}(x_1, x_2) \delta_{x_4, x_1} \delta_{x_2, x_3} \delta \Sigma_{kl}^{cd}(x_3, x_4) \\ &= \frac{1}{2} \int_{x_1, \dots, x_4} \delta \Sigma_{ij}^{ab}(x_1, x_2) \left\{ -[\mathcal{T}^{-1}]_{ji;lk}^{ba;dc}(x_1, x_2) \delta_{x_4, x_1} \delta_{x_2, x_3} + G_{\text{sp}}^{bc}(x_2, x_3) G_{\text{sp}}^{da}(x_4, x_1) \delta_{jk} \delta_{il} \right\} \delta \Sigma_{kl}^{cd}(x_3, x_4). \end{aligned} \quad (\text{C11})$$

The propagator for $\delta \hat{\Sigma}$ is thus

$$\langle \delta \Sigma_{ij}^{ab}(x_1, x_2) \delta \Sigma_{kl}^{cd}(x_3, x_4) \rangle = \langle x_2, x_1; ji; ba | \hat{\mathcal{K}}^{-1} | x_4, x_3; lk; dc \rangle = \langle x_2, x_1; ji; ba | \frac{-1}{\hat{1} - \hat{Y}} \hat{\mathcal{T}} | x_4, x_3; lk; dc \rangle \quad (\text{C12})$$

where the matrix elements of \hat{Y} and $\hat{\mathcal{T}}$ are respectively

$$\langle x_2, x_1; ji; ba | \hat{Y} | x_4, x_3; lk; dc \rangle = \mathcal{T}_{ji;lk}^{ba;dc}(x_1, x_2) G_{\text{sp}}^{bc}(x_2, x_3) G_{\text{sp}}^{da}(x_4, x_1) \quad (\text{C13})$$

and

$$\langle x_2, x_1; ji; ba | \hat{\mathcal{T}} | x_4, x_3; lk; dc \rangle = \mathcal{T}_{ji;lk}^{ba;dc}(x_1, x_2) \delta_{x_1, x_4} \delta_{x_2, x_3}. \quad (\text{C14})$$

This implies that contracting a pair of $\delta \hat{\Sigma}$ amounts to inserting an interaction ladder, as illustrated diagrammatically in Fig. 18. In practice, however, we only keep the first term in the series since higher-order terms are parametrically suppressed by $1/\gamma_{\text{el}}$, as we assumed impurity scattering is the dominating scattering mechanism.

We are now ready to derive S_{int} and $S_{\text{int II}}$. The interaction among $\delta \hat{q}$ arises from the last two terms in the last line of Eq. (C3), which read

$$\delta S_{\text{int}} = -i \gamma_{\text{el}} \text{Tr} \left[\hat{G}_{\text{sp}} \delta \hat{\Sigma} \hat{G}_{\text{sp}} \delta \hat{q} \right] - \frac{\gamma_{\text{el}}^2}{2} \text{Tr} \left[\hat{G}_{\text{sp}} \delta \hat{\Sigma} \hat{G}_{\text{sp}} \delta \hat{q} \hat{G}_{\text{sp}} \delta \hat{\Sigma} \hat{G}_{\text{sp}} \delta \hat{q} \right]. \quad (\text{C15})$$

Consider the expansion

$$\begin{aligned} \langle e^{-\delta S_{\text{int}}} \rangle_{\delta\Sigma} &= \left\langle 1 - \delta S_{\text{int}} + \frac{1}{2!} (-\delta S_{\text{int}})^2 + \dots \right\rangle_{\delta\Sigma} \\ &= \left\langle 1 + \frac{\gamma_{\text{el}}^2}{2} \text{Tr} \left[\hat{G}_{\text{sp}} \delta \hat{\Sigma} \hat{G}_{\text{sp}} \delta \hat{q} \hat{G}_{\text{sp}} \delta \hat{\Sigma} \hat{G}_{\text{sp}} \delta \hat{q} \right] - \frac{\gamma_{\text{el}}^2}{2!} \left(\text{Tr} \left[\hat{G}_{\text{sp}} \delta \hat{\Sigma} \hat{G}_{\text{sp}} \delta \hat{q} \right] \right)^2 + \dots \right\rangle_{\delta\Sigma} \end{aligned} \quad (\text{C16})$$

Consider the second term in Eq. (C16)

$$\begin{aligned} &\left\langle \frac{\gamma_{\text{el}}^2}{2} \text{Tr} \left[\hat{G}_{\text{sp}} \delta \hat{\Sigma} \hat{G}_{\text{sp}} \delta \hat{q} \hat{G}_{\text{sp}} \delta \hat{\Sigma} \hat{G}_{\text{sp}} \delta \hat{q} \right] \right\rangle_{\delta\Sigma} \\ &= \frac{\gamma_{\text{el}}^2}{2} \int \langle G_{\text{sp}}^{aa}(x_1, x_2) \delta \Sigma_{ij}^{ab}(x_2, x_3) G_{\text{sp}}^{bb}(x_3, x_4) \delta q_{jk}^{bc}(x_4, x_5) \delta_{\mathbf{x}_4, \mathbf{x}_5} G_{\text{sp}}^{cc}(x_5, x_6) \delta \Sigma_{kl}^{cd}(x_6, x_7) G_{\text{sp}}^{dd}(x_7, x_8) \delta q_{li}^{da}(x_8, x_1) \delta_{\mathbf{x}_8, \mathbf{x}_1} \rangle_{\delta\Sigma} \\ &\simeq -\frac{\gamma_{\text{el}}^2}{2} \int G_{\text{sp}}^{aa}(x_1, x_2) G_{\text{sp}}^{bb}(x_3, x_4) \delta q_{jk}^{bc}(x_4, x_5) \delta_{\mathbf{x}_4, \mathbf{x}_5} G_{\text{sp}}^{cc}(x_5, x_6) G_{\text{sp}}^{dd}(x_7, x_8) \delta q_{li}^{da}(x_8, x_1) \delta_{\mathbf{x}_8, \mathbf{x}_1} \left[\mathcal{T}_{ji;lk}^{ba;dc}(x_2, x_3) \delta_{x_2, x_7} \delta_{x_3, x_6} \right] \\ &= -\frac{ig^2 \gamma_{\text{el}}^2}{2N} \int G_{\text{sp}}^{aa}(x_1, x_2) G_{\text{sp}}^{bb}(x_3, x_4) \delta q_{jk}^{bc}(x_4, x_5) \delta_{\mathbf{x}_4, \mathbf{x}_5} G_{\text{sp}}^{cc}(x_5, x_3) G_{\text{sp}}^{dd}(x_2, x_8) \delta q_{li}^{da}(x_8, x_1) \delta_{\mathbf{x}_8, \mathbf{x}_1} \\ &\quad \times \left[\gamma_{bc}^s D_{\text{sp}}^{ss'}(x_2, x_3) \gamma_{da}^{s'} \delta_{ij} \delta_{kl} \right] \\ &= -\frac{ig^2 \gamma_{\text{el}}^2}{2N} \int \left[G_{\text{sp}}^{aa}(x_1, x_2) G_{\text{sp}}^{dd}(x_2, x_8) \delta q_{ji}^{da}(x_8, x_1) \delta_{\mathbf{x}_8, \mathbf{x}_1} \gamma_{da}^{s'} \right] D_{\text{sp}}^{ss'}(x_2, x_3) \left[G_{\text{sp}}^{bb}(x_3, x_4) G_{\text{sp}}^{cc}(x_5, x_3) \delta q_{ij}^{bc}(x_4, x_5) \delta_{\mathbf{x}_4, \mathbf{x}_5} \gamma_{bc}^s \right], \end{aligned} \quad (\text{C17})$$

where \int integrates all x_i appearing in the integrand. By switching to momentum space and performing integrals similar to those that appeared in Eq. (C4), we have

$$\begin{aligned} & \left\langle \frac{\gamma_{\text{el}}^2}{2} \text{Tr} \left[\hat{G}_{\text{sp}} \delta \hat{\Sigma} \hat{G}_{\text{sp}} \delta \hat{q} \hat{G}_{\text{sp}} \delta \hat{\Sigma} \hat{G}_{\text{sp}} \delta \hat{q} \right] \right\rangle_{\delta \Sigma} \\ & \simeq -\Gamma_1 \int_{\omega_1, 2, 3, 4, \mathbf{q}} \delta_{\omega_1 + \omega_3, \omega_2 + \omega_4} \text{Tr} [\hat{q}_{ij; \omega_1, \omega_2}(-\mathbf{q}) \hat{\gamma}_{\omega_2, \omega_1}^s] D_{\text{sp}, \omega_2 - \omega_1}^{ss'}(\mathbf{q}) \text{Tr} [\hat{\gamma}_{\omega_4, \omega_3}^{s'} \hat{q}_{ji; \omega_3, \omega_4}(\mathbf{q})], \end{aligned} \quad (\text{C18})$$

where Γ_1 is given in Eq. (5.9).

For the third term in Eq. (C16)

$$\begin{aligned} & -\frac{\gamma_{\text{el}}^2}{2!} \left\langle \left(\text{Tr} \left[\hat{G}_{\text{sp}} \delta \hat{\Sigma} \hat{G}_{\text{sp}} \delta \hat{q} \right] \right)^2 \right\rangle_{\delta \Sigma} \\ & = -\frac{\gamma_{\text{el}}^2}{2} \int \left[G_{\text{sp}}^{aa}(x_1, x_2) \delta \Sigma_{ij}^{ab}(x_2, x_3) G_{\text{sp}}^{bb}(x_3, x_4) \delta q_{ji}^{ba}(x_4, x_1) \delta_{\mathbf{x}_4, \mathbf{x}_1} \right] \\ & \quad \times \left[G_{\text{sp}}^{cc}(x_5, x_6) \delta \Sigma_{kl}^{cd}(x_6, x_7) G_{\text{sp}}^{dd}(x_7, x_8) \delta q_{lk}^{dc}(x_8, x_5) \delta_{\mathbf{x}_8, \mathbf{x}_5} \right]_{\delta \Sigma} \\ & \simeq \frac{\gamma_{\text{el}}^2}{2} \int \left[G_{\text{sp}}^{aa}(x_1, x_2) G_{\text{sp}}^{bb}(x_3, x_4) \delta q_{ji}^{ba}(x_4, x_1) \delta_{\mathbf{x}_4, \mathbf{x}_1} \right] \\ & \quad \times \left[G_{\text{sp}}^{cc}(x_5, x_6) G_{\text{sp}}^{dd}(x_7, x_8) \delta q_{lk}^{dc}(x_8, x_5) \delta_{\mathbf{x}_8, \mathbf{x}_5} \right] \left[\mathcal{T}_{ji; lk}^{ba, dc}(x_2, x_3) \delta_{x_2, x_7} \delta_{x_3, x_6} \right] \\ & = i \frac{\gamma_{\text{el}}^2 g^2}{2N} \int \left[G_{\text{sp}}^{aa}(x_1, x_2) G_{\text{sp}}^{bb}(x_3, x_4) \delta q_{ii}^{ba}(x_4, x_1) \delta_{\mathbf{x}_4, \mathbf{x}_1} \right] \left[G_{\text{sp}}^{cc}(x_5, x_3) G_{\text{sp}}^{dd}(x_2, x_8) \delta q_{jj}^{dc}(x_8, x_5) \delta_{\mathbf{x}_8, \mathbf{x}_5} \right] \left[\gamma_{bc}^s D_{\text{sp}}^{ss'}(x_2, x_3) \gamma_{da}^{s'} \right], \end{aligned} \quad (\text{C19})$$

where \int integrates all x_i appearing in the integrand. By Fourier transforming the above expression and assuming small momentum transfer through the bosonic line, we have

$$-\frac{\gamma_{\text{el}}^2}{2!} \left\langle \left(\text{Tr} \left[\hat{G}_{\text{sp}} \delta \hat{\Sigma} \hat{G}_{\text{sp}} \delta \hat{q} \right] \right)^2 \right\rangle_{\delta \Sigma} \simeq \Gamma_2 \int_{1-4, \mathbf{k}} \delta_{1+3, 2+4} \text{Tr} \left[\hat{q}_{ii; 1, 2}(-\mathbf{k}) \hat{\gamma}_{2, 3}^s \hat{q}_{jj; 3, 4}(\mathbf{k}) \hat{\gamma}_{4, 1}^{s'} \right] \left[\int_{\mathbf{k}'} D_{\text{sp}, 1-4}^{ss'}(\mathbf{k}') \right], \quad (\text{C20})$$

where Γ_2 is given in Eq. (5.9).

Combining Eqs. (C18) and Eq. (C20), we have

$$\langle e^{-\delta S_{\text{int}}} \rangle_{\delta \Sigma} \simeq e^{-S_{\text{int I}} - S_{\text{int II}}}. \quad (\text{C21})$$

Thus, we have recovered $S_{\text{int I}}$ in Eq. (5.7) and $S_{\text{int II}}$ in Eq. (5.8) of the main text.

Appendix D: Expressions for the type-B diagrams

In this appendix, we present the detailed expressions associated with the type-B diagrams shown in Fig. 13. Let's write

$$\delta \pi_{\text{type B}}^R(\Omega, \mathbf{q}) = \sum_i \delta \pi_{\text{type B}, i}^R(\Omega, \mathbf{q}) \quad (\text{D1})$$

where i corresponds to the label of the subfigure. Specifically,

$$\begin{aligned} \delta \pi_{\text{type B, a(i)}}^R(\Omega, \mathbf{q}) &= \frac{C}{2i} \int_{\omega, \xi, \mathbf{k}} D_{\text{scr}, \xi}^R(\mathbf{k}) (F_{\omega} - F_{\omega + \xi}) \left(\frac{1}{F_{\xi}} + F_{\omega} \right) \Delta_{\omega + \xi, \omega - \Omega}^R(\mathbf{k} + \mathbf{q}) \Delta_{\omega + \xi, \omega}^R(\mathbf{k}) \\ &\quad \times \left(\mathbf{q}^2 - i \hbar \bar{g}^2 \Omega \ln \frac{\omega_c}{|\omega|} \right) [\Delta_{\text{FL}, \Omega}^R(\mathbf{q})]^2, \end{aligned} \quad (\text{D2})$$

$$\begin{aligned} \delta\pi_{\text{type B,a(ii)}}^R(\Omega, \mathbf{q}) = & -\frac{C}{2i} \int_{\omega, \xi, \mathbf{k}} D_{\text{scr}, \xi}^R(\mathbf{k})(F_\omega - F_{\omega+\xi}) \left(\frac{1}{F_\xi} + F_{\omega+\Omega} \right) \Delta_{\omega+\xi+\Omega, \omega}^R(\mathbf{k} + \mathbf{q}) \Delta_{\omega+\xi, \omega}^R(\mathbf{k}) \\ & \times \left(\mathbf{q}^2 - ih\lambda\bar{g}^2\Omega \ln \frac{\omega_c}{|\omega + \xi|} \right) [\Delta_{\text{FL}, \Omega}^R(\mathbf{q})]^2, \end{aligned} \quad (\text{D3})$$

$$\begin{aligned} \delta\pi_{\text{type B,b(i)}}^R(\Omega, \mathbf{q}) = & \frac{C}{2i} \int_{\omega, \xi, \mathbf{k}} D_{\text{scr}, \xi}^R(\mathbf{k})(F_\omega - F_{\omega+\xi}) \left(-\frac{1}{F_\xi} + F_{\omega+\xi-\Omega} \right) \Delta_{\omega+\xi, \omega-\Omega}^R(\mathbf{k} + \mathbf{q}) \Delta_{\omega+\xi, \omega}^R(\mathbf{k}) \\ & \times \left(\mathbf{q}^2 - ih\lambda\bar{g}^2\Omega \ln \frac{\omega_c}{|\omega|} \right) [\Delta_{\text{FL}, \Omega}^R(\mathbf{q})]^2, \end{aligned} \quad (\text{D4})$$

$$\begin{aligned} \delta\pi_{\text{type B,b(ii)}}^R(\Omega, \mathbf{q}) = & -\frac{C}{2i} \int_{\omega, \xi, \mathbf{k}} D_{\text{scr}, \xi}^R(\mathbf{k})(F_\omega - F_{\omega+\xi}) \left(-\frac{1}{F_\xi} + F_{\omega+\xi} \right) \Delta_{\omega+\xi+\Omega, \omega}^R(\mathbf{k} + \mathbf{q}) \Delta_{\omega+\xi, \omega}^R(\mathbf{k}) \\ & \times \left(\mathbf{q}^2 - ih\lambda\bar{g}^2\Omega \ln \frac{\omega_c}{|\omega + \xi|} \right) [\Delta_{\text{FL}, \Omega}^R(\mathbf{q})]^2, \end{aligned} \quad (\text{D5})$$

$$\begin{aligned} \delta\pi_{\text{type B,c(i)}}^R(\Omega, \mathbf{q}) = & -\frac{C}{2i} \int_{\omega, \xi, \mathbf{k}} D_{\text{scr}, \xi}^R(\mathbf{k})F_{\omega+\xi}(F_\omega - F_{\omega+\Omega})\Delta_{\omega+\xi, \omega}^R(\mathbf{k})\Delta_{\omega+\Omega+\xi, \omega}^R(\mathbf{k} + \mathbf{q}) \\ & \times \left(\mathbf{q}^2 - ih\lambda\bar{g}^2\Omega \ln \frac{\omega_c}{|\omega + \xi|} \right) [\Delta_{\text{FL}, \Omega}^R(\mathbf{q})]^2, \end{aligned} \quad (\text{D6})$$

$$\begin{aligned} \delta\pi_{\text{type B,c(ii)}}^R(\Omega, \mathbf{q}) = & -\frac{C}{2i} \int_{\omega, \xi, \mathbf{k}} D_{\text{scr}, \xi}^R(\mathbf{k})F_{\omega+\Omega}(F_\omega - F_{\omega+\Omega})\Delta_{\omega+\Omega+\xi, \omega+\Omega}^R(\mathbf{k})\Delta_{\omega+\Omega+\xi, \omega}^R(\mathbf{k} + \mathbf{q}) \\ & \times \left(\mathbf{q}^2 - ih\lambda\bar{g}^2\Omega \ln \frac{\omega_c}{|\omega|} \right) [\Delta_{\text{FL}, \Omega}^R(\mathbf{q})]^2, \end{aligned} \quad (\text{D7})$$

$$\begin{aligned} \delta\pi_{\text{type B,d(i)}}^R(\Omega, \mathbf{q}) = & \frac{C}{2i} \int_{\omega, \xi, \mathbf{k}} D_{\text{scr}, \xi}^R(\mathbf{k})F_\omega(F_\omega - F_{\omega+\Omega})\Delta_{\omega, \omega-\xi}^R(\mathbf{k})\Delta_{\omega+\Omega, \omega-\xi}^R(\mathbf{k} + \mathbf{q}) \\ & \times \left(\mathbf{q}^2 - ih\lambda\bar{g}^2\Omega \ln \frac{\omega_c}{|\omega|} \right) [\Delta_{\text{FL}, \Omega}^R(\mathbf{q})]^2, \end{aligned} \quad (\text{D8})$$

$$\begin{aligned} \delta\pi_{\text{type B,d(ii)}}^R(\Omega, \mathbf{q}) = & \frac{C}{2i} \int_{\omega, \xi, \mathbf{k}} D_{\text{scr}, \xi}^R(\mathbf{k})F_{\omega+\Omega-\xi}(F_\omega - F_{\omega+\Omega})\Delta_{\omega+\Omega, \omega+\Omega-\xi}^R(\mathbf{k})\Delta_{\omega+\Omega, \omega-\xi}^R(\mathbf{k} + \mathbf{q}) \\ & \times \left(\mathbf{q}^2 - ih\lambda\bar{g}^2\Omega \ln \frac{\omega_c}{|\omega - \xi|} \right) [\Delta_{\text{FL}, \Omega}^R(\mathbf{q})]^2, \end{aligned} \quad (\text{D9})$$

and

$$\delta\pi_{\text{type B,c(iii)}}^R(\Omega, \mathbf{q}) + \delta\pi_{\text{type B,c(iv)}}^R(\Omega, \mathbf{q}) \simeq \delta\pi_{\text{type B,d(iii)}}^R(\Omega, \mathbf{q}) + \delta\pi_{\text{type B,d(iv)}}^R(\Omega, \mathbf{q}) \simeq 0. \quad (\text{D10})$$

At $T = 0$, by expanding to leading order of external frequency Ω and momentum \mathbf{q} and making use of the fact that the ξ integral is dominated by the infrared regime at which $\xi \simeq \Omega$, one can cast $\delta\pi_{\text{type B}}^R(\Omega, \mathbf{q})$ into the form of Eq. (7.18), up to logarithmic accuracy.

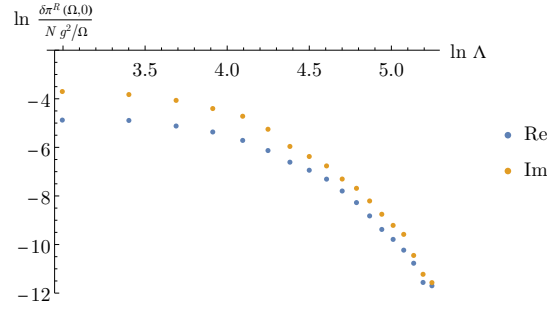


FIG. 19. Log-log plot of the real part (blue) and imaginary part (orange) of the AA density response correction $\delta\pi^R(\Omega, \mathbf{0})$, based on the numerical evaluation of the diagrams in Fig. 12–13 when the external momentum $\mathbf{q} = 0$. We use the parameters $h = 1$, $\lambda = 0.1$, $\bar{g}^2 = 0.25$, $h^2\lambda g^2/\pi N = 10^{-3}$, $\Omega = 0.1$, $T = 0.005$, $\omega_c = \Lambda$. As required by the U(1) Ward identity for electric charge conservation, $\delta\pi^R(\Omega, \mathbf{0}) \rightarrow 0$ as the UV cutoff $\Lambda \rightarrow \infty$.

Appendix E: Numerical verification of the Ward identity

Here, we provide additional numerical evidence that the Ward identity is satisfied at $T \rightarrow 0$. We numerically evaluate the interaction corrections represented by the Feynman diagrams in Fig. 12–13 when the external momentum \mathbf{q} is zero. We perform the integrals by the method of Monte Carlo using *Mathematica*. We employ 10^9 for maximum number of sampling points, 0.15 for “BisectionDithering,” and average over 100 configurations. We use the parameters $h = 1$, $\lambda = 0.1$, $\bar{g}^2 = 0.25$, $h^2\lambda g^2/\pi N = 10^{-3}$, $\Omega = 0.1$, $T = 0.005$, and $\omega_c = \Lambda$. The frequency integral is cut in the infrared by Ω . The dependence on the ultraviolet cutoff Λ of the quantum correction $\delta\pi^R(\Omega, \mathbf{0})$ when $\mathbf{q} = 0$ is shown in Fig. 19 in log scale. It is clear that for a sufficiently large cutoff Λ , the sum $\delta\pi^R(\Omega, \mathbf{0})$ goes to zero, indicating that the Ward identity is satisfied, which is in line with our analytical analysis. Similar behaviors are observed in other parameter sets.

Appendix F: AA integral kernels

1. Intermediate temperature, ignoring dynamical screening

The general form of the kernel \mathcal{I}_1 that determines the finite-temperature AA correction in Eqs. (7.27) and (7.28) is given by

$$\mathcal{I}_1 = \frac{iD\alpha_m}{2} \int_{-\infty}^{\infty} dy \tanh\left(\frac{y}{3}\right) \left\{ \frac{\Theta^2(y) + (D\alpha)^2 \Xi^2(y) + 2i(D\alpha) \Theta(y) \Xi(y) \log\left[\frac{i}{D\alpha} \frac{\Theta(y)}{\Xi(y)}\right]}{\Theta(y) [\Theta(y) + i(D\alpha) \Xi(y)]^3} \right\}, \quad (\text{F1})$$

$$\Theta(y) \equiv y + \bar{g}^2 \left\{ y \ln \left[\frac{\omega_c}{T \max(|y|, J)} \right] + i \frac{\pi}{2} \max(|y|, J) \right\},$$

$$\Xi(y) \equiv iy - \frac{\alpha_m}{\alpha}.$$

The parameter $J = J(2\alpha/\alpha_m)$ stabilizes the MFL self-energy at finite temperature, and arises due to the finite thermal mass coefficient α_m , Eqs. (4.29) and (4.30).

For $\alpha = 0$ (static boson) and $\bar{g}^2 = 0$ (Fermi liquid, vanishing MFL self-energy), Eq. (F1) reduces to Eq. (7.29). Comparisons between this and the general case are exhibited in Figs. 15–17.

2. Incorporating dynamical screening

The AA correction in Eq. (7.33) of the main text involves the kernel \mathcal{M} defined in Eq. (7.34) as

$$\mathcal{M}(\mathbf{a}, \mathbf{b}, m_b^2) = \text{Im} \int_0^\infty dx \frac{x}{(x - i\mathbf{a})^2 [x^2 + (m_b^2 - i\mathbf{a})x - i\mathbf{b}]}. \quad (\text{F2})$$

This integral can be done exactly, the result is

$$\mathcal{M}(\mathbf{a}, \mathbf{b}, m_{\mathbf{b}}^2) = \frac{-1}{4(-m_{\mathbf{b}}^2 \mathbf{a} + \mathbf{b})^2} \left\{ -2 \operatorname{Im} \left[\frac{\pi \mathbf{a}^2 + 4(-m_{\mathbf{b}}^2 \mathbf{a} + \mathbf{b}) + 2\mathbf{b} \ln \frac{\mathbf{a}^2}{\mathbf{b}}}{\zeta} \ln \frac{m_{\mathbf{b}}^2 - i\mathbf{a} - \zeta}{m_{\mathbf{b}}^2 - i\mathbf{a} + \zeta} \right] \right\}, \quad (\text{F3})$$

where

$$\zeta(\mathbf{a}, \mathbf{b}, m_{\mathbf{b}}^2) \equiv \sqrt{(m_{\mathbf{b}}^2 - i\mathbf{a})^2 + 4i\mathbf{b}}. \quad (\text{F4})$$

The remaining frequency integral in the AA correction [Eq. (7.37)] involves the kernel \mathcal{I}_2 defined as

$$\mathcal{I}_2(a, b, m_{\mathbf{b}}^2, T) = \mathcal{I}_{2,1}(a, b, m_{\mathbf{b}}^2, T) + \mathcal{I}_{2,2}(a, b, m_{\mathbf{b}}^2, T), \quad (\text{F5})$$

where

$$\begin{aligned} \mathcal{I}_{2,1}(a, b, m_{\mathbf{b}}^2, T) &= \int_0^{3T} d\xi \frac{\xi}{3T} \mathcal{M}(a\xi, b\xi, m_{\mathbf{b}}^2), \\ \mathcal{I}_{2,2}(a, b, m_{\mathbf{b}}^2, T) &= \int_{3T}^{\infty} d\xi \mathcal{M}(a\xi, b\xi, m_{\mathbf{b}}^2). \end{aligned} \quad (\text{F6})$$

The integrals can again be done exactly. The full expressions are

$$\mathcal{I}_{2,1}(a, b, m_{\mathbf{b}}^2, T) = \frac{1}{24T(b - am_{\mathbf{b}}^2)^2} \left\{ m_{\mathbf{b}}^4 \pi + 12am_{\mathbf{b}}^2 T - 3T(4b + 3\pi a^2 T) - 12bT \ln \frac{3a^2 T}{b} + 2 \operatorname{Im} \left[(m_{\mathbf{b}}^2 + 3iaT) \tilde{\zeta} \ln \frac{m_{\mathbf{b}}^2 - 3iaT - \tilde{\zeta}}{m_{\mathbf{b}}^2 - 3iaT + \tilde{\zeta}} \right] \right\} \quad (\text{F7})$$

and

$$\mathcal{I}_{2,2}(a, b, m_{\mathbf{b}}^2, T) = \frac{1}{16(b - am_{\mathbf{b}}^2)^2} \left[(16 - \pi^2)b + 4a(-4m_{\mathbf{b}}^2 + 3\pi aT) + 4 \ln \frac{3a^2 T}{b} \left(4b - 2am_{\mathbf{b}}^2 + b \ln \frac{3a^2 T}{b} \right) - 8 \operatorname{Re} \left(a \tilde{\zeta} \ln \frac{m_{\mathbf{b}}^2 - 3iaT - \tilde{\zeta}}{m_{\mathbf{b}}^2 - 3iaT + \tilde{\zeta}} \right) - 4 \operatorname{Re} \left(b \ln^2 \frac{m_{\mathbf{b}}^2 - 3iaT - \tilde{\zeta}}{m_{\mathbf{b}}^2 - 3iaT + \tilde{\zeta}} \right) \right] \quad (\text{F8})$$

with

$$\tilde{\zeta} = \sqrt{12ibT + (m_{\mathbf{b}}^2 - 3iaT)^2} \quad (\text{F9})$$

Although the expressions of $\mathcal{I}_{2,1}$ and $\mathcal{I}_{2,2}$ are complicated, their asymptotic behaviors are quite simple. In particular, for $T \gg g^2/N$, we have

$$\mathcal{I}_{2,1}(a, b, m_{\mathbf{b}}^2, T) \simeq \frac{\pi}{8a^2 T}, \quad (\text{F10})$$

$$\mathcal{I}_{2,2}(a, b, m_{\mathbf{b}}^2, T) \simeq -\frac{\pi}{12a^2 T} \quad (\text{F11})$$

On the other hand, in the very low temperature limit $T \ll g^2/N$, we have

$$\mathcal{I}_{2,1}(a, b, m_{\mathbf{b}}^2, T) \simeq -\frac{1}{2b} \ln \left(\frac{a^2 T}{b} \right), \quad (\text{F12})$$

$$\mathcal{I}_{2,2}(a, b, m_{\mathbf{b}}^2, T) \simeq \frac{1}{4b} \ln^2 \left(\frac{a^2 T}{b} \right). \quad (\text{F13})$$

Combining the above expressions gives Eq. (7.38).

[1] C. M. Varma, P. B. Littlewood, S. S.-Rink, E. Abrahams, and A. E. Ruckenstein, Phenomenology of the normal state of Cu-O high-temperature superconductors, Phys. Rev. Lett. **63**, 1996 (1989).

[2] B. Keimer, S. A. Kivelson, M. R. Norman, S. Uchida, and J. Zaanen, From quantum matter to high-temperature superconductivity in copper oxides, Nature **518**, 179 (2015).

- [3] T. Shibauchi, A. Carrington, and Y. Matsuda, A Quantum Critical Point Lying beneath the Superconducting Dome in Iron Pnictides, *Annu. Rev. Condens. Matter Phys.* **5**, 113 (2014).
- [4] H. Kuo, J. Chu, J. Palmstrom, S. Kivelson, and I. Fisher, Ubiquitous signatures of nematic quantum criticality in optimally doped Fe-based superconductors, *Science* **352**, 958 (2016).
- [5] N. E. Hussey, A. P. Mackenzie, J. R. Cooper, Y. Maeno, S. Nishizaki, and T. Fujita, Normal-State Magnetoresistance of Sr_2RuO_4 , *Phys. Rev. B* **57**, 5505 (1998).
- [6] M. Schneider, D. Geiger, S. Esser, U. S. Pracht, C. Stingl, Y. Tokiwa, V. Moshnyaga, I. Sheikin, J. Mravlje, M. Scheffler, and P. Gegenwart, Low-Energy Electronic Properties of Clean CaRuO_3 : Elusive Landau Quasiparticles, *Phys. Rev. Lett.* **112**, 206403 (2014).
- [7] L. Klein, J. S. Dodge, C. H. Ahn, G. J. Snyder, T. H. Geballe, M. R. Beasley, and A. Kapitulnik, Anomalous Spin Scattering Effects in the Badly Metallic Itinerant Ferromagnet SrRuO_3 , *Phys. Rev. Lett.* **77**, 2774 (1996).
- [8] P. B. Allen, H. Berger, O. Chauvet, L. Forro, T. Jarlborg, A. Junod, B. Revaz, and G. Santi, Transport Properties, Thermodynamic Properties, and Electronic Structure of SrRuO_3 , *Phys. Rev. B* **53**, 4393 (1996).
- [9] H. Polshyn, N. Yankowicz, S. Chen, Y. Zhang, K. Watanabe, T. Taniguchi, C. R. Dean, and A. F. Young, Large linear-in-temperature resistivity in twisted bilayer graphene, *Nat. Phys.* **15**, 1011 (2019).
- [10] Y. Cao, D. Chowdhury, D. Rodan-Legrain, O. Rubies-Bigorda, K. Watanabe, T. Taniguchi, T. Senthil, and P. Jarillo-Herrero, Strange Metal in Magic-Angle Graphene with near Planckian Dissipation, *Phys. Rev. Lett.* **124**, 076801 (2020).
- [11] G. R. Stewart, Non-Fermi-Liquid Behavior in d - and f -Electron Metals, *Rev. Mod. Phys.* **73**, 797 (2001).
- [12] Hilbert v. Löhneysen, Achim Rosch, Matthias Vojta, and Peter Wölfle, Fermi liquid instabilities at magnetic quantum phase transitions, *Rev. Mod. Phys.* **79**, 1015 (2007).
- [13] A. Steppke, R. Kuchler, S. Lausberg, E. Lengyel, L. Steinke, R. Borth, T. Lühmann, C. Krellner, M. Nicklas, C. Geibel, F. Steglich, and M. Brando, Ferromagnetic quantum critical point in the heavy-fermion metal $\text{YbNi}_4(\text{P}_{1-x}\text{As}_x)_2$, *Science* **339**, 6112, 933 (2013).
- [14] L. P. Pitaevskii and E. M. Lifshitz, *Physical Kinetics: Volume 10 (Course of Theoretical Physics)*, 1st Ed. (Butterworth-Heinemann, Oxford, England, 1981).
- [15] A. A. Patel and S. Sachdev, Theory of a Planckian Metal, *Phys. Rev. Lett.* **123**, 066601 (2019).
- [16] D. Chowdhury, A. Georges, O. Parcollet, S. Sachdev, Sachdev-Ye-Kitaev Models and Beyond: A Window into Non-Fermi Liquids, arXiv:2109.05037 (2021).
- [17] P. A. Lee and T. V. Ramakrishnan, Disordered electronic systems, *Rev. Mod. Phys.* **57**, 287 (1985).
- [18] F. Evers and A. D. Mirlin, Anderson transitions, *Rev. Mod. Phys.* **80**, 1355 (2008).
- [19] V. M. Galitski, Metallic phase in a two-dimensional disordered Fermi system with singular interactions, *Phys. Rev. B* **72**, 214201 (2005).
- [20] I. Aleiner, B. Altshuler, and M. Gershenson, Interaction effects and phase relaxation in disordered systems, *Waves Random Media* **9**, 201 (1999).
- [21] B. L. Altshuler and A. G. Aronov, Electron-electron interaction in disordered conductors, in *Electron-Electron Interactions in Disordered Systems*, edited by M. Pollak and A. L. Efros (North-Holland, Amsterdam, 1985).
- [22] G. Zala, B. N. Narozhny, and I. L. Aleiner Interaction corrections at intermediate temperatures: Longitudinal conductivity and kinetic equation, *Phys. Rev. B* **64**, 214204 (2001).
- [23] C. Castellani, C. DiCastro, G. Kotliar, and P. A. Lee, Dephasing Time in Disordered Systems, *Phys. Rev. Lett.* **56**, 1179 (1986).
- [24] A. V. Chubukov, S. Sachdev, and J. Ye, Theory of two-dimensional quantum Heisenberg antiferromagnets with a nearly critical ground state, *Phys. Rev. B* **49**, 11919 (1994).
- [25] S. Sachdev, Universal relaxational dynamics near two-dimensional quantum critical points, *Phys. Rev. B* **59**, 14054 (1999).
- [26] S. Sachdev, *Quantum Phase Transitions*, 2nd Ed., Cambridge University Press (2011).
- [27] M. V. Feigel'man, L. B. Ioffe, V. E. Kravtsov, and E. A. Yuzbashyan, Eigenfunction Fractality and Pseudogap State near the Superconductor-Insulator Transition, *Phys. Rev. Lett.* **98**, 027001 (2007).
- [28] M. V. Feigel'man, L. B. Ioffe, V. E. Kravtsov, and E. Cuevas, Fractal superconductivity near localization threshold, *Ann. Phys.* **325**, 1390 (2010).
- [29] I. S. Burmistrov, I. V. Gornyi, and A. D. Mirlin, Enhancement of the Critical Temperature of Superconductors by Anderson Localization, *Phys. Rev. Lett.* **108**, 017002 (2012).
- [30] J. Mayoh, and A. M. García-García, Global critical temperature in disordered superconductors with weak multifractality, *Phys. Rev. B* **92**, 174526 (2015).
- [31] B. Fan and A. M. García-García, Superconductivity at the three-dimensional Anderson metal-insulator transition, *Phys. Rev. B* **102**, 184507 (2020).
- [32] X.-Y. Song, C.-M. Jian, and L. Balents, Strongly Correlated Metal Built from Sachdev-Ye-Kitaev Models, *Phys. Rev. Lett.* **119**, 216601 (2017).
- [33] D. Chowdhury and E. Berg, The unreasonable effectiveness of Eliashberg theory for pairing of non-Fermi liquids, *Ann. Phys.* **417**, 168125 (2020).
- [34] I. Esterlis, H. Guo, A. A. Patel, and S. Sachdev, Large- N theory of critical Fermi surfaces, *Phys. Rev. B* **103**, 235129 (2021).
- [35] E. E. Aldape, T. Cookmeyer, A. A. Patel, E. Altman, Solvable Theory of a Strange Metal at the Breakdown of a Heavy Fermi Liquid, arXiv:2012.00763 (2020).
- [36] D. Chowdhury, Y. Werman, E. Berg, and T. Senthil, Translationally Invariant Non-Fermi-Liquid Metals with Critical Fermi Surfaces: Solvable Models, *Phys. Rev. X* **8**, 031024 (2018).
- [37] W. Choi, O. Tivakol, and Y. B. Kim, Pairing Instabilities of the Yukawa-SYK Models with Controlled Fermion Incoherence, arXiv:2110.02968 (2021).
- [38] A. A. Patel, H. Guo, I. Esterlis, S. Sachdev, Universal T-linear resistivity in two-dimensional quantum-critical metals from spatially random interactions, arXiv:2203.04990 (2022).
- [39] J. A. Damia, S. Kachru, S. Raghu, and G. Torroba, Two-Dimensional Non-Fermi-Liquid Metals: A Solvable Large- N Limit, *Phys. Rev. Lett.* **123**, 096402 (2019).
- [40] P. A. Nosov, I. S. Burmistrov, and S. Raghu, Interaction-Induced Metallicity in a Two-Dimensional Disordered Non-Fermi Liquid, *Phys. Rev. Lett.* **125**,

- 256604 (2020).
- [41] I. Esterlis, H. Guo, A. A. Patel, and S. Sachdev, Large- N theory of critical Fermi surfaces, *Phys. Rev. B* **103**, 235129 (2021).
 - [42] A. Kamenev and A. Levchenko, Keldysh technique and non-linear σ -model: basic principles and applications, *Adv. Phys.* **58**, 197 (2009).
 - [43] A. Kamenev, *Field Theory of Non-Equilibrium Systems*, (Cambridge University Press, Cambridge, England, 2011).
 - [44] Y. Liao, A. Levchenko, and M. S. Foster, Response theory of the ergodic many-body delocalized phase: Keldysh Finkel'stein sigma models and the 10-fold way, *Ann. Phys.* **386**, 97 (2017).
 - [45] M. Le Bellac, *Thermal Field Theory* (Cambridge University Press, 2000).
 - [46] A. M. Finkel'stein, Influence of Coulomb interaction on the properties of disordered metals, *Zh. Eksp. Teor. Fiz.* **84**, 168 (1983) [*Sov. Phys. JETP* **57**, 97 (1983)].
 - [47] D. Belitz and T. R. Kirkpatrick, The Anderson-Mott transition, *Rev. Mod. Phys.* **66**, 261 (1994).
 - [48] I. S. Burmistrov, Finkel'stein Nonlinear Sigma Model: Interplay of Disorder and Interaction in 2D Electron Systems, *Journal of Experimental and Theoretical Physics* **129**, 669 (2019).
 - [49] J. S. Meyer, I. V. Gornyi, and A. Altland, Quantum Critical Fluctuations in Disordered d -Wave Superconductors, *Phys. Rev. Lett.* **90**, 107001 (2003).
 - [50] J. S. Meyer, I. V. Gornyi, and A. Altland, Disorder and Quantum Criticality in d -wave Superconductors, *Int. J. Mod. Phys. B* **18**, 7, 949 (2004).
 - [51] A. Levchenko and J. Schmalian, Transport properties of strongly coupled electron-phonon liquids, *Ann. Phys.* **419**, 168218 (2020).
 - [52] A. Punnoose and A. M. Finkel'stein, Metal-Insulator Transition in Disordered Two-Dimensional Electron Systems, *Science* **310**, 289 (2005).
 - [53] B. L. Altshuler, and A. G. Aronov, Contribution to the theory of disordered metals in strongly doped semiconductors, *Zh. Eksp. Teor. Fiz.*, **77**, 2028 (1979) [*Sov. Phys. JETP* **50**, 968 (1979)].
 - [54] L. Dell'Anna, Disordered d -wave superconductors with interactions, *Nucl. Phys. B* **758**, 255 (2006).
 - [55] L. Dell'Anna, Beta-functions of non-linear σ -models for disordered and interacting electron systems, *Ann. Phys. (Berlin)* **529**, 1600317 (2017).
 - [56] P. A. Lee, N. Nagaosa, and X.-G. Wen, Doping a Mott insulator: Physics of high-temperature superconductivity, *Rev. Mod. Phys.* **78**, 17 (2006).
 - [57] E. Berg, S. Lederer, Y. Schattner, and S. Trebst, Monte Carlo Studies of Quantum Critical Metals, *Annu. Rev. Condens. Matter Phys.* **10**, 63 (2019).
 - [58] S.-S. Lee, Recent Developments in Non-Fermi Liquid Theory, *Annu. Rev. Condens. Matter Phys.* **9**, 227 (2018).
 - [59] J. Rech, C. Pépin, and A. V. Chubukov, Quantum critical behavior in itinerant electron systems: Eliashberg theory and instability of a ferromagnetic quantum critical point, *Phys. Rev. B* **74**, 195126 (2006).
 - [60] S. P. Ridgway and C. A. Hooley, Non-Fermi-Liquid Behavior and Anomalous Suppression of Landau Damping in Layered Metals lose to Ferromagnetism, *Phys. Rev. Lett.* **114**, 226404 (2015).
 - [61] M. A. Metlitski and S. Sachdev, Quantum phase transitions of metals in two spatial dimensions. I. Ising-nematic order, *Phys. Rev. B* **82**, 075127 (2010).
 - [62] M. A. Metlitski and S. Sachdev, Quantum phase transitions of metals in two spatial dimensions. II. Spin density wave order, *Phys. Rev. B* **82**, 075128 (2010).
 - [63] S. Raghu, G. Torroba, and H. Wang, Metallic quantum critical points with finite BCS couplings, *Phys. Rev. B* **92**, 205104 (2015).
 - [64] A. L. Fitzpatrick, S. Kachru, J. Kaplan, and S. Raghu, Non-Fermi-liquid fixed point in a Wilsonian theory of quantum critical metals, *Phys. Rev. B* **88**, 125116 (2013).
 - [65] R. Mahajan, D. M. Ramirez, S. Kachru, and S. Raghu, Quantum critical metals in $d = 3 + 1$ dimensions, *Phys. Rev. B* **88**, 115116 (2013).
 - [66] I. Mandal and S.-S. Lee, Ultraviolet/infrared mixing in non-Fermi liquids, *Phys. Rev. B* **92**, 035141 (2015).
 - [67] S.-S. Lee, Low-energy effective theory of Fermi surface coupled with U(1) gauge field in 2+1 dimensions, *Phys. Rev. B* **80**, 165102 (2009).
 - [68] A. Schliefl, P. Lunts, and S.-S. Lee, Exact Critical Exponents for the Antiferromagnetic Quantum Critical Metal in Two Dimensions, *Phys. Rev. X* **7**, 021010 (2017).
 - [69] S. Sur and S.-S. Lee, Chiral non-Fermi liquids, *Phys. Rev. B* **90**, 045121 (2016).
 - [70] S. Sur and S.-S. Lee, Anisotropic non-Fermi liquids, *Phys. Rev. B* **94**, 195135 (2016).
 - [71] D. F. Mross, J. McGreevy, H. Liu, and T. Senthil, Controlled expansion for certain non-Fermi-liquid metals, *Phys. Rev. B* **82**, 045121 (2010).
 - [72] I. Mandal, Superconducting instability in non-Fermi liquids, *Phys. Rev. B* **94**, 115138 (2016).
 - [73] A. V. Chubukov, Ward identities for strongly coupled Eliashberg theories, *Phys. Rev. B* **72**, 085113 (2005).
 - [74] A. Shekhter and C. M. Varma, Long-wavelength correlations and transport in a marginal Fermi liquid, *Phys. Rev. B* **79**, 045117 (2009).
 - [75] S. Lederer, Y. Schattner, E. Berg, and S. A. Kivelson, Superconductivity and Non-Fermi Liquid Behavior near a Nematic Quantum Critical Point, *Proc. Natl. Acad. Sci. U.S.A.* **114**, 4905 (2017).
 - [76] S.-K. Jian, Z.-Y. Xian, and H. Yao, Quantum Criticality and Duality in the SYK=AdS₂ Chain, *Phys. Rev. B* **97**, 205141 (2018).
 - [77] S. Sachdev, Bekenstein-Hawking Entropy and Strange Metals, *Phys. Rev. X* **5**, 041025 (2015).
 - [78] R. A. Davison, W. Fu, A. Georges, Y. Gu, K. Jensen, and S. Sachdev, Thermoelectric Transport in Disordered Metals without Quasiparticles: The Sachdev-Ye-Kitaev Models and Holography, *Phys. Rev. B* **95**, 155131 (2017).
 - [79] S. Sachdev and J. Ye, Gapless spin-fluid ground state in a random quantum Heisenberg magnet, *Phys. Rev. Lett.* **70**, 3339 (1993).
 - [80] Y. Gu, X.-L. Qi, and D. Stanford, Local Criticality, Diffusion and Chaos in Generalized Sachdev-Ye-Kitaev Models, *J. High Energy Phys.* **05**, 125 (2017).
 - [81] I. Esterlis and J. Schmalian, Cooper pairing of incoherent electrons: An electron-phonon version of the Sachdev-Ye-Kitaev model, *Phys. Rev. B* **100**, 115132 (2019).
 - [82] Y. Wang, Solvable Strong-Coupling Quantum-Dot Model with a Non-Fermi-Liquid Pairing Transition, *Phys. Rev. Lett.* **124**, 017002 (2020).

- [83] D. V. Else and T. Senthil, Strange Metals as Ersatz Fermi Liquids, *Phys. Rev. Lett.* **127**, 086601 (2021).
- [84] B. L. Altshuler, A. G. Aronov, and P. A. Lee, Interaction Effects in Disordered Fermi Systems in Two Dimensions, *Phys. Rev. Lett.*, **44**, 1288 (1980).
- [85] M. S. Foster and E. A. Yuzbashyan, Interaction-mediated surface state instability in disordered three-dimensional topological superconductors with spin SU(2) symmetry, *Phys. Rev. Lett.* **109**, 246801 (2012).
- [86] M. S. Foster, H.-Y. Xie, and Y.-Z. Chou, Topological protection, disorder, and interactions: Survival at the surface of 3D topological superconductors, *Phys. Rev. B* **89**, 155140 (2014).
- [87] S. V. Kravchenko and M. P. Sarachik, Metal-insulator transition in two-dimensional electron systems, *Rep. Prog. Phys.* **67**, 1 (2004).
- [88] A. M. Finkel'stein, Disordered Electron Liquid with Interactions, in *50 Years of Anderson Localization*, edited by E. Abrahams (World Scientific, Singapore, 2010).
- [89] J. Halbinger and M. Punk, Quenched disorder at antiferromagnetic quantum critical points in two-dimensional metals, *Phys. Rev. B* **103**, 235157 (2021).
- [90] H. Yerzhakov and J. Maciejko, Disordered fermionic quantum critical points, *Phys. Rev. B* **98**, 195142 (2018).
- [91] C. Chamon, A. W. W. Ludwig, and C. Nayak, Schwinger-Keldysh approach to disordered and interacting electron systems: Derivation of Finkelstein's renormalization-group equations, *Phys. Rev. B* **60**, 2239 (1999).
- [92] M. S. Foster and A. W. W. Ludwig, Metal-insulator transition from combined disorder and interaction effects in Hubbard-like electronic lattice models with random hopping, *Phys. Rev. B* **77**, 165108 (2008).
- [93] M. S. Foster and A. W. W. Ludwig, Metal-insulator transition in Hubbard-like models with random hopping, *Phys. Rev. B* **74**, 241102(R) (2006).
- [94] A. J. McKane and M. Stone, Localization as an alternative to Goldstone's theorem, *Ann. of Phys.* **131**, 36 (1981).
- [95] M. V. Feigel'man, A. I. Larkin, and M. A. Skvortsov, Keldysh action for disordered superconductors, *Phys. Rev. B* **61**, 12361 (2000).
- [96] I. S. Burmistrov and E. V. Repin, Quantum corrections to conductivity of disordered electrons due to inelastic scattering off magnetic impurities, *Phys. Rev. B* **98**, 045414 (2018).
- [97] B. L. Altshuler, A. G. Aronov, and D. E. Khmelnitsky, Effects of electron-electron collisions with small energy transfers on quantum localisation, *J. Phys. C* **15**, 7367 (1982).
- [98] S. M. Davis and M. S. Foster, Non-Markovian dephasing of disordered quasi-one-dimensional fermion systems, *Phys. Rev. B* **102**, 155101 (2020).
- [99] Y. Liao and M. S. Foster, Dephasing Catastrophe in $4 - \varepsilon$ Dimensions: A Possible Instability of the Ergodic (Many-Body-Delocalized) Phase, *Phys. Rev. Lett.* **120**, 236601 (2018).
- [100] S. Matsuura, P.-Y. Chang, A. P. Schnyder, and S. Ryu, Protected boundary states in gapless topological phases, *New J. Phys.* **15**, 065001 (2013).
- [101] C.-K. Chiu, J. C. Y. Teo, A. P. Schnyder, and S. Ryu, Classification of topological quantum matter with symmetries, *Rev. Mod. Phys.* **88**, 035005 (2016).
- [102] A. P. Schnyder, S. Ryu, A. Furusaki, and A. W. W. Ludwig, Classification of topological insulators and superconductors in three spatial dimensions, *Phys. Rev. B* **78**, 195125 (2008).
- [103] A. Kamenev and A. Andreiev, Electron-electron interactions in disordered metals: Keldysh formalism, *Phys. Rev. B* **60**, 2218 (1999).
- [104] Y. Liao, D. Buterakos, M. Schecter, and S. Das Sarma, Two-dimensional electron self-energy: Long-range Coulomb interaction, *Phys. Rev. B* **102**, 085145 (2020).
- [105] T. C. Wu, H. K. Pal, and M. S. Foster, Topological anomalous skin effect in Weyl superconductors, *Phys. Rev. B* **103**, 104517 (2021).
- [106] S. Das Sarma and Y. Liao, Know the enemy: 2D Fermi liquids, *arXiv:2101.07802* (2021).
- [107] J. A. Damia, M. Solís, and G. Torroba, How non-Fermi liquids cure their infrared divergences, *Phys. Rev. B* **102**, 045147 (2020).
- [108] C. Castellani, C. Di Castro, G. Kotliar, P. A. Lee, and G. Strinati, Heat-transport Ward identity and effective Landau Fermi-liquid parameters in disordered systems, *Phys. Rev. B* **37**, 9046 (1988).
- [109] P. M. Ostrovsky, I. V. Gornyi, and A. D. Mirlin, Interaction-Induced Criticality in \mathbb{Z}_2 Topological Insulators, *Phys. Rev. Lett.* **105**, 036803 (2010).
- [110] Y. Nakajima, T. Metz, C. Eckberg, K. Kirshenbaum, A. Hughes, R. Wang, L. Wang, S. R. Saha, I.-L. Liu, N. P. Butch, D. Campbell, Y. S. Eo, D. Graf, Z. Liu, S. V. Borisenko, P. Y. Zavalij, and J. Paglione, Quantum-critical scale invariance in a transition metal alloy, *Comm. Phys.* **3**, 181 (2020).
- [111] N. Tenen, A. Yu. Kuntsevich, V. M. Pudalov, and M. Reznikov, Spin-Droplet State of an Interacting 2D Electron System, *Phys. Rev. Lett.* **109**, 226403 (2012).
- [112] L. A. Morgun, A. Yu. Kuntsevich, and V. M. Pudalov, Novel energy scale in the interacting two-dimensional electron system evidenced from transport and thermodynamic measurements, *Phys. Rev. B* **93**, 235145 (2016).
- [113] M. E. Peskin and D. V. Schroeder, *An Introduction To Quantum Field Theory* (Addison-Wesley, Reading, MA, 1995).
- [114] R. Nandkishore and L. Levitov, Electron interactions in bilayer graphene: Marginal Fermi liquid and zero-bias anomaly, *Phys. Rev. B* **82**, 115431 (2010).
- [115] A. Abanov and A. V. Chubukov, Interplay between superconductivity and non-Fermi liquid at a quantum critical point in a metal. I. The γ model and its phase diagram at $T = 0$: The case $0 < \gamma < 1$, *Phys. Rev. B* **102**, 024524 (2020).
- [116] Y.-M. Wu, A. Abanov, Y. Wang, and A. V. Chubukov, Interplay between superconductivity and non-Fermi liquid at a quantum critical point in a metal. II. The γ model at a finite T for $0 < \gamma < 1$, *Phys. Rev. B* **102**, 024525 (2020).
- [117] Y.-M. Wu, A. Abanov, and A. V. Chubukov, Interplay between superconductivity and non-Fermi liquid behavior at a quantum critical point in a metal. III. The γ model and its phase diagram across $\gamma = 1$, *Phys. Rev. B* **102**, 094516 (2020).
- [118] S.-S. Zhang, Y.-M. Wu, A. Abanov, and A. V. Chubukov, Interplay between superconductivity and non-Fermi liquid at a quantum critical point in a metal.

- VI. The γ model and its phase diagram at $2 < \gamma < 3$, Phys. Rev. B **104**, 144509 (2021).
- [119] Y.-M. Wu, S.-S. Zhang, A. Abanov, and A. V. Chubukov, Interplay between superconductivity and non-Fermi liquid behavior at a quantum-critical point in a metal. V. The γ model and its phase diagram: The case $\gamma = 2$, Phys. Rev. B **103**, 184508 (2021).
- [120] Y.-M. Wu, S.-S. Zhang, A. Abanov, and A. V. Chubukov, Interplay between superconductivity and non-Fermi liquid at a quantum critical point in a metal. IV. The γ model and its phase diagram at $1 < \gamma < 2$, Phys. Rev. B **103**, 024522 (2021).
- [121] C. P. Nave and P. A. Lee, Transport properties of a spinon Fermi surface coupled to a U(1) gauge field, Phys. Rev. B **76**, 235124 (2007).
- [122] Y. B. Kim, P. A. Lee, and X.-G. Wen, Quantum Boltzmann equation of composite fermions interacting with a gauge field, Phys. Rev. B **52**, 17275 (1995).
- [123] D. B. Gutman and Y. Gefen, Shot noise in disordered junctions: Interaction corrections, Phys. Rev. B **64**, 205317 (2001).